DESIGN AND EVALUATION OF A PULSATING FLOW WIND TUNNEL

by

Amir Tavakoli

Thesis submitted to the Graduate Faculty of the

Virginia Polytechnic Institute and State University

in partial fulfillment of the requirements for the degree of

MASTER OF SCIENCE

in

Mechanical Engineering

APPROVED:

T. E. Diller, Chairman

D. P. Telionis

J. Moore

S. W. Zewari

A. G. Szeless

September, 1982

Blacksburg, Virginia

ACKNOWLEDGEMENTS

I would like to express my sincerest gratitude to Dr. T. E. Diller and D. P. Telionis, my project advisors, under whose supervision this thesis was completed. I am indebted to them for their help, encouragement, and valuable advice in discussing this investigation.

The author extends his thanks to the members of his advisory committee, Dr. T. E. Diller (Chairman), Dr. D. P. Telionis, Dr. S. W. Zewari, Dr. A. G. Szeless, and Dr. J. Moore for their suggestions and help.

The support of this project as part of contract No. DE-AS 05-82E 12022 under the direction of Dr. Oscar Manley from the office of Basic Energy Research, Department of Energy, is gratefully acknowledged.

My many thanks to Byung K. Kim for his cooperation during the experimental investigation.

I wish to express my thanks to Jack Gray, especially to Red Fisher and H. M. Smith for their help in building the wind tunnel.

Finally, I express my many thanks and appreciation to my parents for their support and encouragement along with their benevolence and especially my sister, Fahti, for her constant encouragement and love. To them I dedicate this thesis.

TABLE OF CONTENTS

TABLE OF CONTENTS (CONT'D)

TABLE OF CONTENTS (CONT'D)

LIST OF FIGURES

LIST OF FIGURES (CONT'D)

LIST OF FIGURES (CONT'D)

LIST OF TABLES

LIST OF TABLES (CONT'D)

LIST OF TABLES (CONT'D)

LIST OF TABLES (CONT'D)

NOMENCLATURE

Symbol	Meaning
A	local area of the tunnel
A_o	cross sectional area of test section
C_f	friction coefficient
d	screen wire diameter
$\bar{E}$	average motor voltage
$\tilde{E}$	motor voltage variation
H	shaft input power
h	height of the settling chamber
h_o	height of the test section
h_s	height of the shutters
K	pressure drop coefficient
r	one-half the height of the shutters
S	spacing between the shutters
S_t	spacing between the tunnel floor (or tunnel ceiling) and lower shutter (or upper shutter)
T	cycle period
t	time
$\bar{U}$	average velocity
$\tilde{U}$	periodic velocity
$U = \bar{U} + \tilde{U}$	velocity at test section entrance
U_{max}	maximum value of velocity at test section entrance
U_{min}	minimum value of velocity at test section entrance
u	mean velocity in the settling chamber

u_1	instantaneous velocity in longitudinal direction
u_{1t}	turbulent part of u_1
V_o	velocity in test section
w_o	width of the test section
β	screen open-area ratio
η	blower efficiency
λ	power factor of the tunnel
$\Delta\lambda_{1,2,3}$	the power factor of each component
ν	kinematic viscosity of air
ρ_o	density of air in test section
$\phi_{2...5}$	relative blade orientation in Figure 6 and Table 1
ω	shutters angular velocity

1. INTRODUCTION

Numerous investigators have constructed wind tunnels that generate periodic pulsation of the velocity, but they have reported little information concerning the sinusoidal flow itself. These studies provide information about the mass transfer, heat transfer and stabilities in unsteady flows over specific models, but are not concerned with the quality of pulsating flow.

The present investigation presents the design, construction and performance of a blower wind tunnel that produces nearly sinusoidal velocity pulsations. The flow pulsation is produced by a set of rotating shutters placed at the beginning of the settling chamber inlet. All the shutters are rotated at the same angular velocity with an adjustable frequency from 3.4 to 31.3 Hz.

Previous investigations indicated that flow pulsations may increase heat transfer in the attached and/or separated flow regions. This investigation is part of a larger project to study a possible increased heat transfer and decreased flow resistance in subcritical pulsed flow about stationary cylinders. Producing a reduced flow resistance and increased heat transfer may increase the efficiency of heat exchange systems. The results obtained from the present wind tunnel flow investigation will be used to design a larger wind tunnel for the heat transfer experiments.

2. LITERATURE REVIEW

A wind tunnel is an essential engineering tool for basic research. Since the 1930s, when the strong effect of free-stream turbulence on shear layers became apparent, wind tunnels with low levels of turbulence and unsteadiness were designed. The requirements of general utility for a wind tunnel are perhaps most completely met by the single-return tunnel [1].

Ideally, the wind tunnel designer starts his work by determining the required flow speed and velocity profile of a new tunnel. Consequently most high performance wind tunnels are of the closed-circuit type to ensure a controlled return flow [2]. However, it is possible to achieve high performance from an open-circuit tunnel, thus saving space and construction cost.

Blower tunnels (with the fan at the entrance to the tunnel) facilitate large variation in working section arrangements [2]. A centrifugal fan is preferable to an axial fan in order to cope with the interchangeability in operating conditions. The main advantage of a centrifugal blower, as distinct from an axial fan, is that it performs well over a large range of loads (the whole blade being at the same incidence and hence operating at the same lift coefficient). For ease of changing working sections the exit diffuser is often omitted from small blower tunnels.

The main advantage of open-circuit tunnels is in the saving of space and cost. They are also less sensitive to temperature changes

(usually room volume is much greater than tunnel volume) and the performance of a fan fitted at the upstream end is not affected by the disturbed flow exiting from the working section [2]. The only advantage of a suction tunnel, with a centrifugal or axial fan at exit, is that air coming from the tunnel room may be less disturbed than that coming from a fan [2].

One disadvantage of any open-circuit tunnel with an exit diffuser is that the pressure in the test section is less than atmospheric and so spurious jets issue from holes left unpatched. This can be remedied by obstructing the tunnel outlet and creating an overpressure in the working section or simply by eliminating the exit diffuser.

Higher efficiency wind tunnel means longer tunnel and hence increased cost of construction. The physical location may also be a decisive factor. If the tunnel is to be located in a certain building, or on a specific plot of ground, the designer must consider this factor in the layout.

3. OSCILLATION DEVICES

The phenomenon of rectilinear oscillations was examined in references [3-8]. The rectilinear oscillation is the motion along the direction of the flow. These works [3-8] discuss the effect of flow and airfoil oscillation on the performance of airfoils. The type of motions investigated were oscillations in the magnitude of the oncoming stream, plunging motions of the airfoil, unsteadiness in the third space dimension, compressibility effects, and oscillating shock waves. The present review and investigation is concerned only with the methods and evaluations for producing rectilinear oscillations of the flow.

3.1 Flap Type Oscillator

A flap type oscillator was used to oscillate the flow around a fixed airfoil [9]. This was accomplished by a system of flaps pivoted on the floor and the ceiling of the tunnel upstream of the settling chamber. The flap oscillator is shown in Figure 1 with solid and dashed lines. The two extreme positions of the flaps (along the axis of the tunnel) correspond to zero incidence where the flaps are parallel to the tunnel walls and the highest incidence which corresponds to full blockage of the tunnel.

The peak-to-peak velocity amplitude produced by this device is not given in this report [9]. The velocity waveform in the free stream is not given, but its time variations due to oscillatory disturbances near the airfoil appear smooth at a peak-to-peak amplitude of about 20%. The frequency range in this experiment varied from 0.3 to 2.4 Hz.

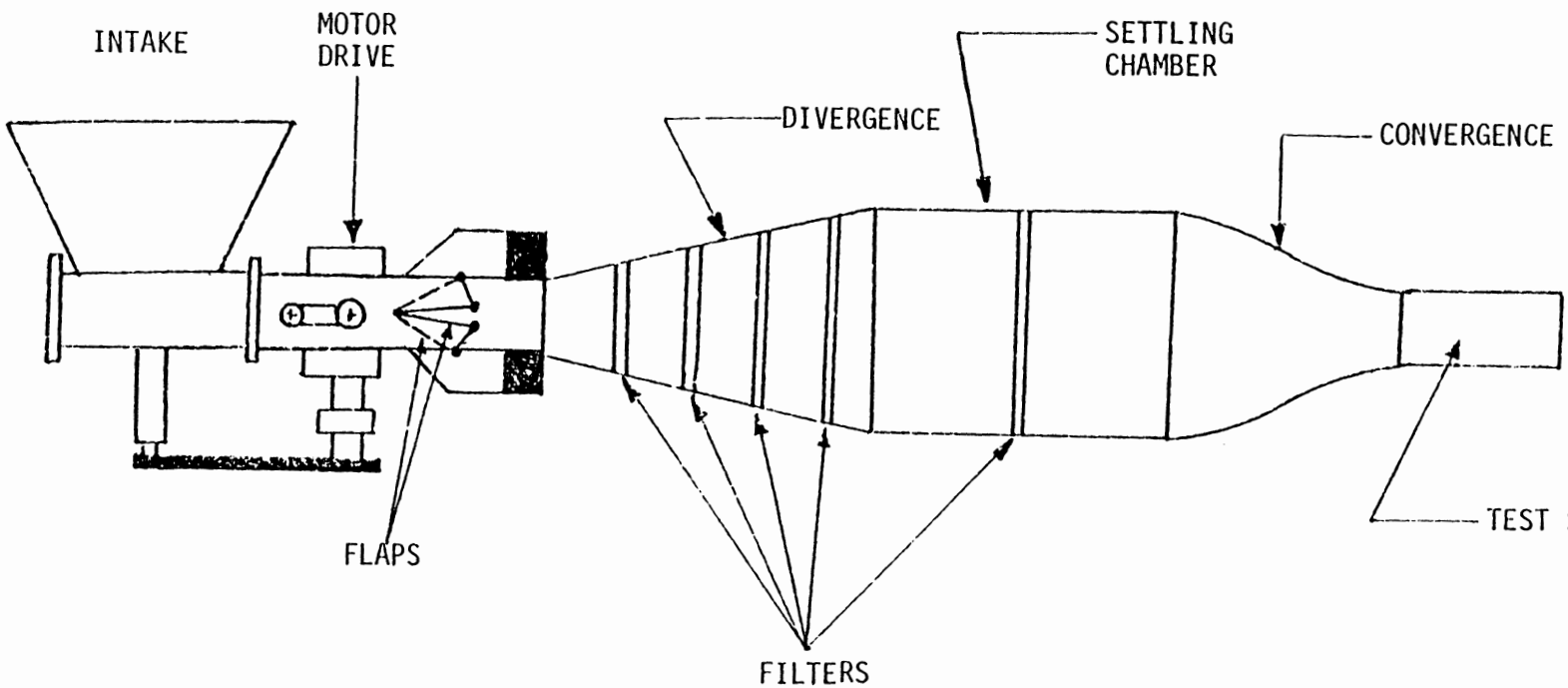

FIGURE 1: THE CNRS WIND TUNNEL WITH FLAP TYPE OSCILLATOR. REFERENCE [9].

3.2 Valve Type Oscillator

Another device that creates flow oscillations was used for an investigation of the oscillatory turbulent flow in a diffuser [10]. The oscillation is provided by a sliding plate valve. Figure 2 illustrates the oscillatory flow wind tunnel. The valve consisted of two adjacent movable slotted plates. A variable speed electric motor was connected to the crankshaft-connecting rod-oscillating plate assembly to provide variable frequency flow oscillations. The amplitude of flow oscillation was controlled by adjusting the stroke of the crankshaft and the length of the connecting rod.

This oscillating valve system generated nearly sinusoidal velocity fluctuations in the frequency range of 5 to 35 Hz. The measured spectral distribution of the flow signal at the diffuser inlet in the absence of valve oscillations was smooth and continuous with no peaks or spikes. The velocity amplitude results are not reported in this publication.

3.3-1 Oscillation by Rotating Shutters

Periodic flow in a wind tunnel produced by rotating shutters was investigated by G. Charnay and J. Mathieu [11]. The periodic flow was obtained in the test section by means of an upstream pulsator. This consisted of a device generating either a periodic loss of head or a periodic change of pressure. It was placed in the settling chamber before the honeycomb. Thus, for the desired range of frequencies, the static pressure in the test section remains practically constant which ensures the flow homogeneity.

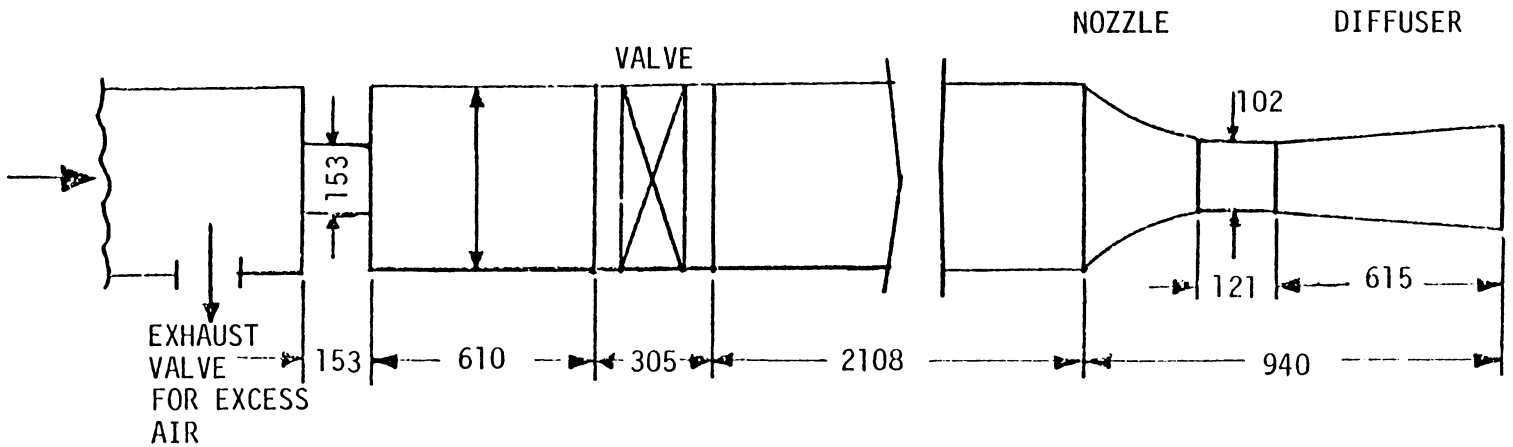

FIGURE 2: SCHEMATIC OF WIND TUNNEL WITH VALVE TYPE OSCILLATOR (DIMENSIONS IN mm). REFERENCE [10].

Figure 3 illustrates the schematic of the tunnel with the pulsating apparatus. The pulsator consisted of eight shutters, all rotating together with an adjustable frequency from 0 to 50 Hz [11]. All shutters were identical although it was possible to introduce a phase shift in their relative movements. Moreover, the shutters reportedly create a reduced turbulence when they are in motion. Thus, the ratio u_{1t}/u_1 is smaller by at least 50 percent than the mean value of the intensities of turbulence measured for a fixed position of the shutters when placed successively, at some angle between 0° and 180°.

Some of the results obtained from this experiment are interesting to note. The intensity of the residual turbulence in the test section is acceptable (less than 0.7 percent) in spite of the presence, upstream, of the pulsating apparatus. This value is not larger than those obtained for other experiments where the oscillatory device was downstream [11-15]. Finally, this wind tunnel is a useful tool for determining the influence of a periodic perturbation on turbulent flows. Unfortunately, the velocity amplitudes and waveforms have not been reported by the authors [11].

3.3-2 Programmable Damper Oscillator

Investigators of unsteady flows normally have little control over the waveform of the flow unsteadiness. In their investigation, R. L.

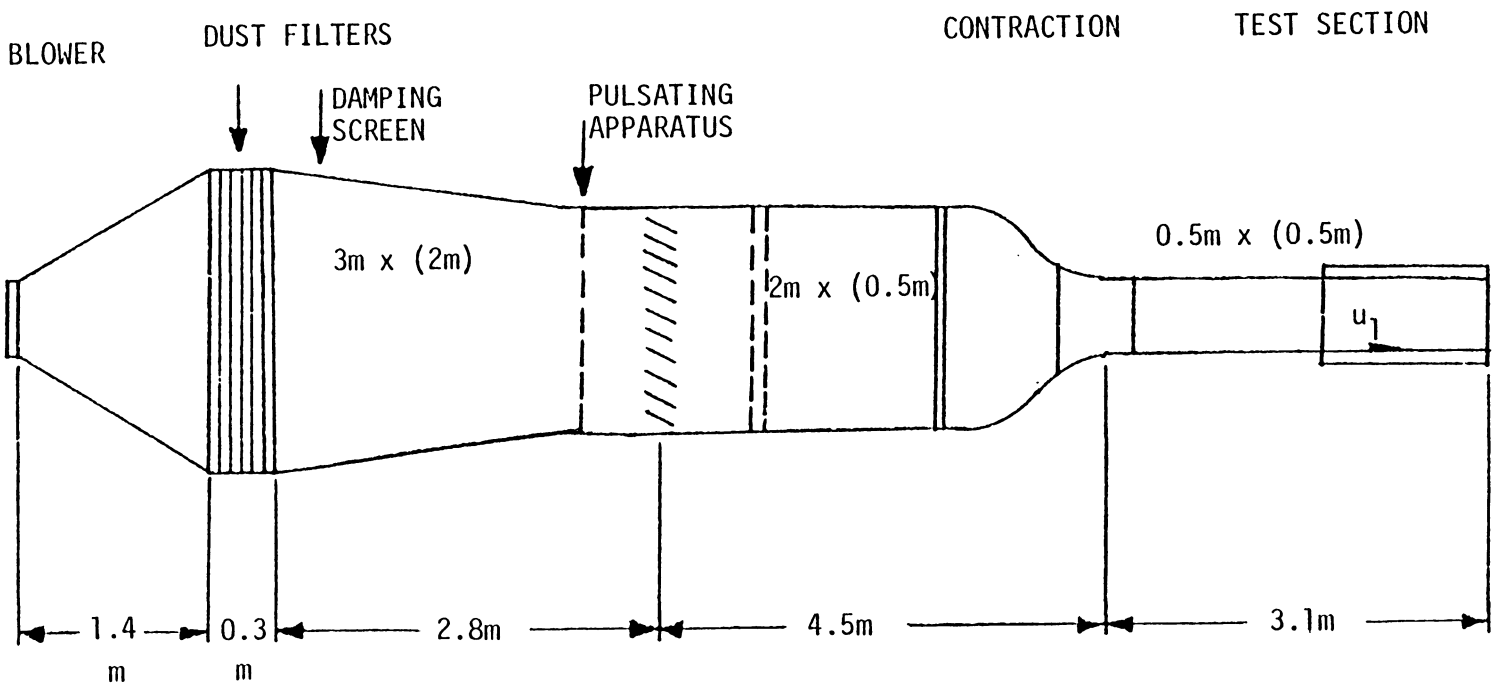

FIGURE 3 : WIND TUNNEL-PULSATING APPARATUS WITH SHUTTERS. REFERENCE [11]

Simpson, J. J. Sallas, and R. E. Nasburg [16] describe a programmable rotating blade damper system that is capable of generating a closely sinusoidal velocity waveform without using wind tunnel resonance. They introduce an improved method of producing a desired periodic velocity waveform by means of a series of rotating blade damper that were controlled and programmed electronically.

The pulsating apparatus consists of fixed blade dampers which control the maximum possible velocity, and the rotating blades which provide the time dependent flow resistance. The rotating blade damper consists of five blades mounted on parallel steel shafts that are supported by ball bearings in the surrounding housing [16]. The cross section of each blade is symmetrical diamond-shaped made out of aluminum. From one to five of the blades may be set at any relative orientation to one another with the remainder in fixed position. The schematic of this pulsating apparatus from the SMU Wind Tunnel is shown in Figure 4.

Meshing spur gears are mounted on shafts outside the housing to provide counterrotation of adjacent blades. Other gears provide a drive-train from a 0.3 (metric) HP/DC motor (with a mechanical advantage of 60 or 300) [16]. The maximum flow frequency is about 2 Hz. The voltage from the programmable angular velocity variation voltage generator causes the rotational speed of the damper blades to vary at desired values but not influence the mean angular velocity. When the frequency and the amplitude of the periodic velocity variation have been selected, the programmable voltage generator is set to produce

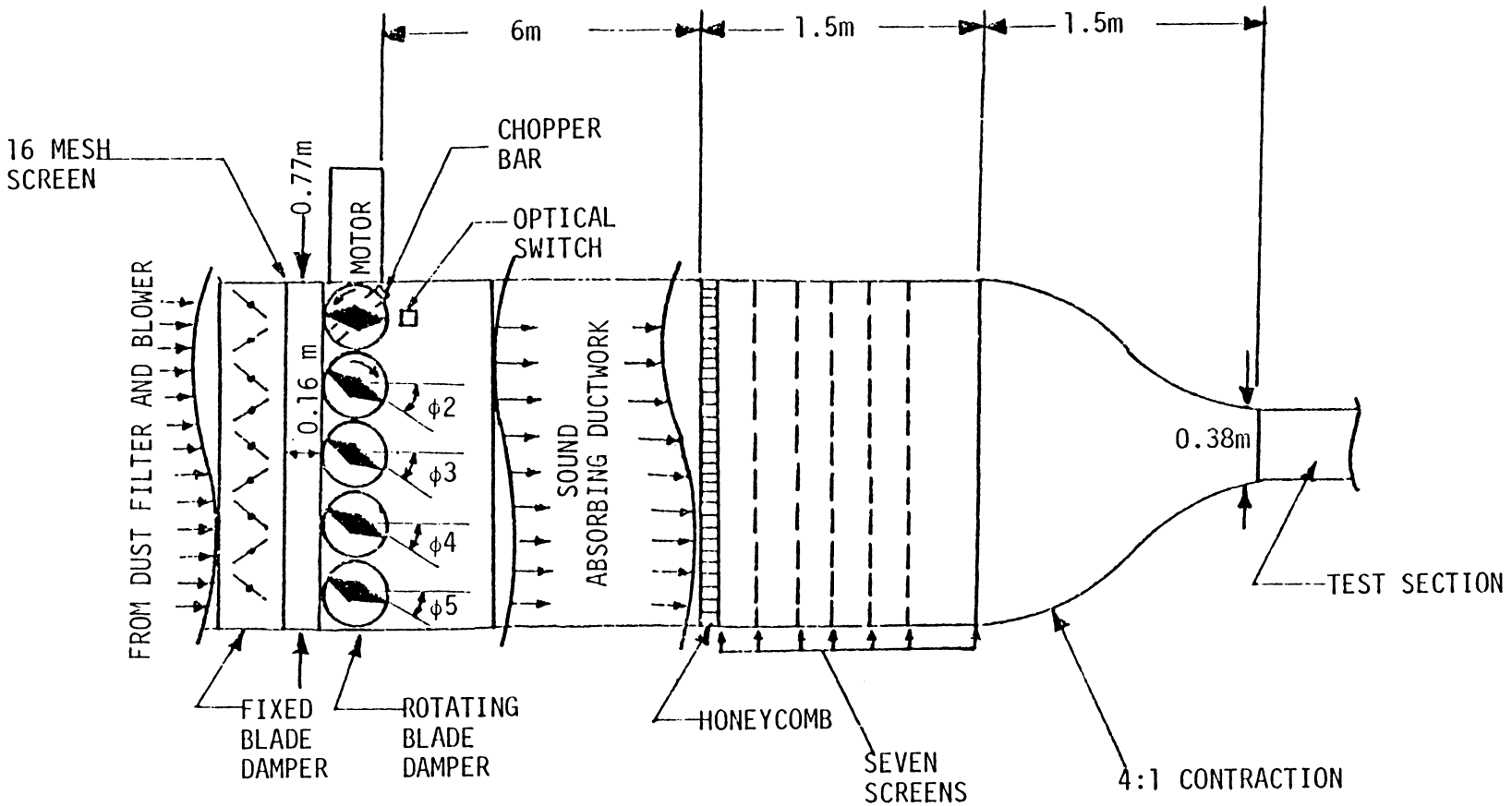

FIGURE 4: SCHEMATIC OF SMU TUNNEL. REFERENCE [16]

the desired waveform. The schematic diagram of the programmable variable angular velocity motor controller is shown in Figure 5. Figure 6 shows several waveforms generated at constant angular velocity with different rotation and orientation of the blades. In Table 1 the relative blade orientation, rotation, and setting are listed.

It is interesting to note how the velocity amplitude and waveform are influenced by the relative orientation of the blades. The velocity amplitude distributions, which are nearly sinusoidal, are obtained by setting the first four blades to zero degree orientation and the last one to 90 degree orientation, or setting the first two blades to zero degree orientation with 90 degree orientation for the remainding fixed nonrotating blades, or finally zero degree orientation for all the blades. As indicated in Table 1 the highest peak-to-peak amplitude was 93%.

The more reasonable velocity waveform is attained by setting the first four blades at zero degree orientation and the fifth blade at 45°. This orientation of the blades gives a 72 percent amplitude which is closest to sinusoidal than the other velocity waveforms shown in Figure 6. It is possible to obtain any intermediate value peak-to-peak velocity variation other than those configurations indicated in Figure 6 by setting the blades to different orientations.

Although this method of generating a periodic flow with a programmable damper was designed for variable angular velocity, the authors [16] do not present any results concerning the variable angular velocity. However, they do include the results obtained with constant angular velocity which are very helpful for the purpose of the present experiment.

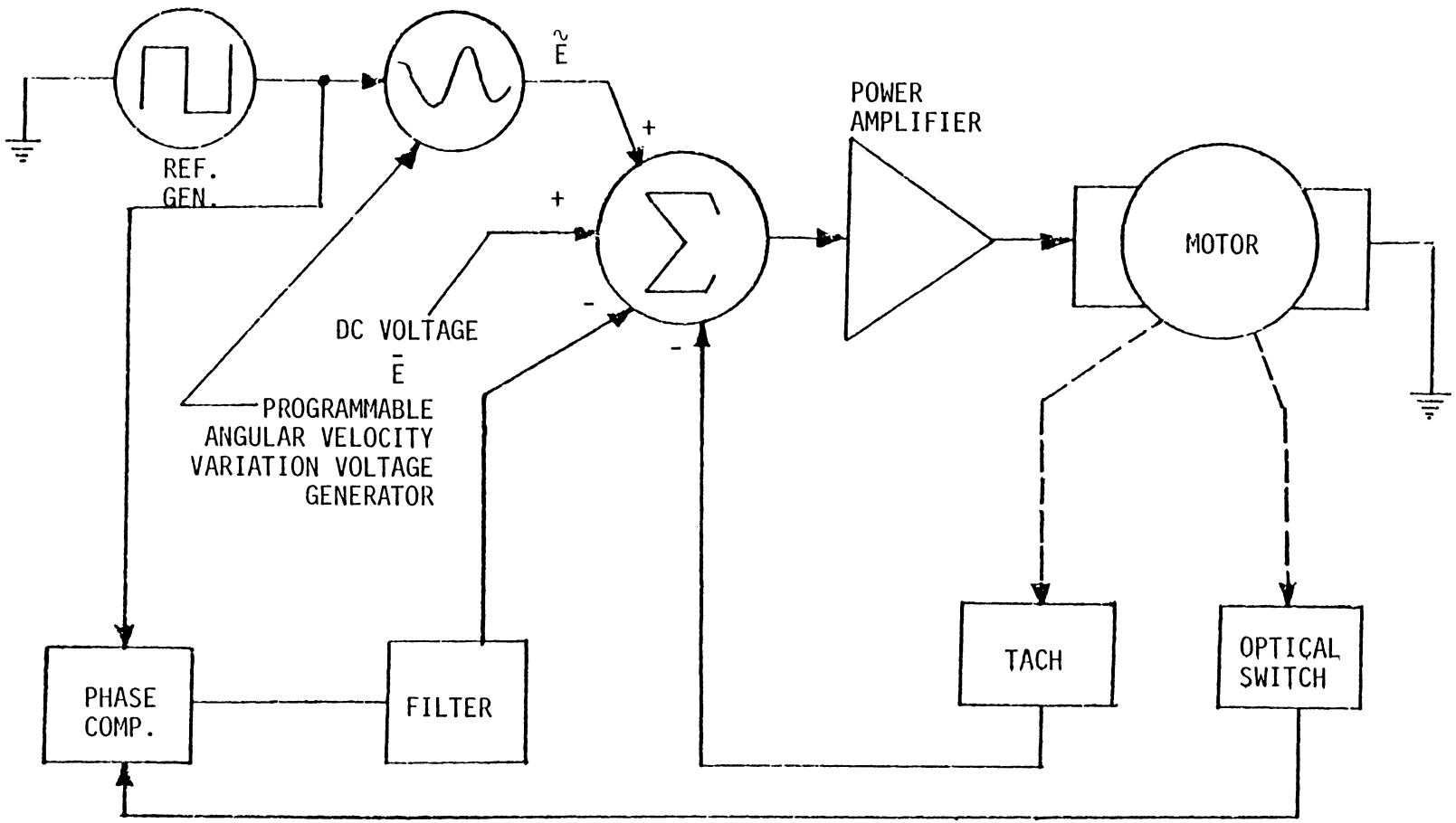

FIGURE 5: SCHEMATIC DIAGRAM OF PROGRAMMABLE VARIABLE ANGULAR VELOCITY MOTOR CONTROLLER. REFERENCE [16].

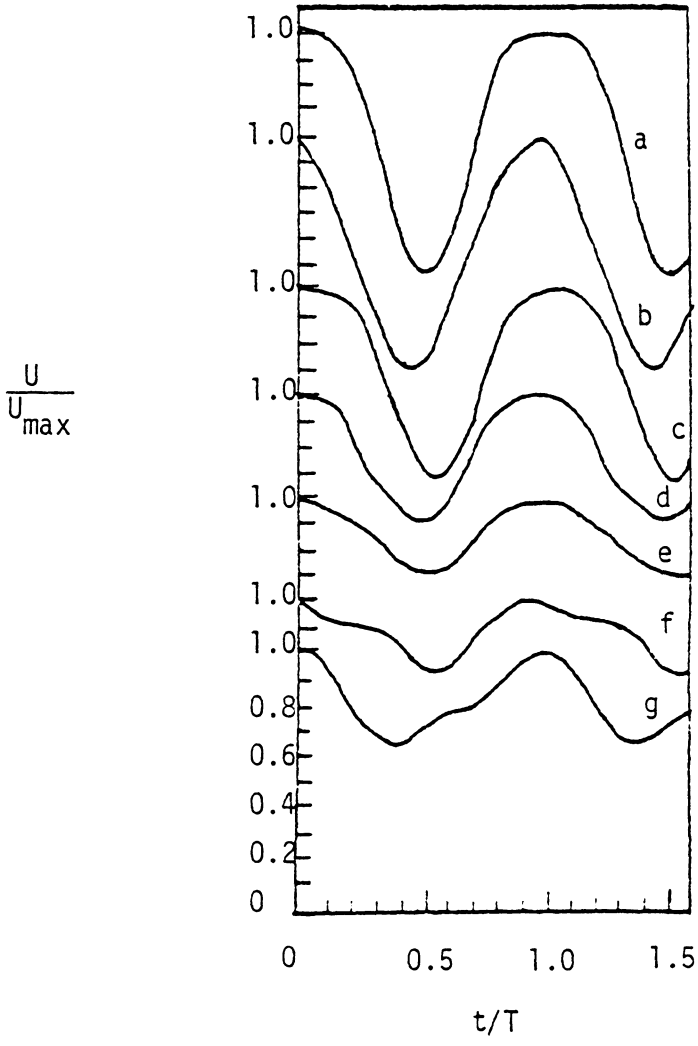

FIGURE 6: SEVERAL WAVEFORMS PRODUCED BY CONSTANT ANGULAR VELOCITY. REFERENCE [16].

TABLE 1. EFFECT OF RELATIVE ORIENTATION OF BLADES ON PEAK-TO-PEAK VELOCITY VARIATION AND WAVEFORM FOR CONSTANT ANGULAR VELOCITY ROTATION OF BLADES. UNDERLINED ANGLES DENOTE FIXED NONROTATING BLADES. REFERENCE [16].

Relative Blade Orientation When First Rotating Blade in Open Position.				$\frac{U_{max}-U_{min}}{U_{max}}$	Waveform shape
ϕ_2	ϕ_3	ϕ_4	ϕ_5		
0	0	0	0	0.93	Fig. 6 (a)
0	$\underline{\pi/2}$	$\underline{\pi/2}$	$\underline{\pi/2}$	0.93	Fig. 6 (b)
0	0	0	$\pi/4$	0.72	Fig. 6 (c)
0	0	0	$\pi/2$	0.49	Fig. 6 (d)
0	0	$\pi/4$	$\pi/4$	0.31	Fig. 6 (e)
0	0	$\pi/2$	$\pi/2$	0.31	Fig. 6 (f)
0	$\pi/3$	$\underline{\pi/2}$	$\underline{\pi/2}$	0.38	Fig. 6 (g)

3.4 Comparison of the Different Types of Pulsating Apparatus

The methods used to produce the flow oscillation were to a certain extent different for the type of application. The waveforms associated with these methods were produced over different frequency ranges.

The best pulsating apparatus for creating a nearly sinusoidal waveform is the programmable damper. This apparatus apparently can produce the desired type of waveform, but the frequency range at which it operates is too small (from 0 to 2 Hz).

The rotating shutter apparatus gives a wide range of oscillating frequency (from 0 to 50 Hz), but sacrifices control of the waveform. However, nearly sinusoidal velocity waveforms were obtained with constant angular velocity for the peak-to-peak velocity amplitudes of 48 percent. To obtain different waveforms the blades could be set to different orientations until the desired waveform of the velocity fluctuation was achieved.

Therefore, because the programmable system limits the frequency range, it does not appear to be advantageous over the constant angular velocity system unless very precise control of the waveform is desired. Consequently, the principle of the constant angular velocity (rotating shutters) is used in the present experiment.

4. WIND TUNNEL COMPONENTS

A wind tunnel consists of five components: blower, diffuser, settling chamber, contraction, and test section. They are explained below.

4.1 Centrifugal Blowers

Centrifugal blowers are normally used to drive open-circuit tunnels from the upstream end. Single-inlet blowers, however, can be installed in one of the corners to drive return-circuit tunnels. Single-inlet blowers produce a vortex-type flow (due to the asymmetric positioning of the impeller) which would aid wall flow attachment in the diffuser [2]. This compensates for the non-uniformity of the flow (which can be improved by placing screens in the settling chamber). Overall, single-inlet centrifugal blowers with backward-facing impellers are usually adequate for driving blower tunnels.

4.2 Screens

Wind tunnel screens are normally made of metal wires interwoven to form square or rectangular meshes. Screens make the flow velocity profiles more uniform by imposing a static pressure drop proportional to velocity squared and thus reduce the boundary layer thickness in the test section so that the ability to overcome a given pressure gradient is increased [2].

Screens that have very low open-area ratio ($\sim$0.3) generate an overshoot that is caused by streamline inclination close to the edge of boundary layer. Screens with low open-area ratio ($<$0.57) also produce

instabilities that result from coalition of jets to form longitudinal vortices which persist through the contraction. For an open-area ratio in the range of 0.57 - 0.7, it is better to have a smaller mesh (usually 16 x 18 mesh per inch) for the reduction of pre-existing turbulence [2].

4.3 Diffuser

The flow through a diffuser depends on its geometry defined by the inlet to exit area ratio, diffuser angle, wall contour, and diffuser cross-sectional shapes. Other parameters like the velocity profile, turbulence level, boundary layer control method, and the presence of separation could also affect the flow thus making it very difficult to predict. The separation in the diffuser can be avoided by boundary layer control. The general method of controlling the boundary layer is by installing gauze screens in the diffuser. A screen would not only remove the effects of boundary layer growth but also the early stage separation. The basic rule is to place screens where the diffuser wall angle changes suddenly, since these are the places where the flow is most likely to separate.

The diffuser included angle is usually between 6° to 8° for best flow steadiness. The area ratio should not exceed 2.5. It is important to have a reasonable degree of flow steadiness in the diffuser, otherwise, the pressure recovery tends to fluctuate with time and, therefore, the tunnel speed also fluctuates. Thus, depending on minimum number of screens required in the diffuser, maximum allowable overall pressure drop coefficient, the area ratio, and the diffuser angle, one can build a diffuser to operate successfully.

4.4 Honeycomb

Honeycombs are effective for removing swirl and lateral mean velocity variation, as long as the flow yaw angles are not greater than about 10°. Large yaw angles cause the honeycomb cells to stall which reduces their effectiveness besides increasing the pressure loss [2]. For maximum overall benefit the cell length should be about 6-8 times its diameter. The cell size should be smaller than the smallest lateral wavelength of the velocity variation (roughly 150 cells per settling chamber diameter).

4.5 Contractions

A contraction:

(i) Increases the mean velocity which allows the honeycomb and screens to be placed in a low speed region, thus reducing pressure losses [2].

(ii) Reduces both mean and fluctuating velocity variations to a smaller fraction of the average velocity [2].

The most important single parameter in determining these effects is c, the contraction ratio. By making the contraction very long, it is always possible to avoid separation in it. But this contributes to the tunnel length, cost, and exit boundary layer thickness. In a contraction whose cross-sectional aspect ratio changes along its length, the effect of boundary layer migration can be reduced by adding small 45° corner fillets to avoid separation.

The solution of the Laplace equation or the Stokes-Beltrami equation [2,18] is relatively easy for simple geometries for contraction design. The actual shape of the contraction contour is not as important as near the ends where the smoothness of contour form is much more critical than exact dimensions. Generally the end contours of the contraction are designed such that at least the first and second derivatives of the curve are zero or very small. Contraction ratios between about 6 and 9 are normally used at least for the smaller tunnels.

4.6 Working Section

Working section design is totally dependent on the requirements of the individual experimenter. Blower tunnels are more flexible in accepting a variety of working sections (with and without exit diffuser) [2]. The flow nonuniformities often fix the minimum length of the working section.

5. DESIGN OF THE WIND TUNNEL

The wind tunnel consists of five components: blower, diffuser, settling chamber, contraction, and test section. The design considerations for each part are explained below.

5.1 Selection of the Blower

A 4-hp blower is used to draw room air into the tunnel. The blower characteristic curve was not known prior to the assembly of the wind tunnel. From the measured mean velocity and diffuser pressure measurements, while calibrating the tunnel, a blower characteristic curve was estimated. This is shown in Figure 7. Since the power required to draw air was conservatively calculated to be 3 hp, this 4-hp centrifugal blower is suffucient for the experiment. The width and height of the discharge duct are 53.3 cm (21-in) and 63.2 cm(24 7/8 - in), respectively. The blower has a mean wheel diameter of 51 cm(20 - in) with 13 blades and operates at 1140 RPM.

5.2 Design of the Diffuser

The 66.0 cm(26-in) long diffuser is connected to the blower with a short rubber boot to reduce the transmission of vibration from the blower to the diffuser. The diffuser angles are designed for about 6 degrees on the side view and 8 degrees on the top view. The diffuser outlet and the settling chamber are 76 cm(30-in) in height and 71 cm (28-in) in width. The diffuser is made out of 1.9 cm(3/4-in) thick plywood with rectangular cross section. The area ratio of the diffuser is 1.6.

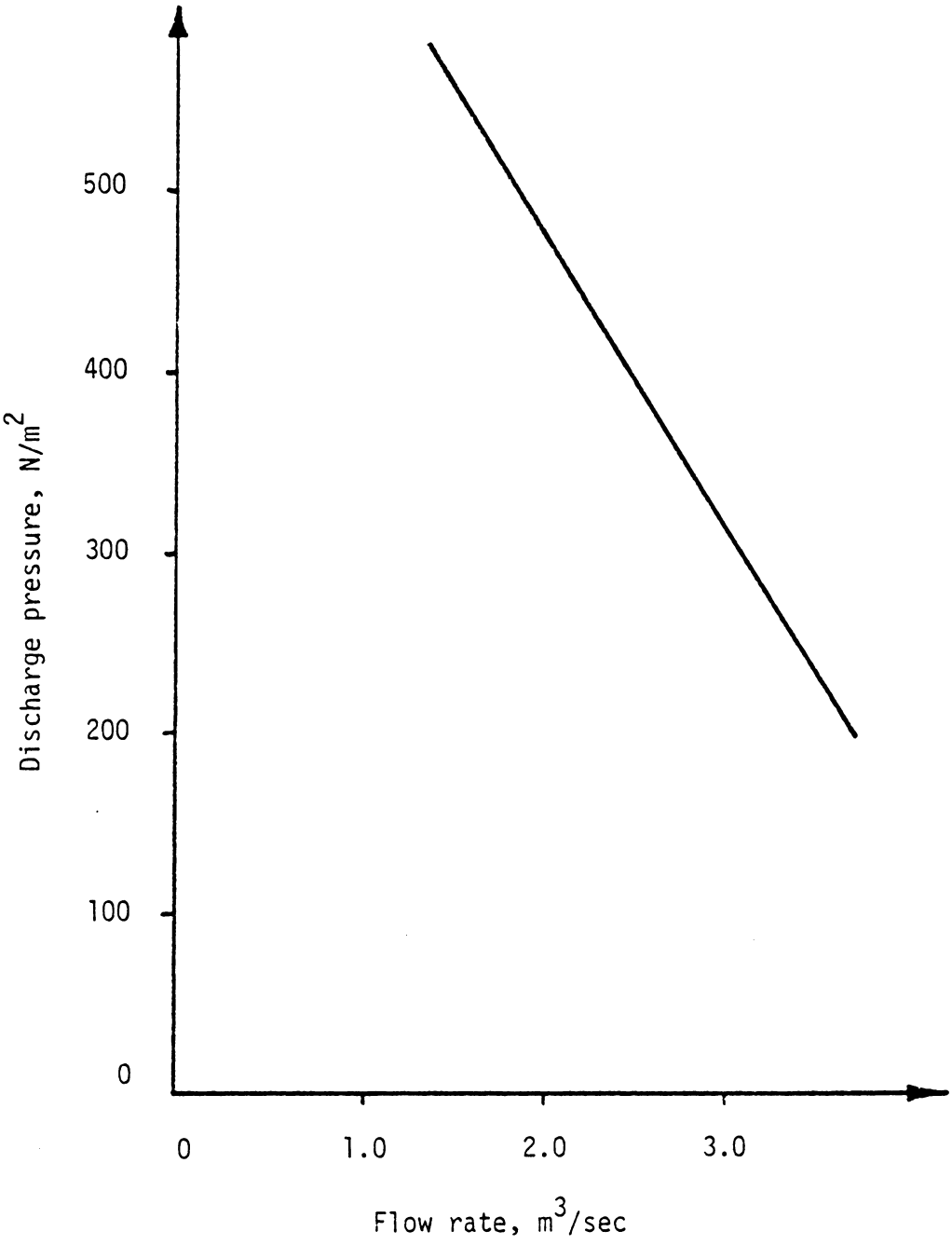

Figure 7: Characteristic curve of the blower

5.3 Design of the Settling Chamber

The settling chamber consists of the shutters box, honeycomb, and screens. The length of the settling chamber is 107 cm(42-in) with 25 cm(10-in) open space after the shutters box before the honeycomb. The 71 cm(28-in) x 76 cm(30-in) settling chamber is made out of 1.9 cm (3/4-in) thick plywood.

5.3-1 Honeycomb

The paper honeycomb used in this experiment has a cell size of 1.3 cm(1/2-in) with a thickness of 7.6 cm(3-in) in the streamwise direction. The honeycomb is placed 38 cm(15-in) from the entrance of the settling chamber.

5.3-2 Screens

As was learned from the literature review, it is important to use the right screen mesh and open area ratio for flow homogeneity. Five series of fiberglass screens of 18x16 mesh per inch are used with a 67.2 percent open area ratio. Each screen has a pressure drop coefficient of 0.99 (see page 29). The first screen is 8.9 cm(3 1/2-in) downstream of the honeycomb. The remaining screens are spaced alternatively 10 cm (4-in) and 8.9 cm(3 1/2 in) apart with 8.9 cm(3 1/2-in) space from the last one to the contraction inlet.

5.4 Contraction Design

The contraction is connected to the settling chamber outlet and is made out of 16-gauge galvanized steel. The contraction ratio is 6:1

with an inlet area of 71 cm x 76cm (28-in x 30-in) reducing to 25 cm x 36 cm(10-in x 14-in) within an 81 cm(32-in) length in the streamwise direction.

The contraction inlet and outlet are designed for zero slope on sides and tops in order to have flow uniformity at the inlet and outlet. The zero slope at the inlet takes 6 cm(2 3/8-in) of the contraction length and is the same for the outlet. The contraction contours are four circles each with different radius. The circles were then drawn in a 69 cm(27 1/4-in) length in order to obtain the best possible and smoothest contours. The side view of the contraction has the circles with 45 cm(17 13/16-in) and 61 cm(24 1/16-in) radii where the top view is designed of circles with 61 cm(24 1/8-in) and 79 cm(31 1/4-in) radii. The centers of the circles lie on the lines where the zero slope ends on top and side views.

To build the contraction, the side and top views were divided into sections of 2.5 cm(1-in) increment and then each section was projected down to find the length of the projected contour. The projected length of the side was 44 cm(17 3/8-in) and that of the top portion was 43 cm(16 3/4-in). The projected top and side views were attached by welding them down from the inlet to the outlet of the contraction. Tables 2 and 3 show the streamwise and vertical segments for drawing the projected contours of the side and top, respectively.

5.5 Test Section Design

The 124 cm(49-in) long test section is made out of 1 cm (3/8-in)

TABLE 2: THE PROJECTED INCREMENTS OF CONTRACTION SIDE VIEW CONTOUR

Increments of Projected Contour	
Streamwise direction, cm	Vertical direction, cm
6.0	12.7
11.4	12.8
16.4	13.4
21.7	14.6
27.0	16.1
32.4	18.1
37.9	20.8
43.6	24.0
49.3	28.3
55.0	31.6
60.6	34.3
65.9	36.2
71.1	37.5
77.2	37.9
79.8	38.1
85.8	38.1

TABLE 3: THE PROJECTED INCREMENTS OF CONTRACTION TOP VIEW CONTOUR

Increments of Projected Contour	
Streamwise direction, cm	Vertical direction cm
6.0	17.8
11.0	17.9
16.1	18.4
21.7	19.2
27.1	20.3
32.2	21.9
38.7	23.8
44.6	26.0
51.3	28.6
57.5	31.0
63.3	33.0
68.9	34.3
74.1	35.1
79.5	35.6
82.6	35.6
87.9	35.6

thick plexiglas which is connected to the contraction outlet. The cross-sectional area of the test section is a 25 cm x 36 cm (10-in x 14-in) rectangle. A rubber gasket is placed between the contraction and test section joint to avoid any air leakage.

5.6 Determination of the Tunnel Power Factor

After estimating the size and configuration of the wind tunnel, the next design step is to determine the tunnel power factor, λ (equal to $H/(1/2\ \rho_o V^3_o A_o)$, where H is the shaft input power and subscript o denotes the working section conditions) [2]. Once the tunnel power factor is obtained, the fan size and drive unit can be selected. It is not essential to accurately estimate the power factor, however, adequate extra power can be installed to cope with a variety of model or test section configurations which are not known in advance.

The major pressure losses in a wind tunnel are due to resistive components such as screens, honeycomb, and friction on the tunnel walls. To calculate the total pressure loss due to each component, it is possible to estimate each loss separately, and then divide the sum by the blower efficiency η, typically between 0.75 to 0.8, to give the tunnel power factor. The typical calculations of pressure losses for the designed wind tunnel shown in Figure 8 are given below.

(i) Losses due to skin friction:

$$\eta\ \Delta\lambda_1 = \frac{\Delta P}{\frac{1}{2}\rho_o V_o^2} = \left(\frac{A_o}{A}\right)^2 \int C_f \frac{S}{A}\, dx$$

where S is the duct local perimeter and knowing that the area ratio is

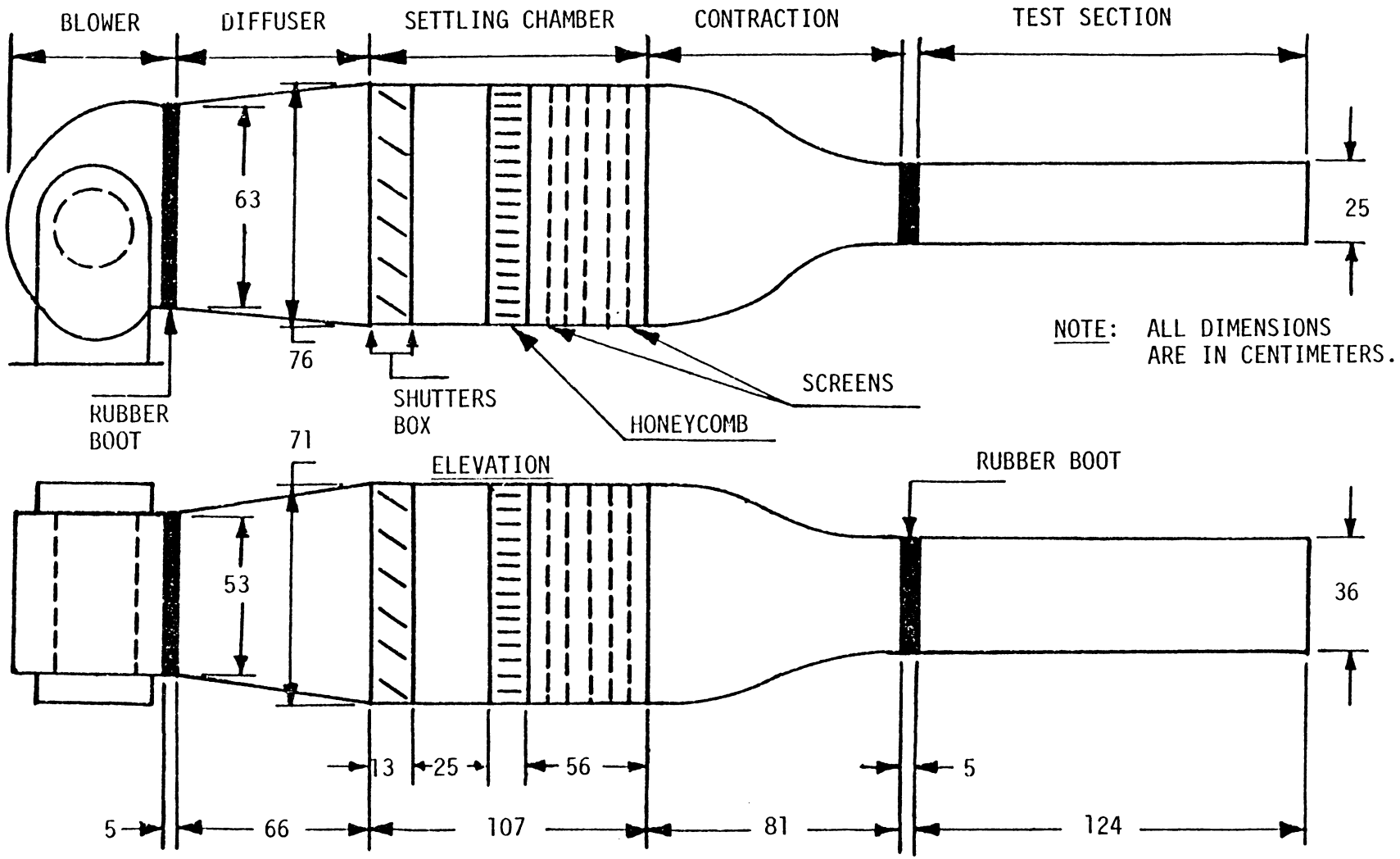

FIGURE 8: THE PULSATING FLOW WIND TUNNEL

the reciprocal of the velocity ratio. It is usually necessary only to estimate skin friction losses in the test section where $A_o/A = 1.0$. The skin friction losses in other components do not contribute significantly but, those in the diffuser are accounted for in the efficiency.

Therefore, $\eta\Delta\lambda_1 \tilde{=} C_f \frac{SL}{A}$ [2], where L is the test section length. Assuming $C_f = 0.003$ [2], the power factor in the test section is

$$\eta\Delta\lambda_1 = 0.003 \frac{2\ (35\ cm + 25\ cm)(124\ cm)}{35\ cm \times 25\ cm}$$

$$= 0.0504$$

(ii) Losses due to screens and honeycomb:

These losses are calculated from the equation given below:

$$\eta\Delta\lambda_2 = K \left[\frac{A_o}{A}\right]^2$$

For this tunnel with five screens (all in the settling chamber) with K = 0.99, a honeycomb with K = 0.5, and a contraction ratio of 6,

$$\eta\Delta\lambda_2 = 0.5 \left[\frac{1}{6}\right]^2 + 5 \times 0.99 \left[\frac{1}{6}\right]^2$$

$$\eta\Delta\lambda_2 = 0.151$$

The pressure drop coefficient through the screens is calculated from the equation given below [2]:

$$K_s = 6.5 \left(\frac{1-\beta}{\beta^2}\right)\left(\frac{V_3 d}{\beta\nu}\right)^{-\frac{1}{3}}$$

$$K_s = 6.5 \left[\frac{1-0.672}{(0.672)^2}\right] \left[\frac{(4.17\ \frac{m}{sec})(0.011\ in \times 0.0254\ \frac{m}{in})}{(0.672)(1.6\times10^{-5})\ \frac{m^2}{sec}}\right]^{-\frac{1}{3}}$$

$$K_s = 0.99$$

(iii) Loss of total head at the exit of an open-circuit tunnel.

In an open-circuit tunnel, the amount of kinetic energy lost at the exit and dissipated into heat adds to the total losses.

$$\eta\Delta\lambda_3 = \left(\frac{A_o}{A_{out}}\right)^2$$

But, since there is no exit diffuser, this value would be 1 for this blower tunnel. Therefore, the estimated overall tunnel power factor is,

$$\lambda = \sum_{n=1}^{3} \Delta\lambda_n/\eta \cong \frac{0.0504 + 0.151 + 1}{0.75}$$

$$\lambda = 1.59$$

for the tunnel considered in our present experiment.

Now the fan static pressure must be determined in order to select the optimum fan size. Here the dynamic pressure rise through the blower is so small that it is usually neglected and can be considered as a factor of safety in the calculation.

The average velocity in the test section of the tunnel was selected to be 25 m/sec (82 ft/sec) without the shutters in the upstream of the settling chamber. The average velocity in the test section with shutters was selected to be 12.5 m/sec (41 ft/sec) so that a 50 percent velocity reduction is achieved in the test section (theoretically).

The velocities at each section of the tunnel (i.e., Figure 9) must be known in order to calculate the pressure drops at these sections. For this reason the continuity equation is used to obtain the unknown velocities at each section since the area of each section is known. It should be noted that the calculated pressure drops are doubled as a safety factor to account for the unknown pressure losses in each section.

5.7 Calculation of Velocity and Pressure Drop at Each Section of the Tunnel Without the Shutters (See Figure 9)

5.7-1 Pressure Drop in Test Section

The velocity at 1 is the same as that of 2 since the areas at these sections are identical. Thus, the pressure drop in the test section is determined to be

$$\Delta P_{T.S.} = [(\eta \Delta \lambda_1)(\frac{1}{2} \rho_o V_2^2] \; 2$$

$$\Delta P_{T.S.} = [(0.0504)(\frac{1}{2})(1.19065 \frac{kg}{m^3})(25 \frac{m}{sec})^2] \; 2$$

$$\Delta P_{T.S.} = 37.5 \text{ Pa}$$

5.7-2 Pressure Drop in Contraction

Using the continuity equation at sections 2 and 3, the velocity at section 3 is found to be

$$V_3 A_3 = V_2 A_2$$

$$V_3 = V_2(\frac{A_2}{A_3})$$

$$V_3 = (25 \frac{m}{sec})(\frac{1}{6})$$

$$V_3 = 4.17 \text{ m/sec}$$

Therefore, the pressure drop in the 81 cm (32-in.) long contraction is

$$\Delta P_c = [\frac{1}{2} \rho_o V_2^2 K_c] \; 2$$

$$\Delta P_c = [\frac{1}{2} (1.19065 \frac{kg}{m^3})(25 \frac{m}{sec})^2 (0.29)] \; 2$$

$$\Delta P_c = 216 \text{ Pa}$$

where K_c is the pressure drop coefficient in the contraction.

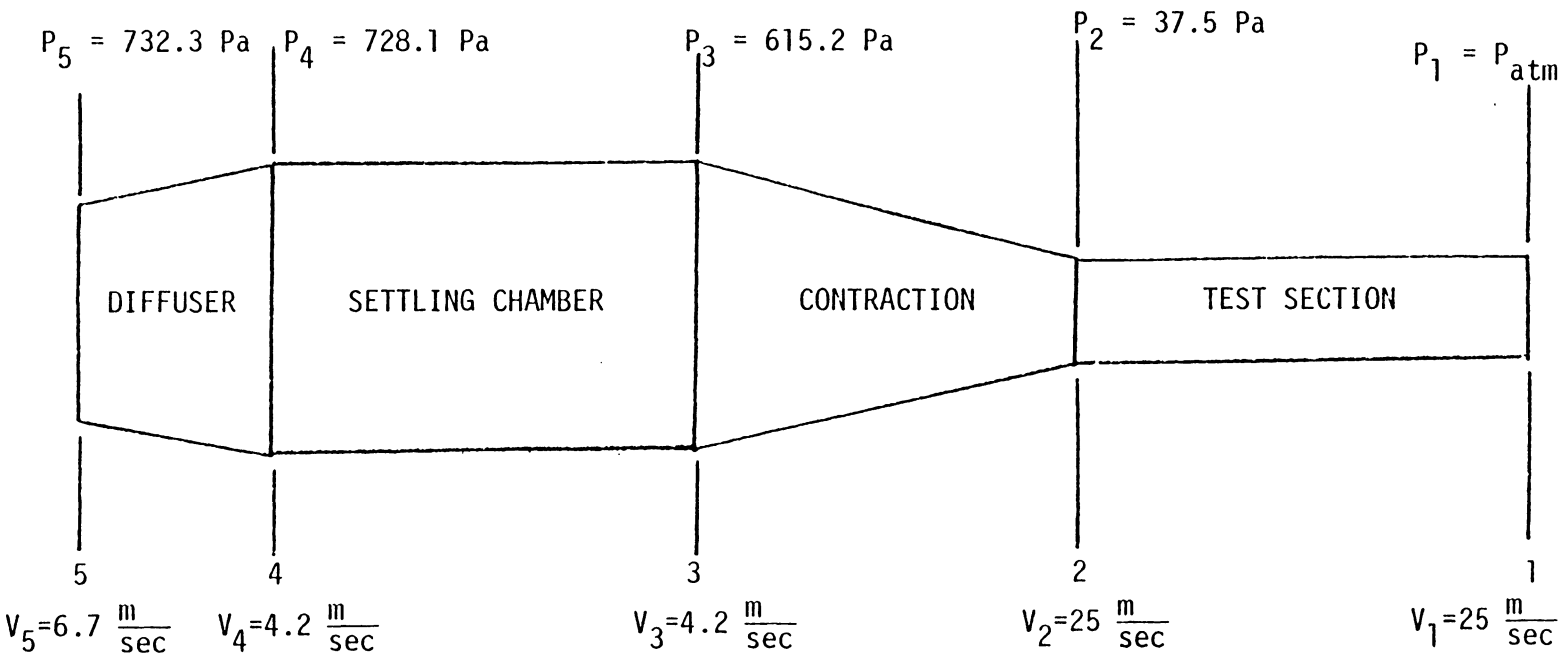

FIGURE 9: DISTRIBUTION OF VELOCITY AND PRESSURE AT EACH SECTION OF THE WIND TUNNEL WITHOUT PULSATING APPARATUS

5.7-3 Settling Chamber Pressure Drop

There are two pressure drops in the settling chamber. One is through five screens and the other through the honeycomb. Therefore, the pressure drop through the screens is

$$\Delta P_s = [\tfrac{1}{2} \rho_o V_3^2 K_s S] \; 2$$

where S and K_s are the number of screens and pressure drop coefficient through the screens, respectively.

$$\Delta P_s = [\tfrac{1}{2} (1.19065 \tfrac{kg}{m^3})(4.17 \tfrac{m}{sec})^2 (0.99)(5)] \; 2$$

$$\Delta P_s = 102.5 \text{ Pa}$$

Now the pressure drop in the honeycomb is calculated

$$\Delta P_{h.c.} = [\tfrac{1}{2} \rho_o V_3^2 K_{h.c.}] \; 2$$

where $K_{h.c.}$ is the pressure drop coefficient through the honeycomb.

$$\Delta P = [\tfrac{1}{2} (1.19065 \tfrac{kg}{m^3})(4.17 \tfrac{m}{sec})^2 (0.5)] \; 2$$

$$\Delta P = 10.4 \text{ Pa}$$

5.7-4 Pressure Drop in Diffuser

The area ratio of the diffuser is made to be 1.6 where the diffuser angles are about 6^o on the side view and about 8^o on the top view. So, the pressure drop in the diffuser is calculated after finding the diffuser inlet velocity.

$$V_4 A_4 = V_5 A_5$$

$$V_5 = V_3(\tfrac{A_4}{A_5}) \qquad \text{(where } V_4 = V_3\text{)}$$

$$V_5 = (4.17 \tfrac{m}{sec})(1.6)$$

$$V_5 = 6.67 \frac{m}{sec}$$

The pressure drop is then obtained using

$$\Delta P_D = [\frac{1}{2} \rho_o V_5^2 K_D] \; 2$$

where K_D is the diffuser pressure drop coefficient.

$$\Delta P_D = [\frac{1}{2} (1.19065 \frac{kg}{m^3})(6.67 \frac{m}{sec})^2 (0.384)] \; 2$$

$$\Delta P_D = 20.3 \text{ Pa}$$

The energy equation, between the two sections of each component, is now applied to obtain the pressure at each section of the tunnel, as numbered, since the pressure drop through each component is known.

Apply energy equation at 1 and 2 for the test section.

$$P_2 + \frac{1}{2} \rho_o V_2^2 = P_1 + \frac{1}{2} \rho_o V_1^2 + \Delta P_{T.S.}$$

But, V_1 is equal to V_2 and P_1 is the atmospheric pressure. Therefore,

$$P_2 = \Delta P_{T.S.}$$

$$P_2 = 37.5 \text{ Pa}$$

The same procedure leads to determination of contraction inlet pressure.

$$P_3 + \frac{1}{2} \rho_o V_3^2 = P_2 + \frac{1}{2} \rho_o V_2^2 + \Delta P_c$$

$$P_3 = 37.5 \frac{N}{m^2} + \frac{1}{2} (1.19065 \frac{kg}{m^3})[(25 \frac{m}{sec})^2 - (4.17 \frac{m}{sec})^2] + 216 \frac{N}{m^2}$$

$$P_3 = 615.2 \text{ Pa}$$

Since the exit and inlet velocities in the settling chamber are the same, the pressure at section 4 is obtained by summing the pressure at section 3 with the pressure drops through screens and honeycomb in the settling chamber.

$$P_4 = P_3 + \Delta P_{h.c.} + \Delta P_s$$

$$P_4 = 615.2 \frac{N}{m^2} + 10.4 \frac{N}{m^2} + 102.5 \frac{N}{m^2}$$

$$P_4 = 728.1 \text{ Pa}$$

The inlet pressure to the diffuser is determined by applying the energy equation at sections 4 and 5.

$$P_5 + \frac{1}{2} \rho_o V_5^2 = P_4 + \frac{1}{2} \rho_o V_4^2 + \Delta P_D$$

$$P_5 = 728.1 \frac{N}{m^2} + \frac{1}{2}(1.19065 \frac{kg}{m^3})[4.17 \frac{m}{sec})^2 - (6.67 \frac{m}{sec})^2] + 20.3 \frac{N}{m^2}$$

$$P_5 = 732.3 \text{ Pa}$$

Now the required fan power is obtained by

$$\text{Power} = F.\bar{V} = (P_{05}A)\bar{V}$$

where P_{05} is the total pressure (static and dynamic) at section 5, A is the test section cross-section area, and $\bar{V}$ is the velocity in the test section.

$$P_{05} = P_5 + \frac{1}{2} \rho_o V_5^2$$

$$P_{05} = 732.3 \frac{N}{m^2} + \frac{1}{2}(1.19065 \frac{kg}{m^3}) (6.67 \frac{m}{sec})^2$$

$$P_{05} = 758.8 \text{ Pa}$$

$$\text{Power} = (758.8 \frac{N}{m^2})[10 \text{ in} \times 14 \text{ in} \times (2.54 \frac{cm}{in})^2 (\frac{m^2}{10000 \text{ cm}^2})](25 \frac{m}{sec})$$

$$\text{Power} = 1713.4 \frac{N \cdot m}{sec} (\frac{J}{sec})$$

$$\text{Power} = 1713.4 \text{ W} = 1.7134 \text{ kw}$$

Thus, the horsepower of the fan required to draw air into the tunnel with a 75% efficiency is

$$HP = \frac{(1.7134 \text{ kw})(1.341 \frac{HP}{kw}}{0.75}$$

$$HP = 3.07$$

Consequently, the existing 4 hp fan meets the requirements for this tunnel.

5.8 Procedure to Determine the Shutters Spacing

The spacing between the shutters is an important factor in producing the oscillatory flow amplitude in the tunnel. In order to determine the shutter spacing, one has to know the pressure distribution on both sides of the shutters. Again, the continuity and energy equations are used to find the velocities and, hence, pressures at each section of the tunnel with the shutters box shown in Figure 10.

The calculations are given for a velocity in the test section of 12 $\frac{m}{sec}$ when the shutters are placed in the upstream of the settling chamber. Therefore, the pressure losses in the components of the tunnel would be different than those when the shutters are not placed. The same procedure is used as before starting from the test section.

$$\Delta P_{T.S.} = 2\left[\frac{L}{2} \rho_o V_1^2 K_s\right]$$

$$\Delta P_{T.S.} = 2\left[(\frac{1}{2})(1.19065 \frac{kg}{m^3})(12 \frac{m}{sec})^2(0.0504)\right]$$

$$\Delta P_{T.S.} = 8.64 \text{ Pa}$$

Applying the energy equation between sections 1 and 2, would result in the pressure at section 2 since the pressure at 1 is atmospheric.

$$P_2 + \frac{1}{2} \rho_o V_2^2 = P_1 + \frac{1}{2} \rho_o V_1^2 + \Delta P_{T.S.}$$

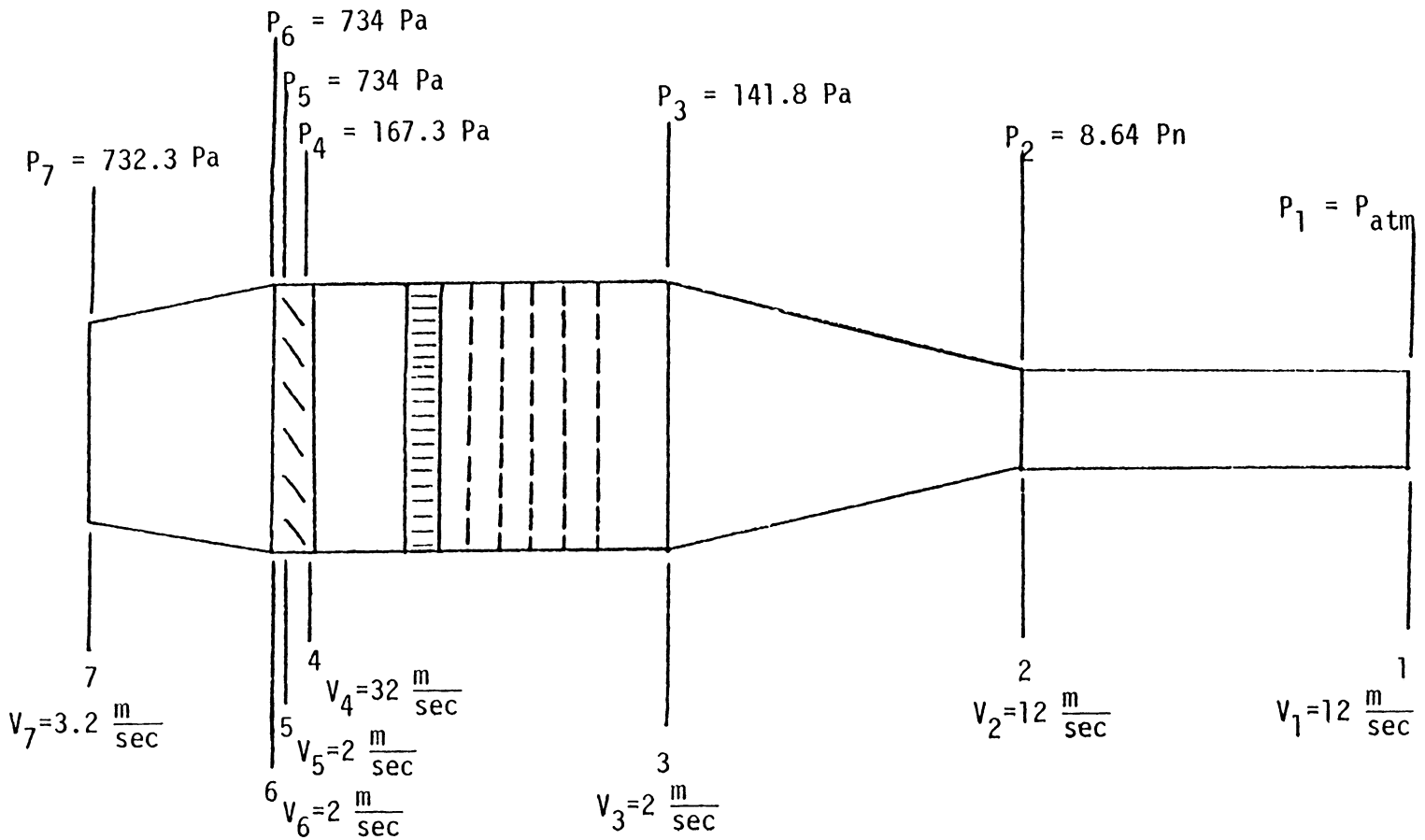

FIGURE 10: DISTRIBUTION OF VELOCITY AND PRESSURE MAGNITUDES AT EACH SECTION OF THE WIND TUNNEL WITH PULSATING APPARATUS

$$P_2 = \Delta P_{T.S.}$$

$$P_2 = 8.64 \text{ Pa}$$

Noting that V_1 and V_2 are the same.

The pressure loss in the contraction is calculated as follows:

$$V_3 = V_2\left(\frac{A_2}{A_3}\right)$$

$$V_3 = \left(12 \frac{m}{sec}\right)\left(\frac{1}{6}\right)$$

$$V_3 = 2 \frac{m}{sec}$$

Therefore;

$$\Delta P_c = 2 \left[\frac{1}{2} \rho_o V_2^2 K_c\right]$$

$$\Delta P_c = 2 \left[\frac{1}{2}\left(1.19065 \frac{kg}{m^3}\right)\left(12 \frac{m}{sec}\right)^2(0.29)\right]$$

$$\Delta P_c = 49.8 \text{ Pa}$$

and the inlet pressure to the contraction is

$$P_3 + \frac{1}{2} \rho_o V_3^2 = P_2 + \frac{1}{2} \rho_o V_2^2 + \Delta P_c$$

$$P_3 = 8.64 \frac{N}{m^2} + \frac{1}{2}\left(1.19065 \frac{kg}{m^3}\right)\left[\left(12 \frac{m}{sec}\right)^2 - \left(2 \frac{m}{sec}\right)^2\right] + 49.8 \frac{N}{m^2}$$

$$P_3 = 141.8 \text{ Pa}$$

Accordingly, the pressure at state 4 is obtained by summing the pressure drop through the honeycomb and screens with the exit pressure in the settling chamber.

$$P_4 = P_3 + \Delta P_{h.c.} + \Delta P_s$$

but

$$\Delta P_{h.c.} = 2 \left[\frac{1}{2} \rho_o V_3^2 K_{h.c.}\right]$$

and

$$\Delta P_s = 2\ [\tfrac{1}{2}\ \rho_o V_3^2\ K_s\ S]$$

where $K_{h.c.}$, K_s, and S are the pressure coefficients through honeycomb, the pressure coefficient through screens, and the number of screens, respectively. Therefore;

$$\Delta P_{h.c.} = 2\ [\tfrac{1}{2}\ (1.19065\ \tfrac{kg}{m^3})(2\ \tfrac{m}{sec})^2(0.5)]$$

$$\Delta P_{h.c.} = 1.9\ Pa$$

and

$$\Delta P_s = 2\ [\tfrac{1}{2}\ (1.19065\ \tfrac{kg}{m^3})(2\ \tfrac{m}{sec})^2(0.99)(5)]$$

$$\Delta P_s = 23.6\ Pa$$

so

$$P_4 = 141.8\ \tfrac{N}{m^2} + 1.9\ \tfrac{N}{m^2} + 23.6\ \tfrac{N}{m^2}$$

$$P_4 = 167.3\ Pa$$

The diffuser inlet pressure is obtained by summing the static and dynamic pressures of the fan as follows:

$$P_{o7} = P_7 + \tfrac{1}{2}\ \rho_o V_7^2$$

where V_7 is determined by the continuity equation applied between sections 2 and 7.

$$V_7 A_7 = V_2 A_2$$

$$V_7 = V_2(\frac{A_2}{A_7})$$

$$V_7 = 12\ \tfrac{m}{sec}(\frac{35cm\ x\ 25cm}{53cm\ x\ 63cm})$$

$$V_7 = 3.2 \frac{m}{sec}$$

Thus;

$$P_{o7} = 732.3 \frac{N}{m^2} + \frac{1}{2} (1.19065 \frac{kg}{m^3})(3.2 \frac{m}{sec})^2$$

$$P_{o7} = 738.4 \text{ Pa}$$

Using the same procedure as before, the diffuser exit pressure is determined assuming that P_7 is the same as P_5 in the previous section.

$$V_6 A_6 = V_7 A_7$$

$$V_6 = V_7 (\frac{A_7}{A_6})$$

$$V_6 = (3.2 \frac{m}{sec})(\frac{53cm \times 63cm}{76cm \times 71cm})$$

$$V_6 = 1.99 \frac{m}{sec}$$

The pressure loss in the diffuser is then

$$\Delta P_D = 2 [\frac{1}{2} \rho_o V_6^2 K_D]$$

$$\Delta P_D = 2 [\frac{1}{2} (1.19065 \frac{kg}{m^3})(1.99 \frac{m}{sec})^2 (0.384)]$$

$$\Delta P_D = 1.81 \text{ Pa}$$

and

$$P_{o7} = P_7 + \frac{1}{2} \rho_o V_7^2 = P_6 + \frac{1}{2} \rho_o V_6^2 + \Delta P_D$$

$$P_6 = 732.3 \frac{N}{m^2} + \frac{1}{2} (1.19065 \frac{kg}{m^3})[(3.2 \frac{m}{sec})^2 - (1.99 \frac{m}{sec})^2] - 1.81 \frac{N}{m^2}$$

$$P_6 = 734 \text{ Pa}$$

Applying the Bernoulli Equation between sections 4 and 5, the velocity through the shutter spacing is determined.

$$P_5 + \frac{1}{2} \rho_o V_5^2 = P_4 + \frac{1}{2} \rho_o V_4^2$$

$$V_4 = \left[\frac{2(P_5 - P_4)}{P_o} + V_5^2\right]^{\frac{1}{2}}$$

$$V_4 = \left[\frac{2(734\ \frac{N}{m^2} - 167.3\ \frac{N}{m^2})}{1.19065\ \frac{kg}{m^3}}\ (\frac{kg \cdot m}{sec^2 N}) + (1.99\ \frac{m}{sec})^2\right]^{\frac{1}{2}}$$

$$V_4 = 32\ \frac{m}{sec}$$

It is now possible to obtain the shutters area and spacing between shutters using the continuity equation between sections 2 and 4.

$$V_2 A_2 = V_4 A_4$$

$$V_2 A_2 = V_5 A_s C_d$$

where C_d is, the discharge coefficient associated for the flow between the shutters, taken to be 0.80. Therefore,

$$A_s = (12\ \frac{m}{sec})(25.4 \times 36\ cm^2)/(32\ \frac{m}{sec})(0.80)$$

$$A_s = 420\ cm^2\ (65\text{-}in^2)$$

but

$$A_s = (5S)(W)$$

where S is the spacing and W is the width of the settling chamber.

$$S = \frac{420\ cm^2}{5(71)\ cm}$$

$$S = 1.18\ cm\ (0.464\text{-}in)$$

It must be mentioned that the actual diffuser inlet pressure was measured to be about 436 Pa. This is much lower than the assumed pressure of 732.3 Pa at the blower discharge. The calculated blower

discharge pressure would be 539 Pa if the pressure losses in the wind tunnel components were not doubled. This calculated pressure is higher than 436 Pa. Therefore, the blower discharge pressure of 732.3 Pa was overestimated and doubling the pressure loss was not needed.

5.9 Design of the Shutters Box

The shutters box consisted of six rotating blades with 1.18 cm (0.464-in) spacing between each shutter. The spacing between the upper shutter and the wind tunnel ceiling is 0.59 cm (0.232-in) and between the lower shutter and the wind tunnel floor is 0.59 cm (0.232-in) also. The shutters' length is about 70 cm (27.75-in) where only 0.64 cm ($\frac{1}{4}$ -in) spacing is allowed between the sides of the tunnel and the shutters. The maximum thickness of the diamond-shaped cross section of the shutters is 1.63 cm (0.64-in). The shutters box is made from 1.27 cm ($\frac{1}{2}$ -in) plywood while the shutters themselves are made out of 16-gauge galvanized steel which was smoothened with body putty, sanded and painted. The schematic of a shutter is shown in Figure 11.

The shutters box is 13 cm (5-in) long and can be removed any time for repair or changes. Knowing the spacing between the shutters, the height of the shutters can be calculated as follows:

$$\begin{bmatrix}\text{Height of the} \\ \text{settling chamber}\end{bmatrix} = 6 \begin{bmatrix}\text{Height of} \\ \text{shutters}\end{bmatrix} + 5 \begin{bmatrix}\text{Spacing between} \\ \text{shutters}\end{bmatrix} + 2 \begin{bmatrix}\text{Spacing between the tunnel} \\ \text{floor and lower shutter}\end{bmatrix}$$

$$h = 6\, h_s + 5S + 2\, S_t$$

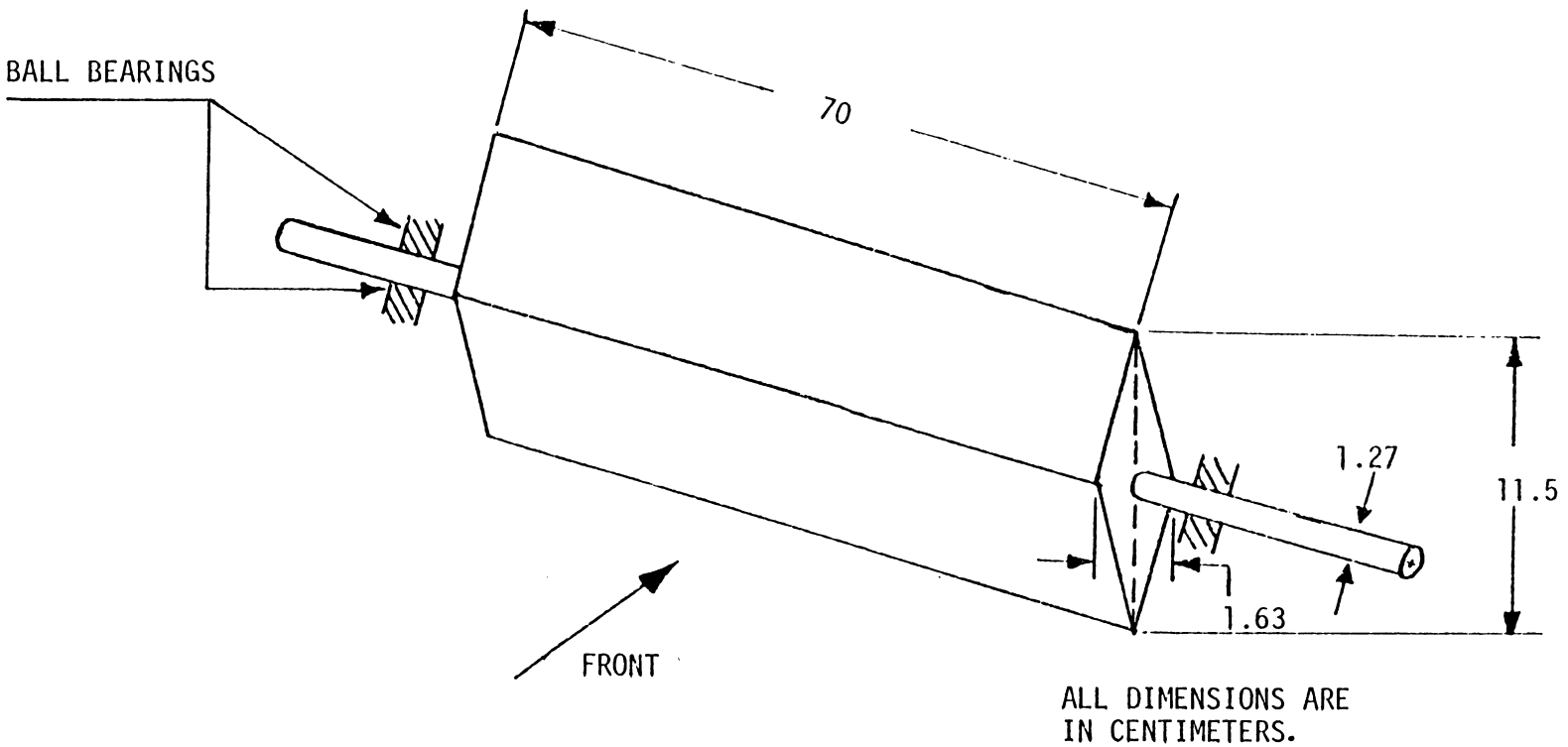

FIGURE 11: SCHEMATIC OF A SHUTTER DESIGN

where 6 corresponds to six shutters, 5 corresponds to five spacing between the shutters, and 2 corresponds to two spacing between the tunnel ceiling (or tunnel floor) and upper shutter (or lower shutter). Therefore

$$76 \text{ cm} = 6\ h_s + 5(1.18 \text{ cm}) + 2\ (0.59 \text{ cm})$$

$$h_s = 11.5 \text{ cm } (4.53\text{-in})$$

The schematic of the shutters box is shown in Figure 12.

5.10 Drive Unit of the Shutters

The shutters are mounted on parallel steel shafts that are supported by ball bearings on the outside housing of the tunnel. The diameter of the shaft is 1.27 cm ($\frac{1}{2}$ - in). The shutter rotation is provided by a set of timing pulleys that are driven by a 2 hp/AC motor. It was decided to rotate the top three shutters in clockwise sense and the rest in the opposite sense. The senses can be switched by simply changing the windings in the motor. The 13-teeth timing pulleys to drive the device have a 1 cm ($\frac{3}{8}$-in) pitch with a pitch diameter of 4 cm (1.552-in). The 2.5 cm (1-in) wide timing belts have 40-teeth with a length of 38 cm (15-in).

The relative speed ratio of the shutters is 1.00 and the rotation is provided by a set of timing pulleys with a speed ratio of 1.9 connected to the motor shaft and shutter No. 4. To generate various speeds of the shutters, a 3 hp mechanical variable speed motor is used with the same timing pulleys of 1.9 speed ratio. The variable speed motor has an angular velocity range of 213 to 1200 RPM.

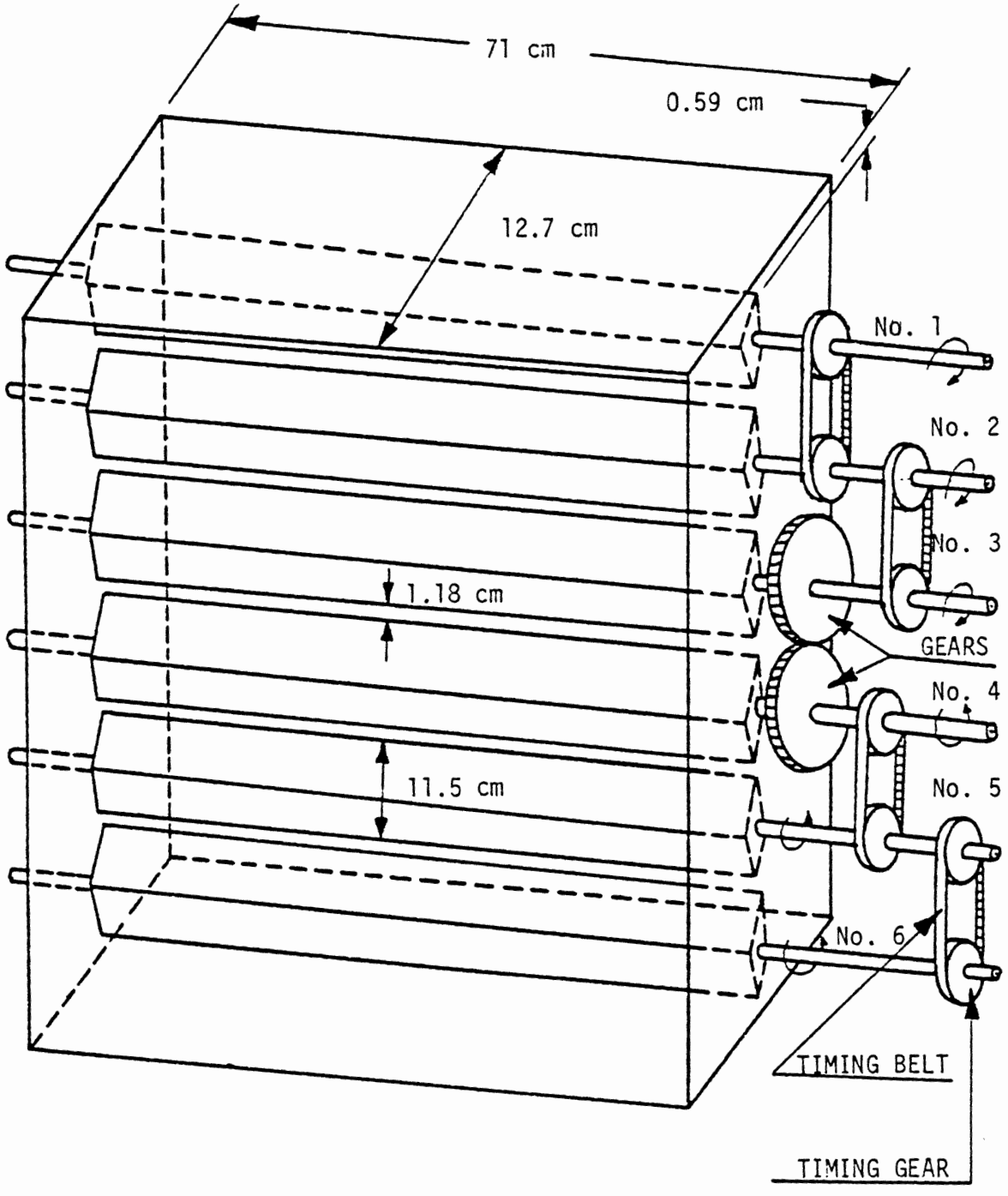

FIGURE 12: SCHEMATIC OF THE SHUTTERS BOX

6. EXPERIMENTAL INVESTIGATION

6.1 Instruments

To measure the mean velocities in the streamwise direction in the air flow a hot-wire anemometer was used. The hot-wire was operated by a Disa Constant Temperature Anemometer type 55D01. The output of the Anemometer was connected to a Disa Linearizer type 55D10. The output of the hot-wire was read on an Autoranging Digital Voltmeter type 2427 (Brüel & Kjaer Copenhagen).

The Linearizer output was also connected to a Hewlett Packard Digital Signal Analyzer type 5420A through a Tektronix AM502 Differential Amplifier Filter and a Hewlett Packard Analog/Digital Converter type 54410A to obtain the flow waveforms at different shutters settings and frequencies. A reluctance transducer model 3045A was mounted on the shaft of the shutters No. 4 to measure the shutter frequency, and to provide a trigger to the Digital Signal Analyzer. The flow frequency was then read on a Hewlett Packard Digital Frequency Counter type 5326B.

The hot-wire anemometer was attached to a traversing mechanism by a holder to obtain the mean velocities and hence the flow uniformity at different points in the y and z directions of the test section. The y and z directions are along the height and width of the test section shown in Figure 13, respectively. The traversing mechanism was mounted 45.7 cm (18-in) from the test section entrance through a 10.2 cm(4-in) long x 17.8 cm(7-in) wide hole cut symmetrically on top of the test section.

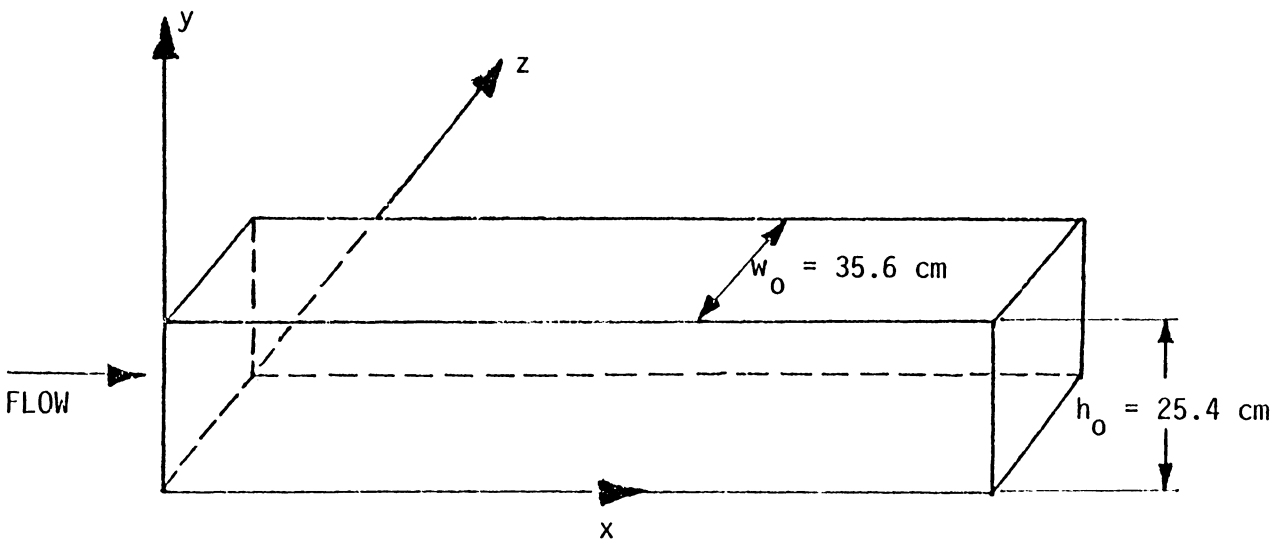

FIGURE 13: THE COORDINATE SYSTEM USED FOR FLOW UNIFORMITY IN THE TEST SECTION

It was supported by a flat steel plate on top of the test section. Another hole of the same size was cut to provide an access to the hot-wire and pitot tube for convenience. The center-to-center distance of the holes was 22.9 cm(9-in). The traversing was achieved by two stepping motors through a Superior Electric preset indexer with count insertion. Two-hundred steps (one cycle) indexing corresponded to 1.27 cm(0.5-in) displacement in the y-direction and 0.14 cm(0.055-in) in the z-direction.

The hot-wire itself was placed in the holder at 30.5 cm(12-in) from the entrance to the test section with its tip at about 10 cm(4-in) from the right-hand side wall and 15 cm(6-in) from the top wall of the test section, for velocity measurements at different frequencies.

A pitot tube was mounted at 30.5 cm(12-in) from the test section inlet with its tip at about 5.0 cm(2-in) from the right-hand side wall and 10 cm(4-in) from the top wall. The output of the pitot tube was read on a manometer and used for calibration of the hot-wire.

To determine the pressure variation in the diffuser a Statham Laboratories Pressure Transducer serial no. 543 was mounted on the diffuser 20. cm(8-in) from the shutters box through a 0.64 cm(1/4-in) hole and it was connected to the Digital Signal Analyzer through a Vishay/Ellis-11 power supply.

A Hewlett Packard plotter model T225A was connected to the Digital Signal Analyzer to obtain the plots of the pressure distributions, velocity waveforms and corresponding frequency plots.

6.2 Instrumentation and Measurements

6.2-1 Vibration And Necessary Modifications

There was very little noise and vibration when the wind tunnel was running by itself. When the shutters were turned on with the blower, the pressure in the diffuser excited the top plate of the blower. This resulted in the noise and vibration of the top plate of the blower, the diffuser and hence, the test section and hot-wire. To reinforce the blower four lengths of 3.8 cm(1 1/2-in) x 3.8 cm(1 1/2-in) angle iron were installed on the top plate of the blower 10 cm(4-in) apart. This greatly reduced the vibration and noise.

It was also noticed that the rubber boot between the blower and the diffuser was stretched because of the force exerted from the blower to the diffuser when both the blower and shutters were running at the same time. This problem was solved by connecting the diffuser stand to the blower by two reinforced rubber belts on both sides of the diffuser. The rubber belts were then able to keep the diffuser from moving and to resist the exerted force from the blower to the diffuser.

One of the purposes of reducing the vibration was to keep the hot-wire probe and test section stable. After the preliminary vibration reduction on the blower and diffuser, the hot-wire and test section were still vibrating at the higher frequencies. To eliminate this vibration two steps were taken. First, a rubber boot was connected between the contraction outlet and test section inlet to diminish vibration coming from the contraction to the test section. The rubber boot reduced the test section vibration some. Second, it was noticed that the test section and stand had a light weight and could therefore be driven by small

forces. Hence, four 50-lbs dead weights were mounted near the top of the test section stand, closest to the test section itself. The installation of the weights was achieved by mounting two steel bars on the rear and front sides of the stand. This procedure eliminated any noticeable vibration of the test section and hot-wire.

6.2-2 Calibration

The hot-wire was calibrated against the pitot tube in the wind tunnel over the velocity range of 15 to 30 $\frac{m}{sec}$. The shutters were used to block the flow for the velocity range specified. The calibration was achieved for the shutters angles of zero degree. It was repeated several times to check for variation and found to remain unchanged. One of the calibration curves is shown in Figure 14. After the calibration was performed, the oncoming flow was shown to be uniform under steady state and unsteady conditions along the y and z directions of the test section. Tables 4 and 5 indicate the steady state uniformity of the flow along with turbulence levels when the shutters are in open and closed positions, respectively. The unsteady flow uniformity was checked at different frequencies for shutters setting B when the flow was not blocked. An example of this uniformity is indicated in Table 6 at a frequency of 16 Hz.

The unsteady flow uniformity was also checked at various frequencies for the condition when both the upper and lower plates of the shutters box were removed. Table 7 indicates the uniformity at one of these frequencies (3.4 Hz) for the specified shutters setting. It must

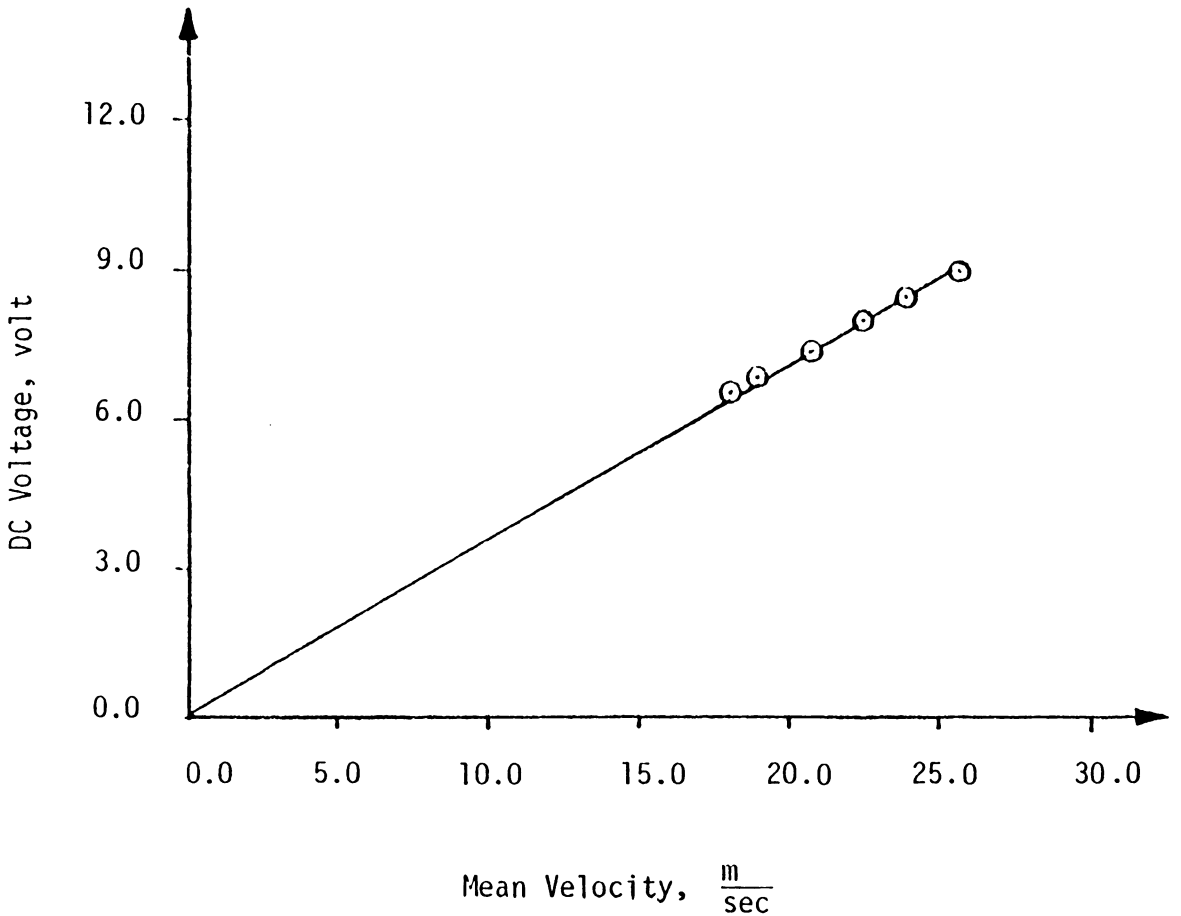

FIGURE 14: CALIBRATION CURVE OF THE HOT-WIRE

TABLE 4: STEADY STATE FLOW UNIFORMITY AND TURBULENCE LEVEL FOR SHUTTERS IN OPEN POSITION

$\frac{y}{h_o}$	$\frac{z}{w_o}$	Mean Velocity (m/sec)	Turbulence Level (%)
0.264	0.5	26.7	0.207
0.303	0.5	26.7	0.20
0.343	0.5	26.9	0.185
0.382	0.5	26.9	0.205
0.421	0.5	27.0	0.184
0.461	0.5	27.0	0.194
0.5	0.5	27.3	0.186
0.539	0.5	27.0	0.194
0.579	0.5	27.0	0.184
0.618	0.5	26.9	0.205
0.657	0.5	26.9	0.185
0.697	0.5	26.7	0.20
0.736	0.5	26.7	0.207

TABLE 5: STEADY STATE FLOW UNIFORMITY AND TURBULENCE LEVEL FOR SHUTTERS IN CLOSED POSITION

$\frac{y}{h_o}$	$\frac{z}{w_o}$	Mean Velocity (m/sec)	Turbulence Level (%)
0.264	0.5	17.0	0.43
0.303	0.5	17.0	0.43
0.343	0.5	17.0	0.415
0.382	0.5	17.1	0.414
0.421	0.5	17.1	0.399
0.461	0.5	17.1	0.414
0.5	0.5	17.2	0.413
0.539	0.5	17.1	0.414
0.579	0.5	17.1	0.399
0.618	0.5	17.1	0.414
0.657	0.5	17.0	0.415
0.697	0.5	17.0	0.43
0.736	0.5	17.0	0.43

TABLE 6: FLOW UNIFORMITY FOR SHUTTERS SETTING B AT 16 Hz

$\frac{y}{h_o}$	$\frac{z}{w_o}$	Mean Velocity (m/sec)
0.126	0.374	29.3
0.173	0.374	29.3
0.224	0.374	29.3
0.276	0.374	29.3
0.327	0.374	29.3
0.374	0.374	29.3
0.402	0.374	29.3
0.449	0.374	29.3
0.5	0.374	29.5
0.551	0.374	29.5
0.598	0.374	29.6
0.65	0.374	29.6
0.700	0.374	29.6
0.748	0.374	29.6
0.800	0.374	29.6
0.850	0.374	30.0
0.902	0.374	30.2
0.950	0.374	30.2
0.5	0.053	30.0
0.5	0.174	29.6

Table 6: cont'd.

$\frac{y}{h_o}$	$\frac{z}{w_o}$	Mean Velocity (m/sec)
0.5	0.281	29.6
0.5	0.374	29.6
0.5	0.643	29.6
0.5	0.730	29.6
0.5	0.837	29.6
0.5	0.95	29.6

TABLE 7 : FLOW UNIFORMITY AT 3.4 Hz FOR SHUTTERS SETTING A WHEN BOTH UPPER AND LOWER PLATES OF SHUTTERS BOX ARE REMOVED.

$\frac{y}{h_o}$	$\frac{z}{w_o}$	Mean Velocity (m/sec)
0.055	0.5	16.5
0.157	0.5	16.1
0.256	0.5	16.1
0.354	0.5	16.1
0.457	0.5	16.1
0.555	0.5	16.1
0.657	0.5	16.1
0.744	0.5	16.1
0.756	0.5	16.1
0.843	0.5	16.1
0.5	0.037	14.6
0.5	0.334	16.0
0.5	0.427	16.0
0.5	0.5	16.1
0.5	0.643	16.1
0.5	0.722	16.1
0.5	0.947	16.0

be noted that the velocity corresponding to point ($\frac{y}{h_o}$ = 0.5, $\frac{z}{w_o}$ = 0.037) was measured in the boundary layer.

The pressure transducer used to determine the pressure distributions in the diffuser was also calibrated against the manometer with the Digital Signal Analyzer in the steady state environment of the diffuser. The calibration curve is shown in Figure 15 and one of the pressure distribution plots used to calibrate the transducer is indicated in Figure 16. The calibration curve was then used to obtain pressure distribution in the diffuser for the desired shutters settings and frequency range.

6.2-3 Shutters Settings

Preliminary adjustments of the shutters were achieved by changing the shutters angles to determine the best velocity waveforms with the highest obtainable amplitude for the flow frequency range of 3.4 to 31.3 Hz. The flow in the test section was again calibrated for uniformity at the desired shutters setting and frequency range. These results are indicated in Tables 6 and 7 for the desired conditions.

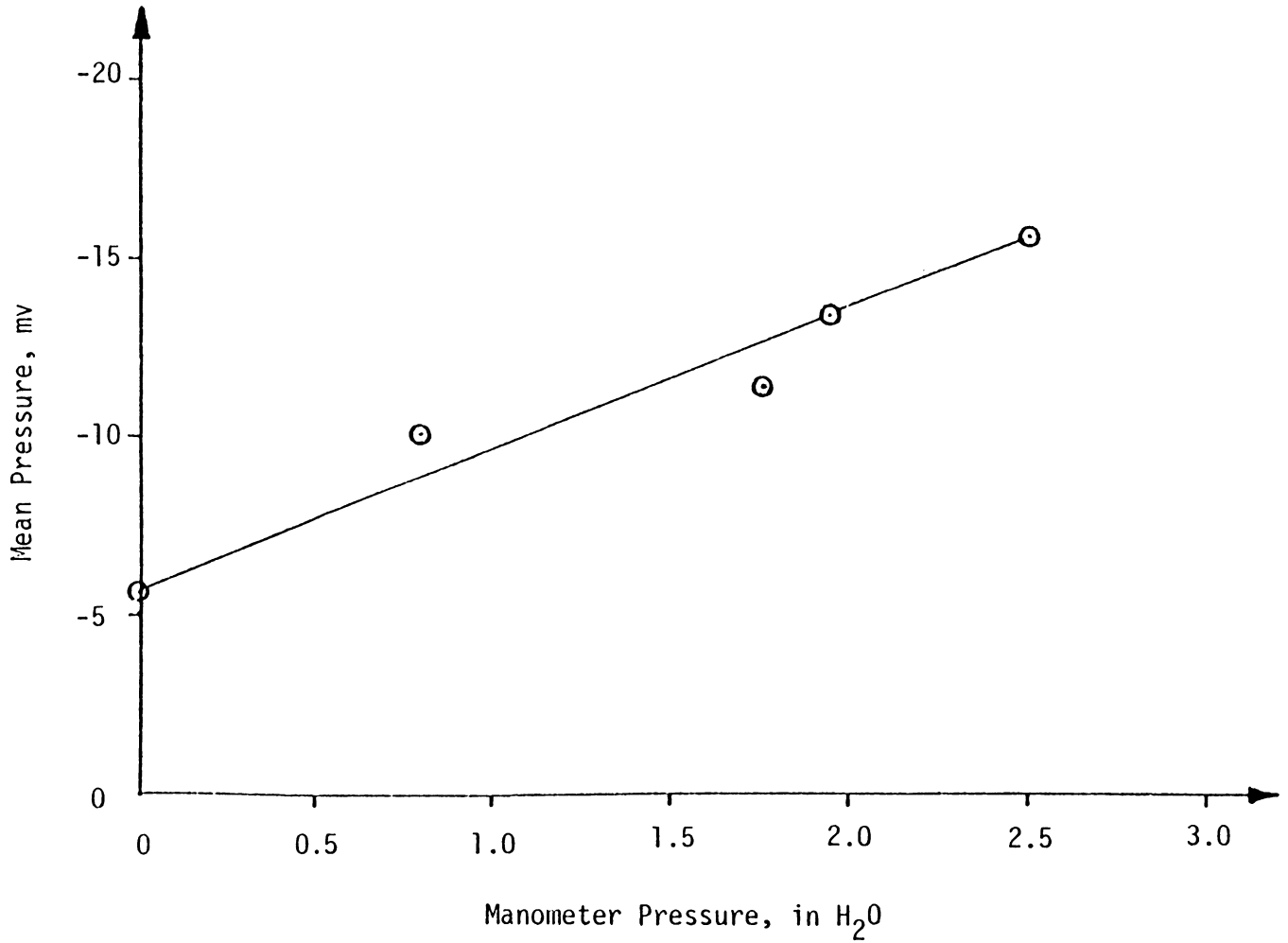

FIGURE 15: CALIBRATION CURVE FOR PRESSURE DISTRIBUTION IN THE DIFFUSER

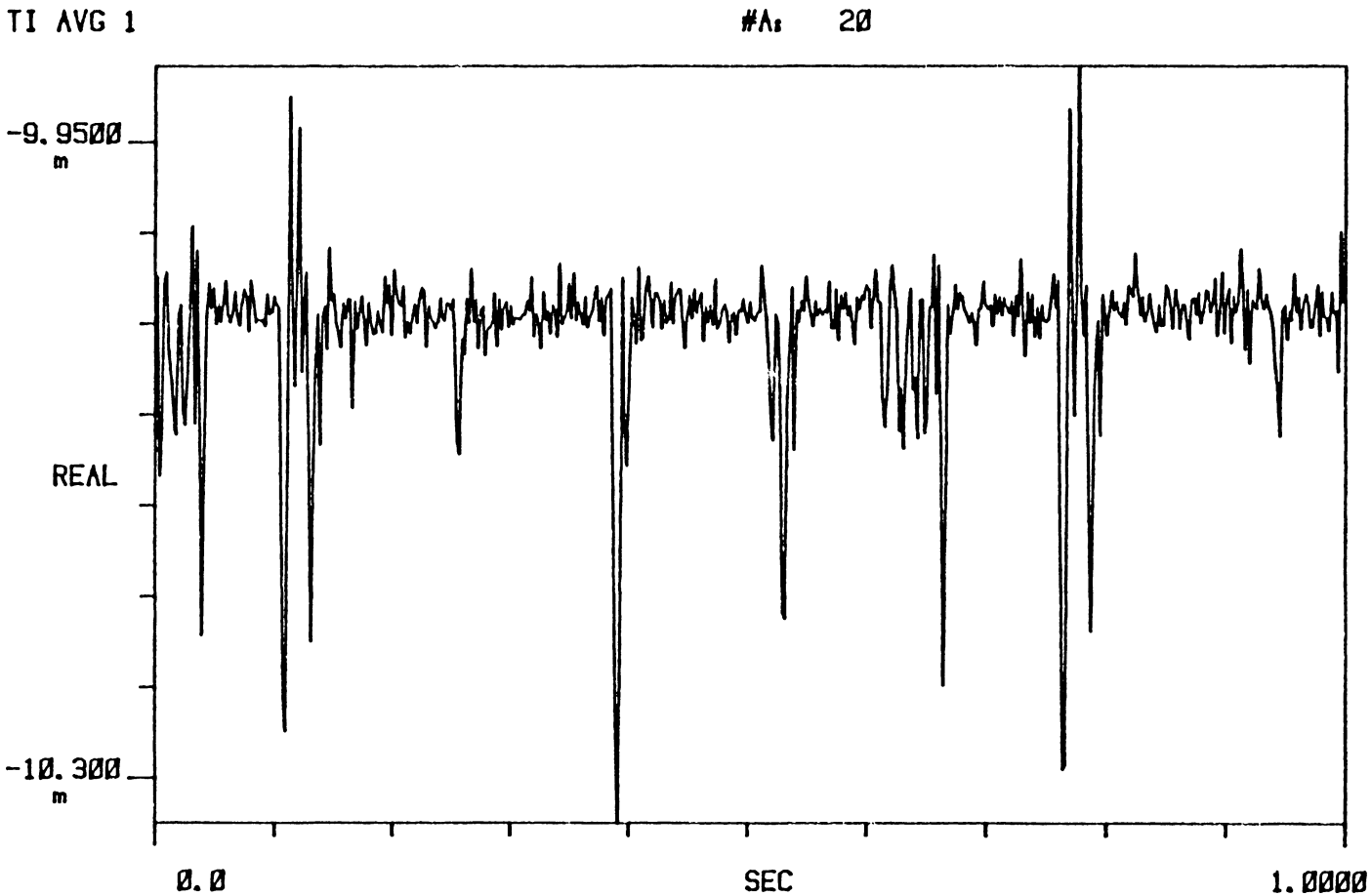

FIGURE 16: A SAMPLE OF PRESSURE VARIATION IN THE DIFFUSER FOR CALIBRATION AT SHUTTERS SETTING A (U = 15 m/sec).

7. RESULTS

The flow measurements were obtained for a pulsation frequency range of 3.4 to 31.3 Hz. The velocity waveforms were measured in the test section over this range for different shutters settings and physical arrangements of the wind tunnel.

First, all the shutters were set at zero degree relative to shutter No. 1 (see Figure 12) in the clockwise sense and velocity waveforms were obtained. Sample velocity waveforms are shown in Figures 17, 18, and 19 for shutters setting A at 3.4 Hz, 16 Hz, and 31.3 Hz, respectively. Setting A corresponds to zero degree angle for all the shutters. Setting B corresponds to 30° angle for shutters No. 2 and 5, and the rest at zero degree. The abscissa of these figures is time and the ordinate axis given in voltage is proportional to velocity. The calibration curves for velocity and pressure are shown in Figures 14 and 15, respectively. Because these velocity distributions were not suitable the relative orientations of the shutters were changed to obtain better waveforms. It was known from the literature that the relative orientation of the shutters influences the amplitudes of the velocity variation and the velocity waveforms in this type of tunnel. Tables 8 and 9 illustrate several configurations with different amplitudes that resulted from constant angular velocity rotation of the shutters. The velocity waveforms were obtained for two different mean velocities. The lower velocity was achieved by partly blocking the flow at the blower inlet.

It was thought that the pressure build-up in the diffuser could have some effect on the velocity waveform and its amplitude. Therefore,

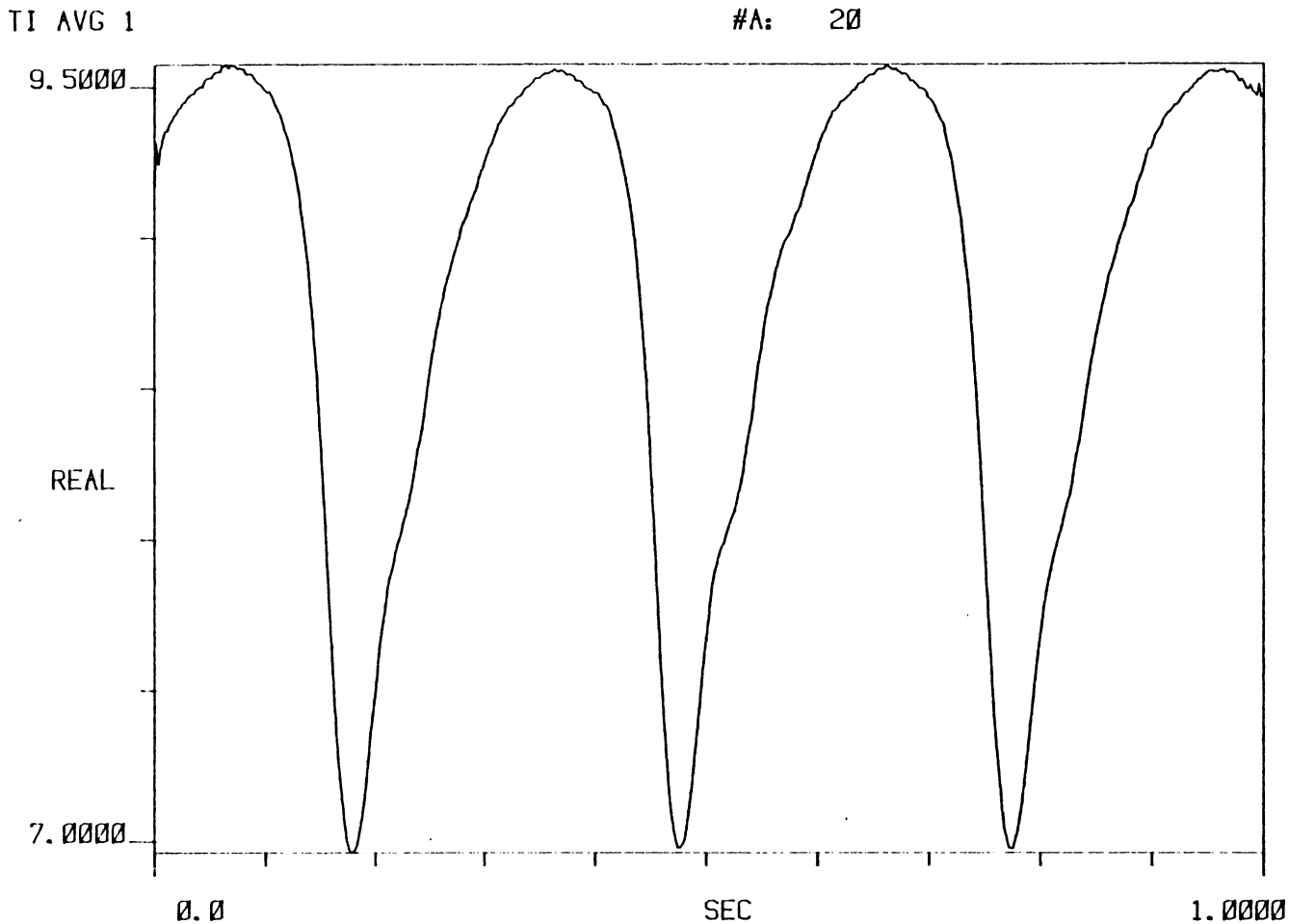

FIGURE 17: SAMPLE VELOCITY WAVEFORM FOR SHUTTERS SETTING A AT 3.4 Hz (U = 30 m/sec).

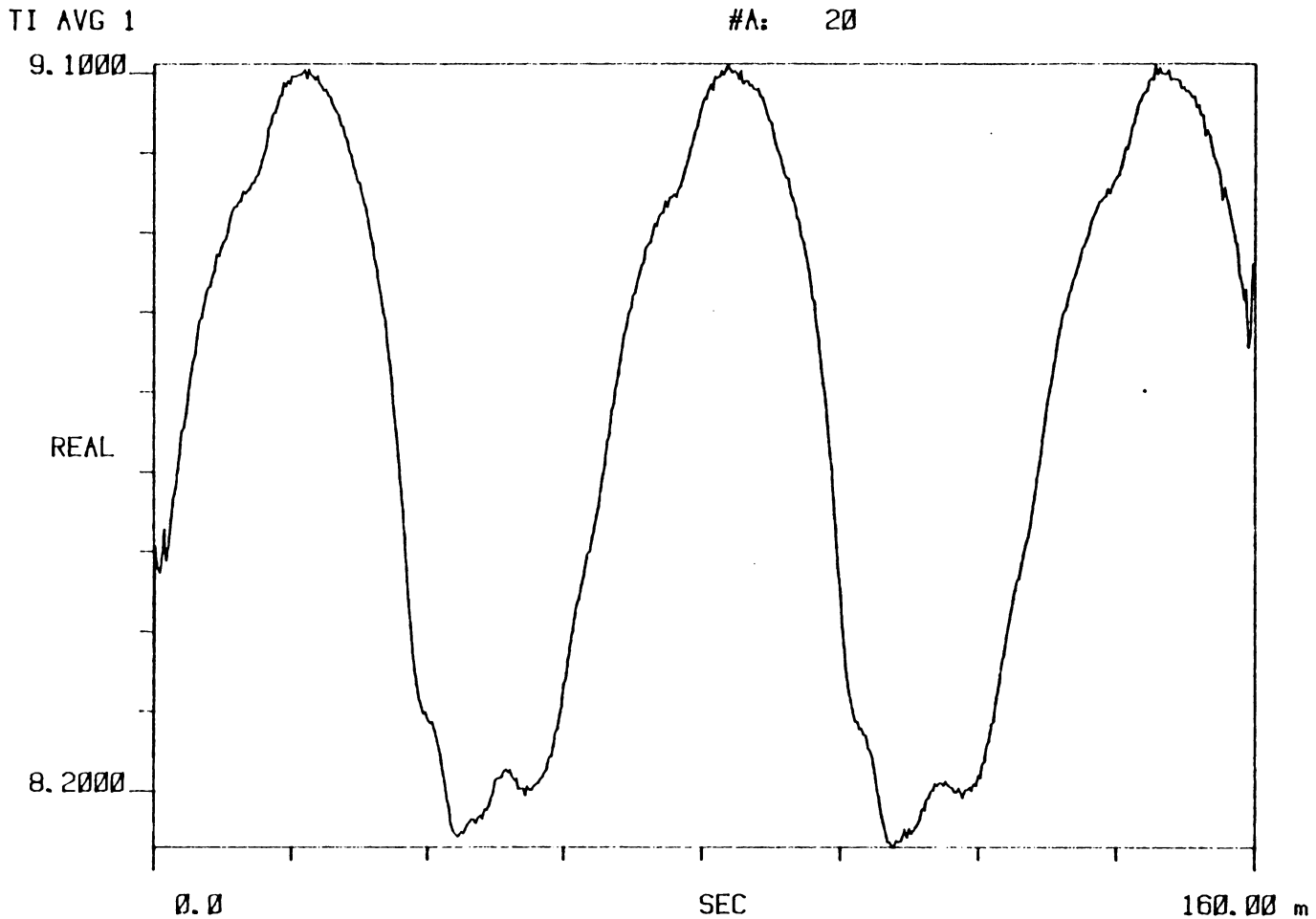

FIGURE 18: SAMPLE VELOCITY WAVEFORM FOR SHUTTERS SETTING A AT 16 Hz (U = 30 m/sec).

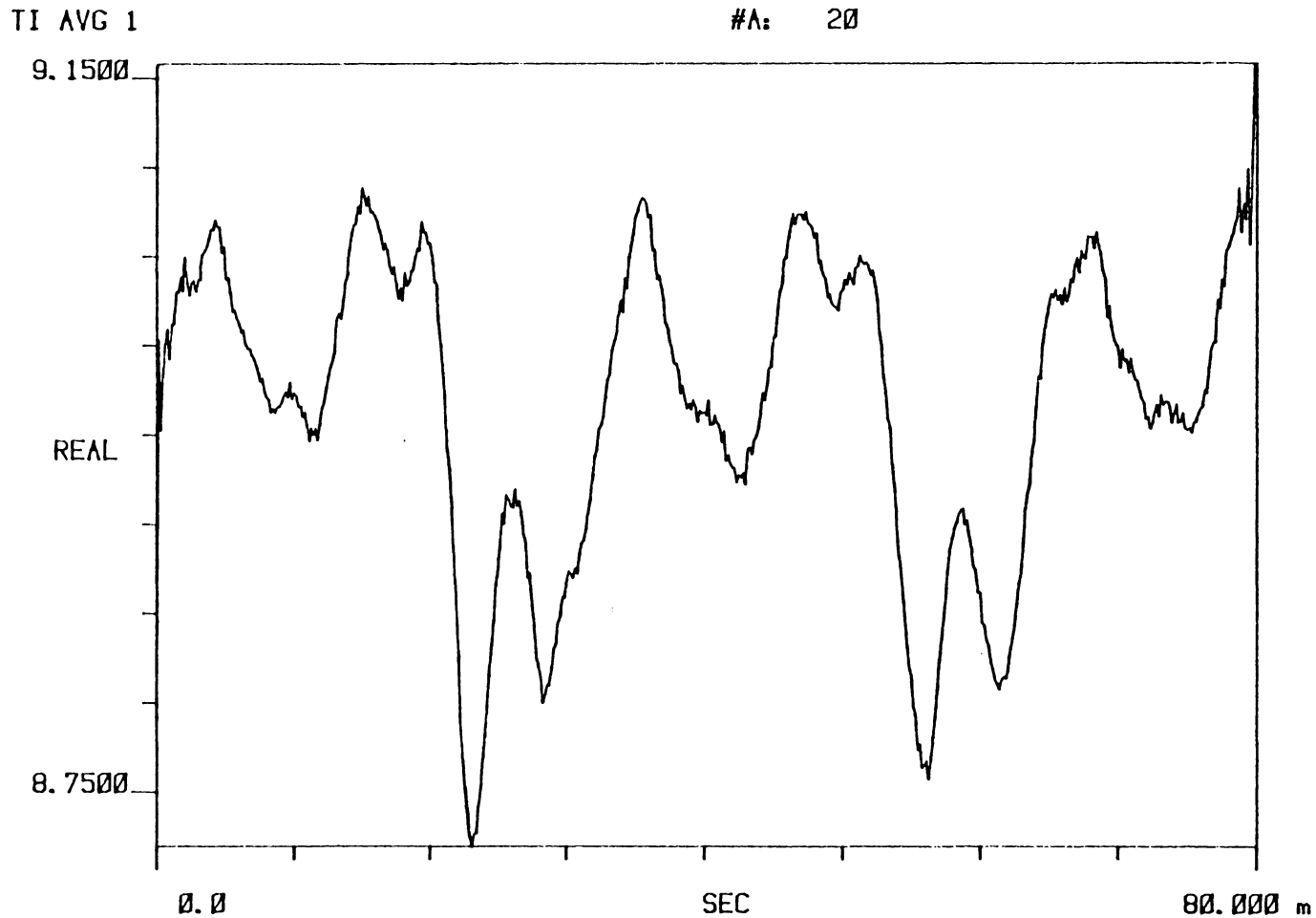

FIGURE 19: SAMPLE VELOCITY WAVEFORM FOR SHUTTERS SETTING A 31.3 Hz (U = 30 m/sec).

TABLE 8 : THE PEAK-TO-PEAK AMPLITUDES AND MEAN VELOCITIES OF VELOCITY WAVEFORMS AT DIFFERENT SHUTTERS SETTINGS FOR FLOW NOT BLOCKED.

Flow Frequency, Hz	Mean Velocity, m/s			Peak-to-Peak Amplitude, m/s			Mean Velocity, m/s			Peak-to-Peak Amplitude, m/s		
	Shutters Setting A, Degree						Shutters Setting B, Degree					
	0	0	0	0	0	0	0	30	0	0	30	0
3.38	27.0			6.90			29.0			3.40		
5.08	27.0			5.60			29.0			2.80		
6.8	27.0			4.50			29.0			2.40		
10.0	27.0			3.2			28.6			2.00		
16.0	27.7			2.70			28.6			2.08		
19.2	28.0			2.40			28.0			1.80		

TABLE 8 : cont'd.

Flow Frequency, Hz	Mean Velocity, m/s			Peak-to-Peak Amplitude, m/s			Mean Velocity, m/s			Peak-to-Peak Amplitude, m/s		
	Shutters Setting C, Degree						Shutters Setting D, Degree					
	0	30	0	0	0	0	0	0	0	0	0	30
3.38	28.0			7.20			27.0			7.10		
5.08	28.0			5.60			27.7			5.80		
6.8	27.7			4.80			27.7			4.60		
10.0	27.7			3.40			27.7			3.10		
16.0	27.7			3.10			28.0			3.00		
19.2	28.0			2.55			28.6			2.30		

TABLE 8 : cont'd.

Flow Frequency, Hz	Mean Velocity, m/s			Peak-to-Peak Amplitude, m/s			Mean Velocity, m/s			Peak-to-Peak Amplitude, m/s		
	Shutters Setting E, Degree						Shutters Setting F, Degree					
	0	0	0	0	45	0	0	0	0	0	45	90
3.38	27.0			5.80			30			1.58		
5.08	27.7			4.40			29.5			1.20		
6.8	27.7			3.80			29.5			1.20		
10.0	28.0			2.80			29.5			1.00		
16.0	28.0			2.60			29.0			1.40		
19.2	28.6			2.20			29.0			1.10		

TABLE 8: cont'd.

Flow Frequency, Hz	Mean Velocity, m/s			Peak-to-Peak Amplitude, m/s		
	Shutters Setting G, Degree					
	45	35	0	0	0	0
3.38	29.5			3.40		
5.08	29.5			2.80		
6.8	29.0			2.70		
10.0	29.0			2.15		
16.0	29.0			2.20		
19.2	28.6			1.90		

TABLE 9 : THE PEAK-TO-PEAK AMPLITUDES AND MEAN VELOCITIES OF VELOCITY WAVEFORMS AT DIFFERENT SHUTTERS SETTINGS FOR FLOW BLOCKED.

Flow Frequency, Hz	Mean Velocity, m/s			Peak-to-Peak Amplitude, m/s			Mean Velocity, m/s			Peak-to-Peak Amplitude, m/s		
	Shutters Setting A, Degree						Shutters Setting B, Degree					
	0	0	0	0	0	0	0	30	0	0	30	0
3.38	19.4			2.25			15.0			1.17		
5.08	18.0			1.875			15.0			1.05		
6.8	16.2			1.813			15.0			1.95		
10.0	16.0			1.25			15.2			1.88		
16.0	15.6			0.95			15.0			0.75		
19.2	15.6			0.75			15.5			0.45		

pressure waveforms were obtained with a pressure transducer in the diffuser. One of these pressure waveforms for a frequency of 5.0 Hz is shown in Figure 20.

To release the transitory pressure build-up in the diffuser, first the upper plate of the shutters box and then both the upper and lower plates were removed and velocity measurements along with pressure distributions in the diffuser were obtained. The pressure release generally facilitated better velocity waveforms and higher amplitudes. Tables 10 and 11 illustrate the results at various frequencies and shutters settings for the case where the upper plate of the shutter box is removed. Figures 21 through 23 are sample velocity waveforms for shutters setting B obtained in this case at 3.4 Hz, 16 Hz, and 31.1 Hz, respectively. The waveforms were obtained for two different mean velocities.

The peak-to-peak and base pressures of the pressure waveforms in the diffuser are indicated in Tables 12 and 13 at various shutters settings and frequencies when the upper plate is removed.

To obtain more of pressure release in the diffuser when the air flow contacted the shutters, both the upper and lower plates of the shutter box were removed. This gave the best velocity waveforms with the highest amplitudes for the pulsation frequency range of 3.4 to 10 Hz. Table 14 indicates two shutters settings with different amplitudes and frequencies for this condition. Sample velocity waveforms are shown in Figures 24, 25, and 26 for shutters setting A at 3.4 Hz, 16 Hz, and 31.3 Hz, respectively. The velocity waveforms

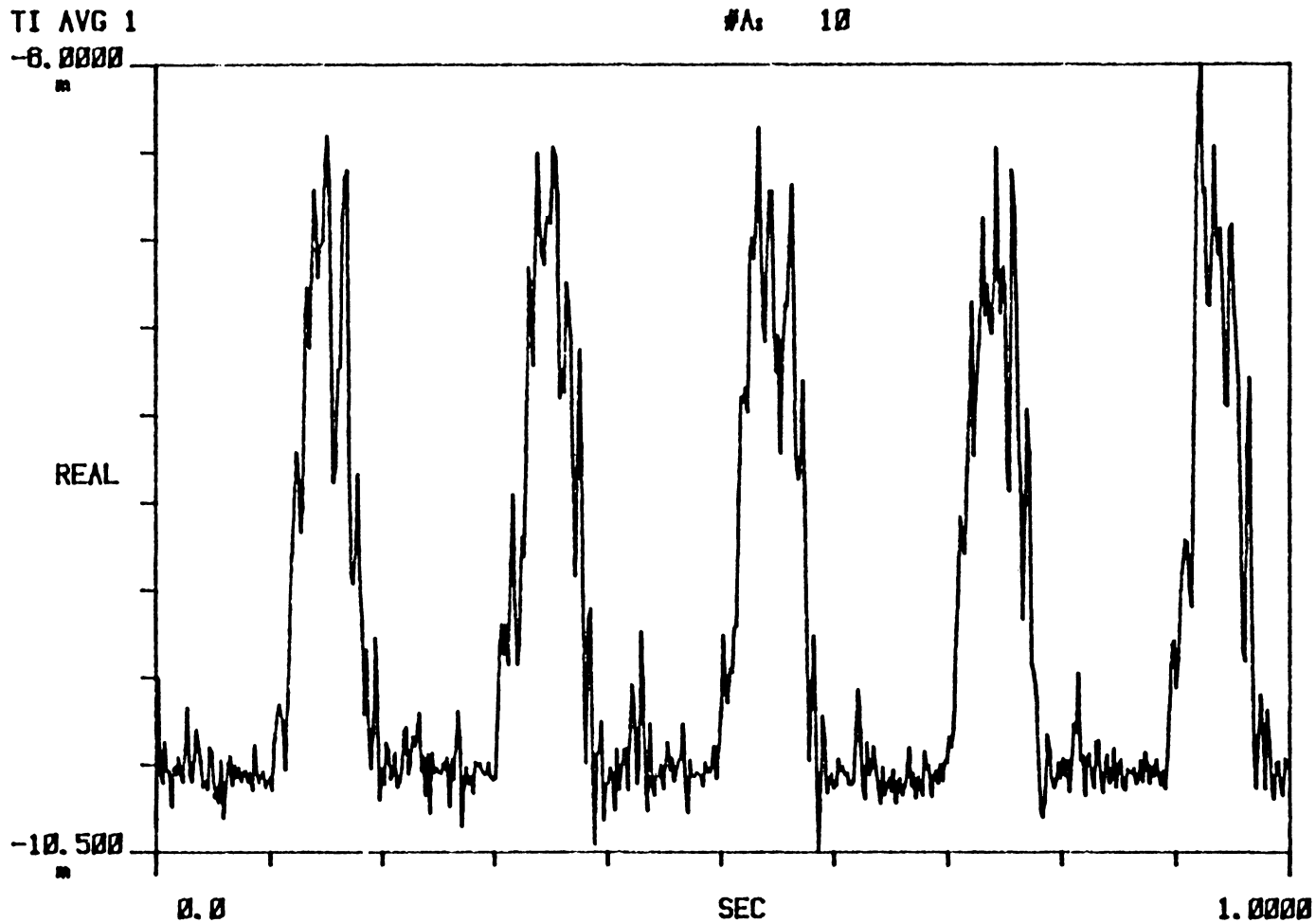

FIGURE 20: SAMPLE PRESURE VARIATION IN THE DIFFUSER FOR SHUTTERS SETTING B AT 5 HZ. BOTH PLATES ARE REMOVED (U = 17 m/sec).

TABLE 10: THE PEAK-TO-PEAK AMPLITUDES AND MEAN VELOCITIES OF VELOCITY WAVEFORMS AT DIFFERENT SHUTTERS SETTINGS FOR UPPER PLATE REMOVED.

Flow Frequency, Hz	Mean Velocity, m/s			Peak-to-Peak Amplitude, m/s			Mean Velocity, m/s			Peak-to-Peak Amplitude, m/s		
	Shutters Setting A, Degree						Shutters Setting B, Degree					
	0	0	0	0	0	0	0	30	0	0	30	0
3.38	19.6			6.5			22.3			4.0		
5.08	20.3			5.4			22.1			3.0		
6.8	20.5			4.0			22.3			2.5		
10.0	20.0			3.0			22.0			2.4		
16.0	20.0			2.50			22.0			1.9		
19.2	20.0			2.4			22.0			1.8		
31.34	20.0			2.3			22.0			2.10		

TABLE 11: THE PEAK-TO-PEAK AMPLITUDES AND MEAN VELOCITIES OF VELOCITY WAVEFORMS AT DIFFERENT SHUTTERS SETTINGS FOR UPPER PLATE REMOVED. THE FLOW IS BLOCKED.

Flow Frequency, Hz	Mean Velocity, m/s			Peak-to-Peak Amplitude, m/s		
	Shutters Setting B, Degree					
	0	30	0	0	30	0
3.38	9.80			1.35		
5.08	9.90			1.10		
6.8	9.80			0.90		
10.0	9.6			0.76		
16.0	9.5			0.70		
19.2	9.5			0.55		
31.34	9.5			0.73		

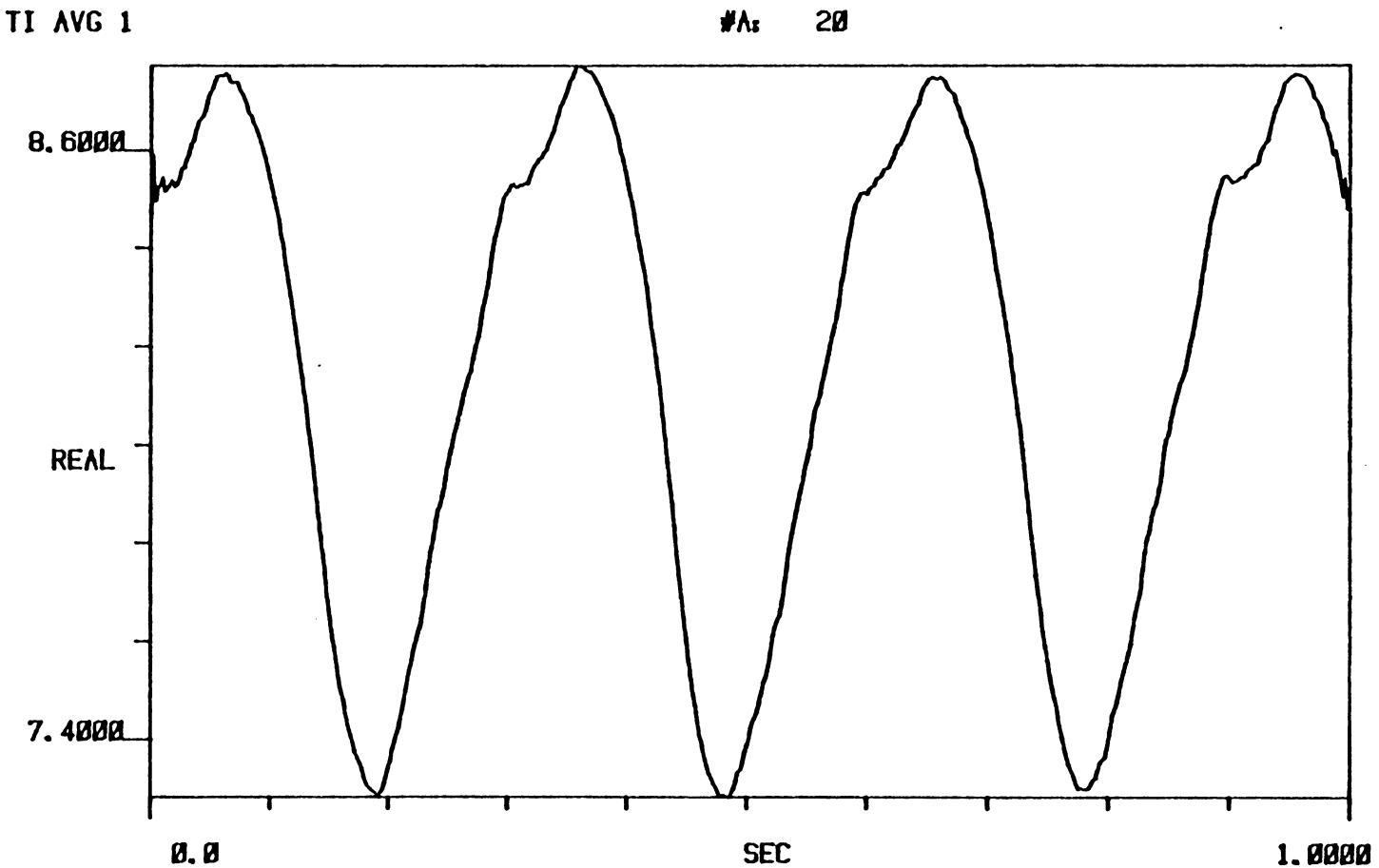

FIGURE 21: SAMPLE VELOCITY WAVEFORM FOR SHUTTERS SETTING B AT 3.4 Hz. UPPER PLATE IS REMOVED (U = 22 m/sec).

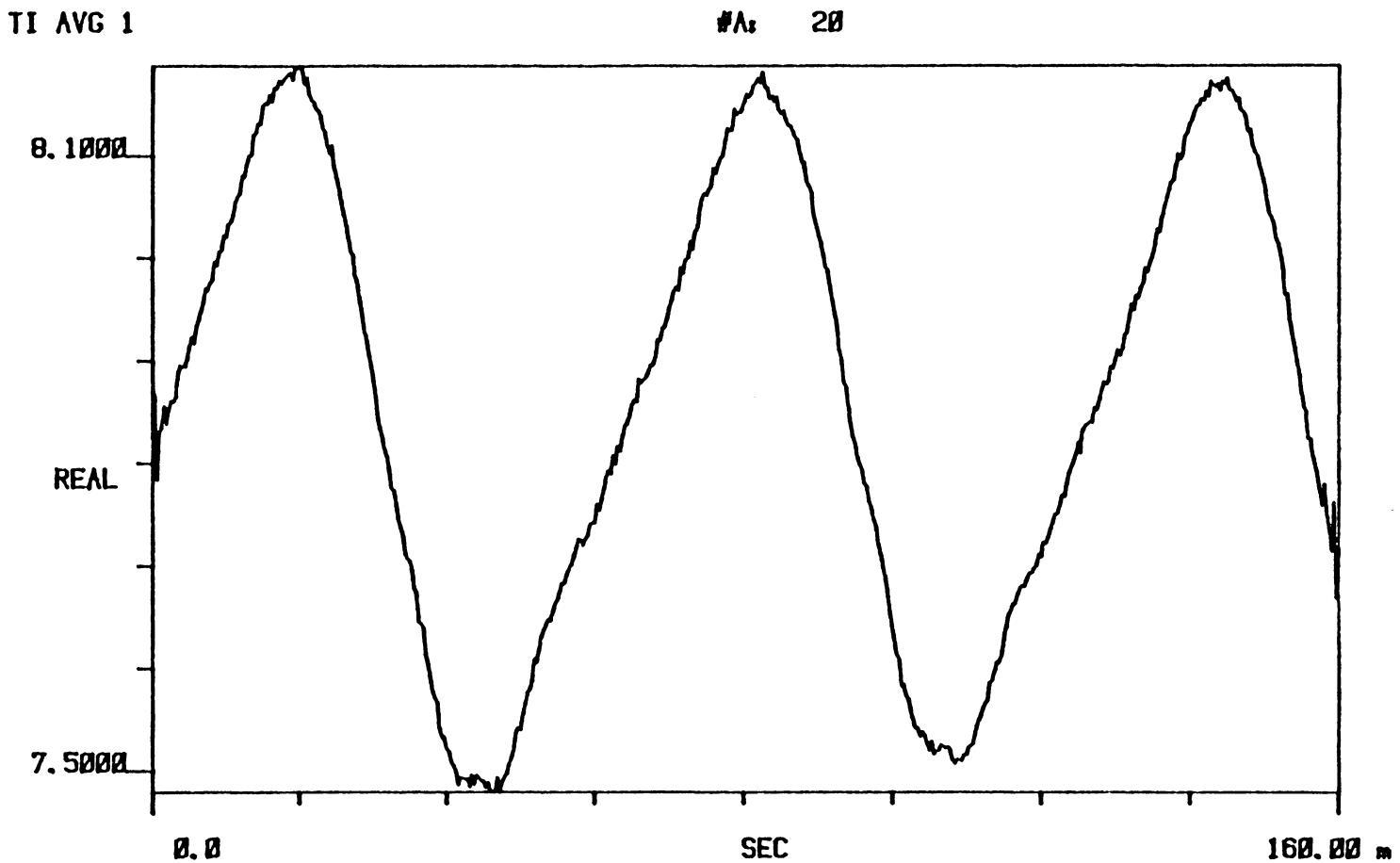

FIGURE 22: SAMPLE VELOCITY WAVEFORM FOR SHUTTERS SETTING B at 16 Hz. UPPER PLATE IS REMOVED (U = 22 m/sec).

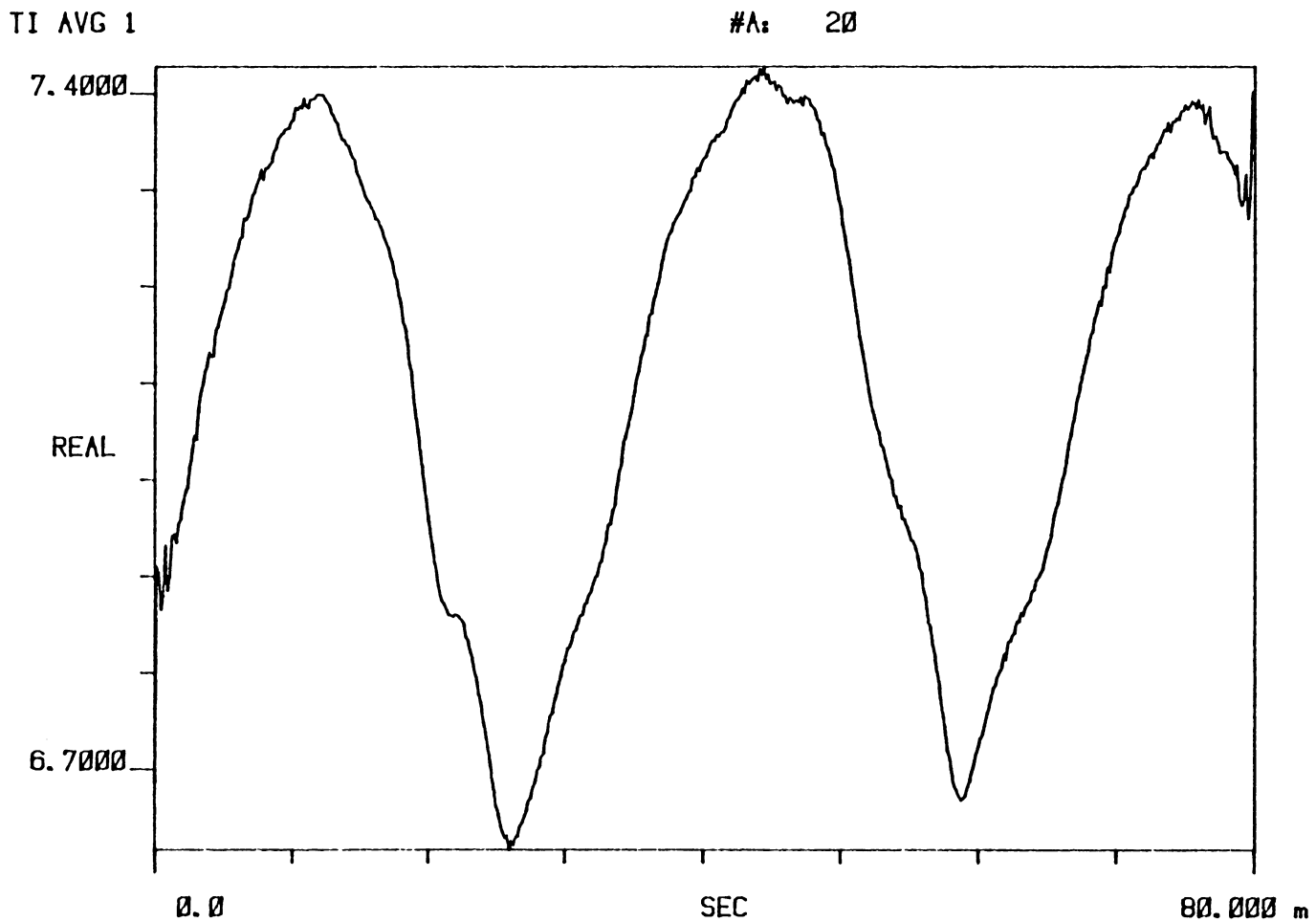

FIGURE 23: SAMPLE VELOCITY WAVEFORM FOR SHUTTERS SETTING B AT 31.3 Hz. UPPER PLATE IS REMOVED (U = 22 m/sec).

TABLE 12: THE PEAK-TO-PEAK AND BASE PRESSURES OF THE PRESSURE DISTRIBUTIONS IN THE DIFFUSER FOR DIFFERENT SHUTTERS SETTINGS AND FREQUENCIES WHEN FLOW IS NOT BLOCKED AND UPPER PLATE IS REMOVED.

Flow Frequency, Hz	Peak-to-Peak Pressure, in H_2O			Base Pressure, in H_2O			Peak-to-Peak Pressure, in H_2O			Base Pressure, in H_2O		
	Shutters Settings A, Degree						Shutters Settings B, Degree					
	0	0	0	0	0	0	0	30	0	0	30	0
3.38	0.28			1.1			0.54			2.46		
5.08	0.85			1.1			1.33			2.32		
6.8	1.12			1.1			1.20			1.1		
10.0	1.24			1.1			1.26			1.1		
16.0	1.24			1.1			1.2			1.1		
19.2	1.24			1.1			1.09			1.1		
31.34	1.75			1.05			2.30			1.95		

TABLE 13: THE PEAK-TO-PEAK AND BASE PRESSURES OF THE PRESSURE DISTRIBUTIONS IN THE DIFFUSER FOR DIFFERENT FREQUENCIES AND SHUTTERS SETTING WHEN FLOW IS BLOCKED AND UPPER PLATE IS REMOVED.

Flow Frequency, Hz	Peak-to-Peak Pressure, in H_2O			Base Pressure, in H_2O		
	Shutters Settings B, Degree					
	0	30	0	0	30	0
3.38	0.13			0.01		
5.08	0.15			0.0		
6.8	0.85			1.25		
10.0	0.62			1.15		
16.0	0.48			1.15		
19.2	0.38			1.05		
31.34	1.47			0.84		

TABLE 14: THE PEAK-TO-PEAK AMPLITUDES AND MEAN VELOCITIES OF VELOCITY WAVEFORMS AT DIFFERENT SHUTTERS SETTINGS AND FREQUENCIES FOR BOTH PLATES REMOVED.

Flow Frequency, Hz	Mean Velocity, m/s			Peak-to-Peak Amplitude, m/s			Mean Velocity, m/s			Peak-to-Peak Amplitude, m/s		
	Shutters Setting A, Degree						Shutters Setting B, Degree					
	0	0	0	0	0	0	0	30	0	0	30	0
3.38	16.5			5.40			17.2			3.60		
5.08	16.6			3.80			17.0			2.42		
6.8	16.6			3.0			17.0			1.85		
10.0	16.2			2.0			16.6			1.70		
16.0	16.0			2.0			16.0			1.3		
19.2	16.0			2.0			16.0			1.25		
31.34	16.0			1.95			16.0			1.87		

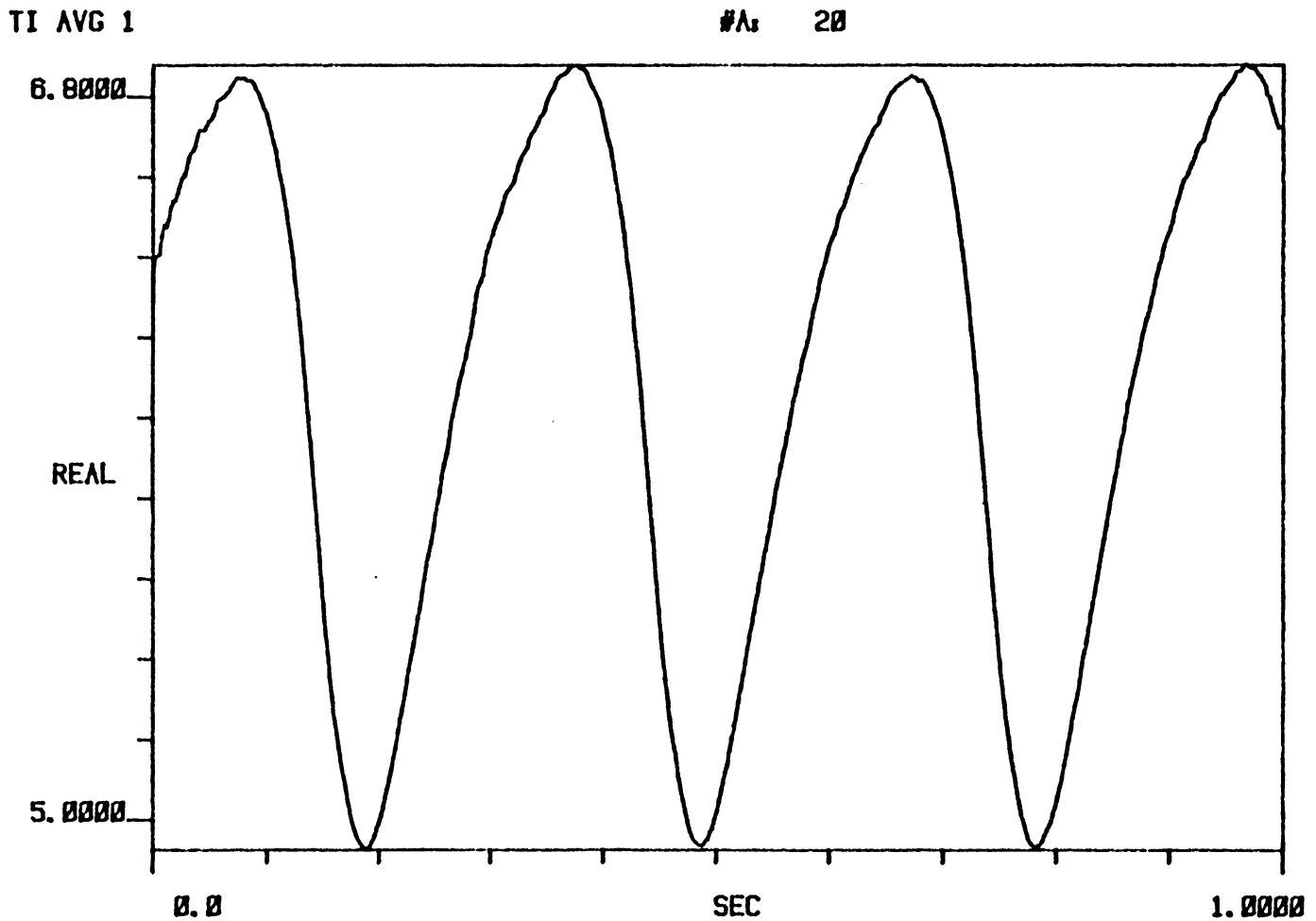

FIGURE 24: SAMPLE VELOCITY WAVEFORM FOR SHUTTERS SETTING A AT 3.4 Hz. BOTH PLATES ARE REMOVED (U = 16 m/sec).

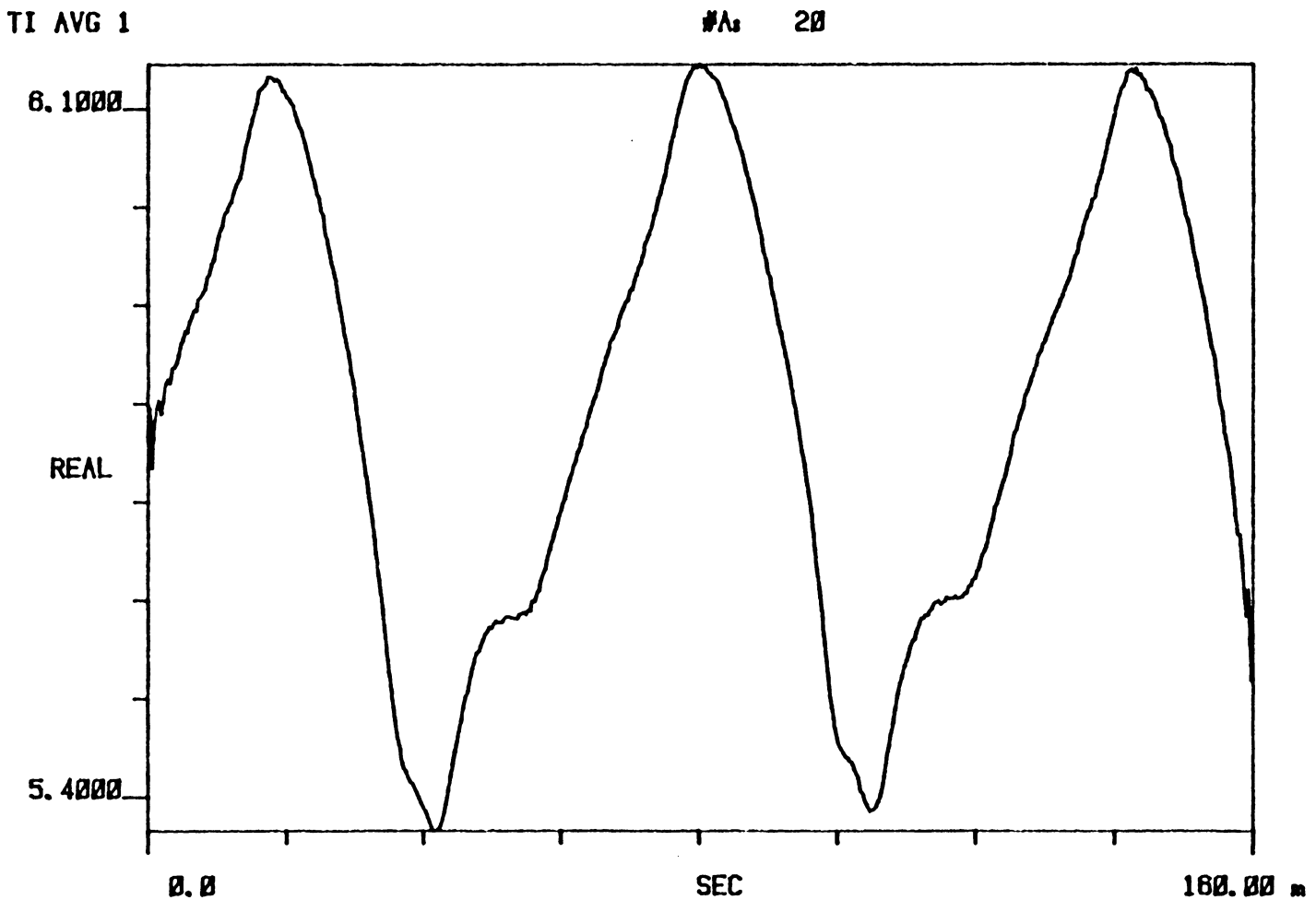

FIGURE 25: SAMPLE VELOCITY WAVEFORM FOR SHUTTERS SETTING A AT 16 Hz. BOTH PLATES ARE REMOVED (U = 16 m/sec).

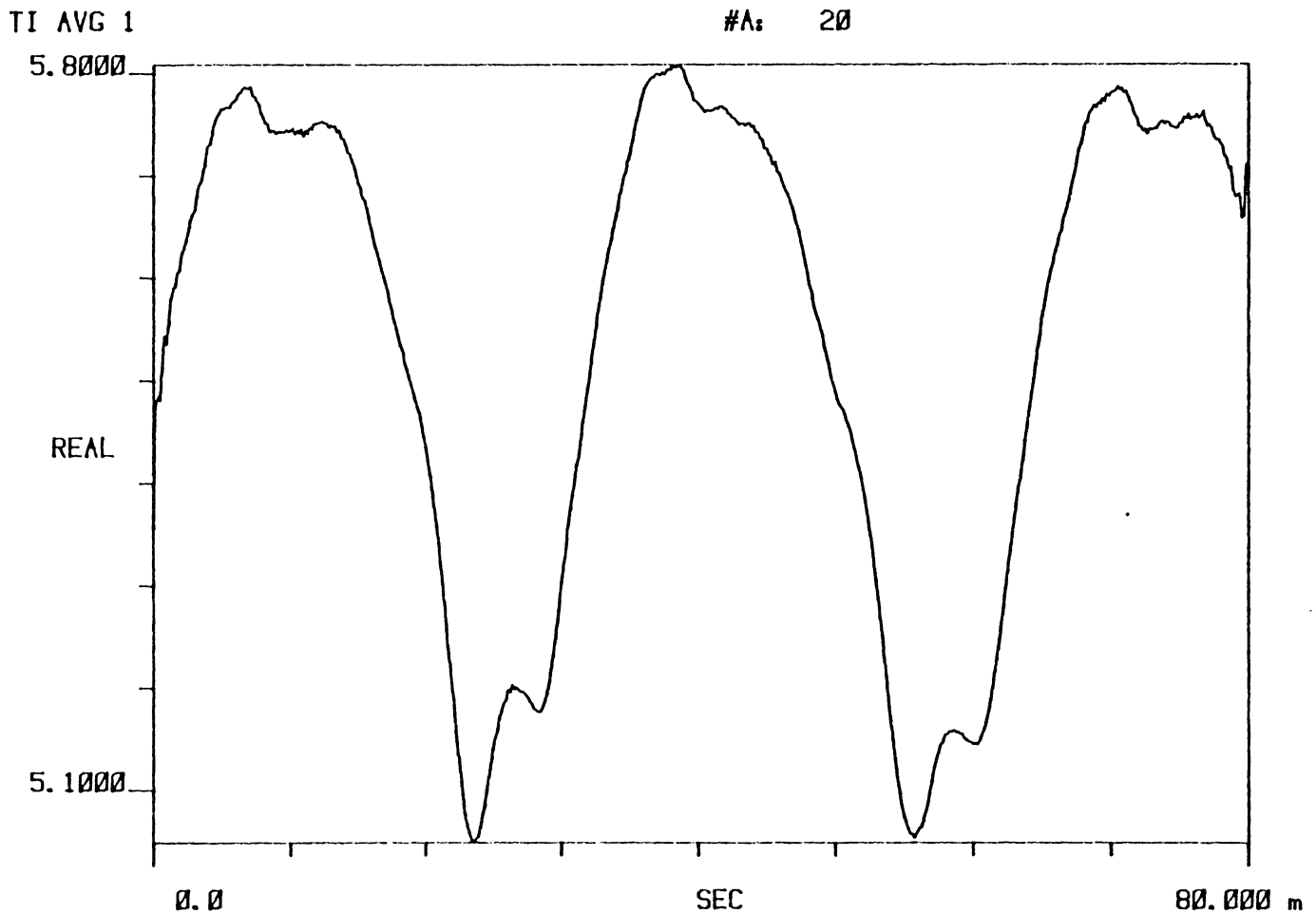

FIGURE 26: SAMPLE VELOCITY WAVEFORM FOR SHUTTERS SETTING A AT 31.3 Hz. BOTH PLATES ARE REMOVED (U = 16 m/sec).

were obtained for a mean velocity of 17.0 $\frac{m}{sec}$. Because of the pressure release the mean velocities were considerably lower than for the other conditions.

Table 15 indicates the peak-to-peak and base pressures of the pressure waveforms in the diffuser at different shutters settings and frequencies when both the upper and lower plates are removed.

The velocity waveforms for each shutters setting were compared at the same frequency in order to determine the best velocity waveforms with the highest obtainable amplitude. The best velocity waveforms with the highest amplitudes were obtained at the same shutters setting, but different physical arrangements of the tunnel, for low and high frequency ranges. These waveforms are shown in Figures 27, 29, 31, 33, 36, 38, and 41. The dashed curves represent true sinusoidal waveforms at the specified frequencies with the same amplitudes.

The best velocity waveforms at low frequency range were obtained with shutters setting B. The conditions were for the flow not blocked at the blower inlet and both the upper and lower plates of the shutters box removed. The flow frequency range was from 3.4 to 10.0 Hz for the setting and conditions mentioned above. The velocity waveforms and corresponding frequency spectra are shown in Figures 27 through 34. The corresponding typical pressure waveform is shown in Figure 35.

The best velocity waveforms over the frequency range of 16 to 19.2Hz were obtained for flow not blocked and the upper plate of the shutters box removed for setting B. The amplitude obtained with this setting

TABLE 15: THE PEAK-TO-PEAK AND BASE PRESSURES OF THE PRESSURE DISTRIBUTIONS IN THE DIFFUSER FOR DIFFERENT FREQUENCIES AND SHUTTERS SETTINGS WHEN THE FLOW IS NOT BLOCKED AND BOTH PLATES ARE REMOVED.

Flow Frequency, Hz	Peak-to-Peak Pressure, in H_2O			Base Pressure, in H_2O			Peak-to-Peak Pressure, in H_2O			Base Pressure, in H_2O		
	Shutters Settings A, Degree						Shutters Settings B, Degree					
	0	0	0	0	0	0	0	30	0	0	30	0
3.38	1.15			1.1			0.18			1.1		
5.08	1.16			0.84			0.13			1.1		
6.8	1.27			1.1			1.25			1.05		
10.0	1.31			1.1			1.35			1.05		
16.0	1.25			1.04			1.0			0.84		
19.2	1.27			1.04			1.0			0.84		
31.34	1.35			0.47			1.1			0.35		

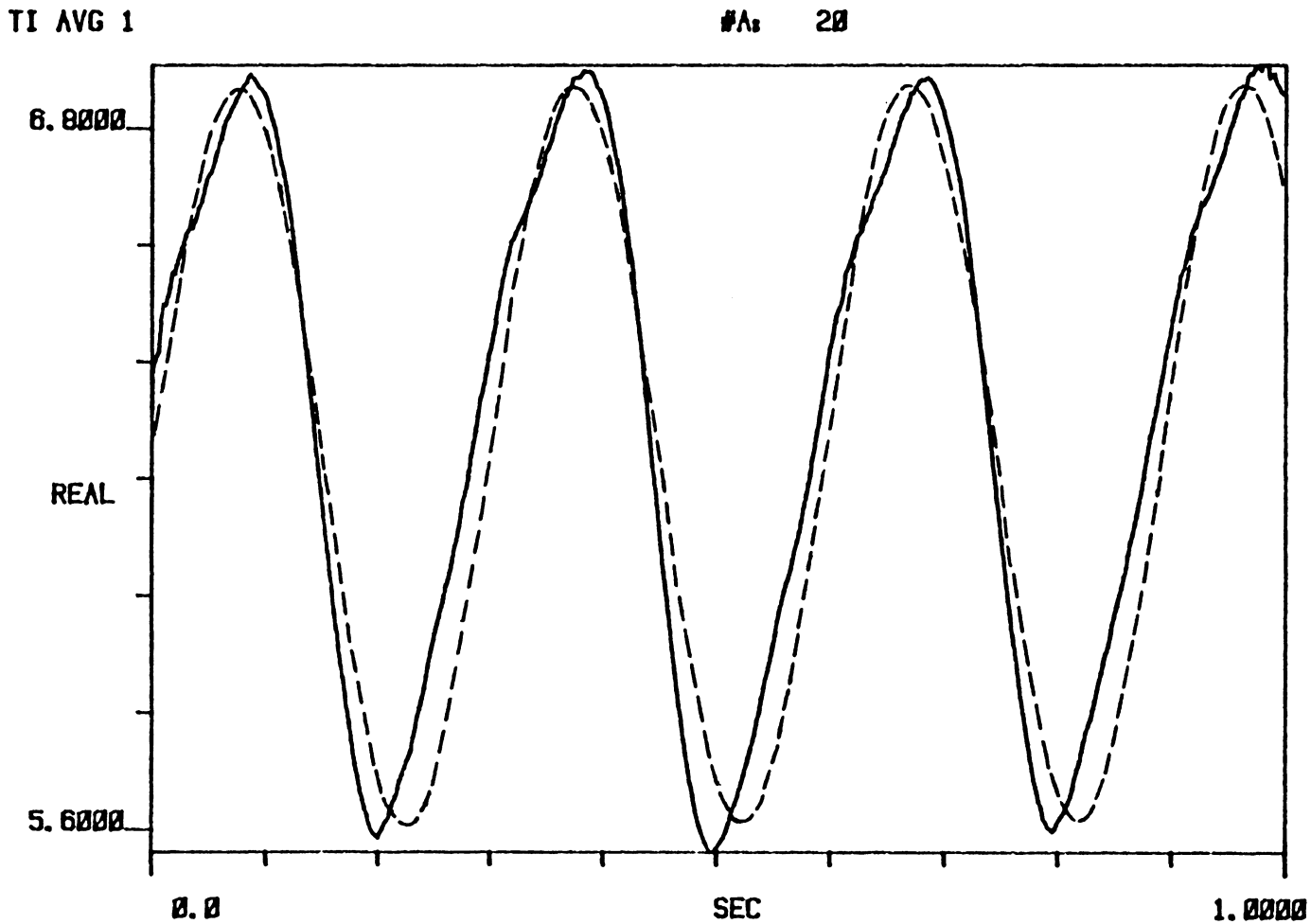

FIGURE 27: THE BEST VELOCITY WAVEFORM FOR SHUTTERS SETTING B AT 3.4 Hz. BOTH PLATES ARE REMOVED (U = 17 m/sec).

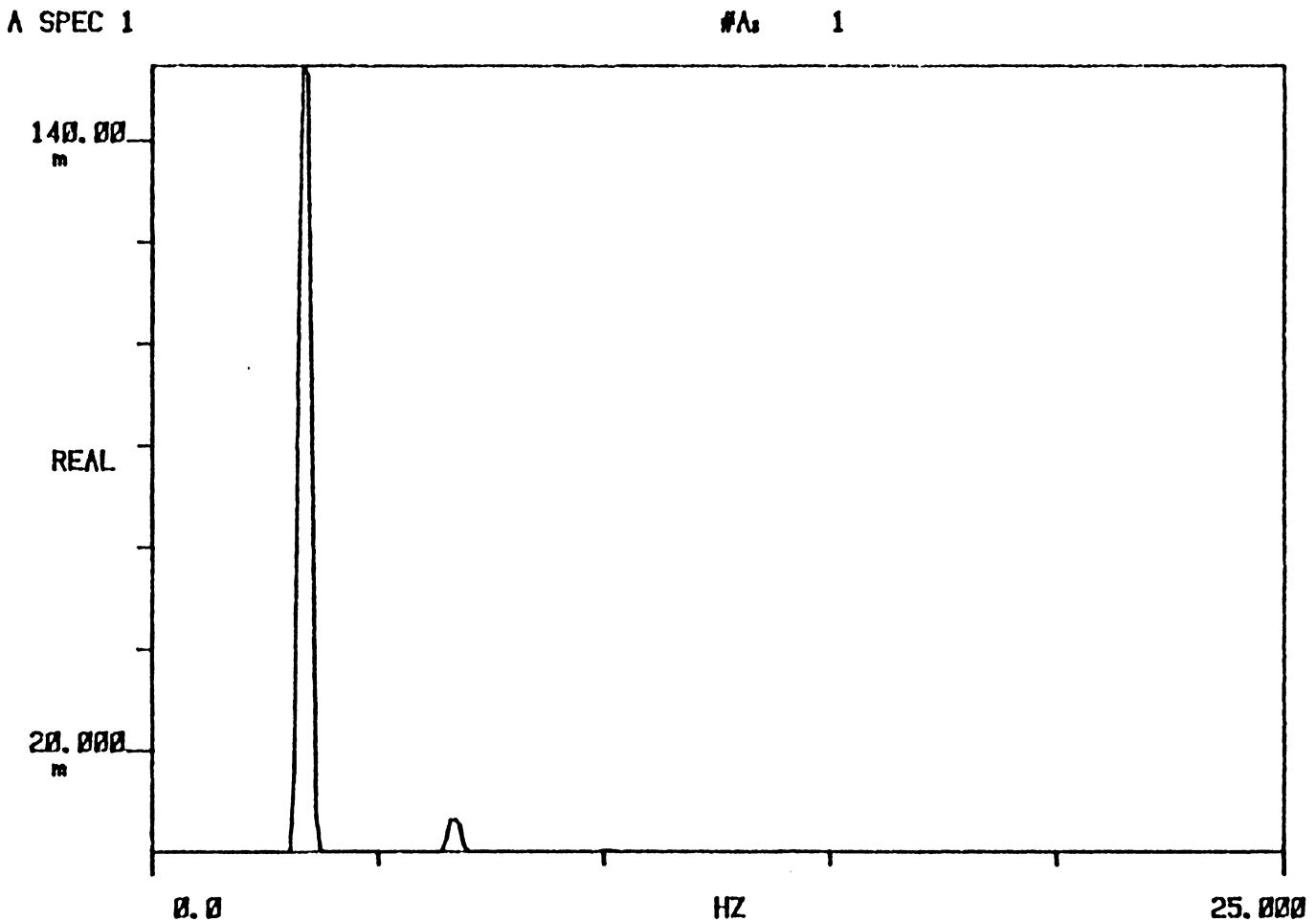

FIGURE 28: THE FREQUENCY SPECTRUM AT 3.4 Hz FOR SHUTTERS SETTING B. BOTH PLATES ARE REMOVED (U = 17 m/sec).

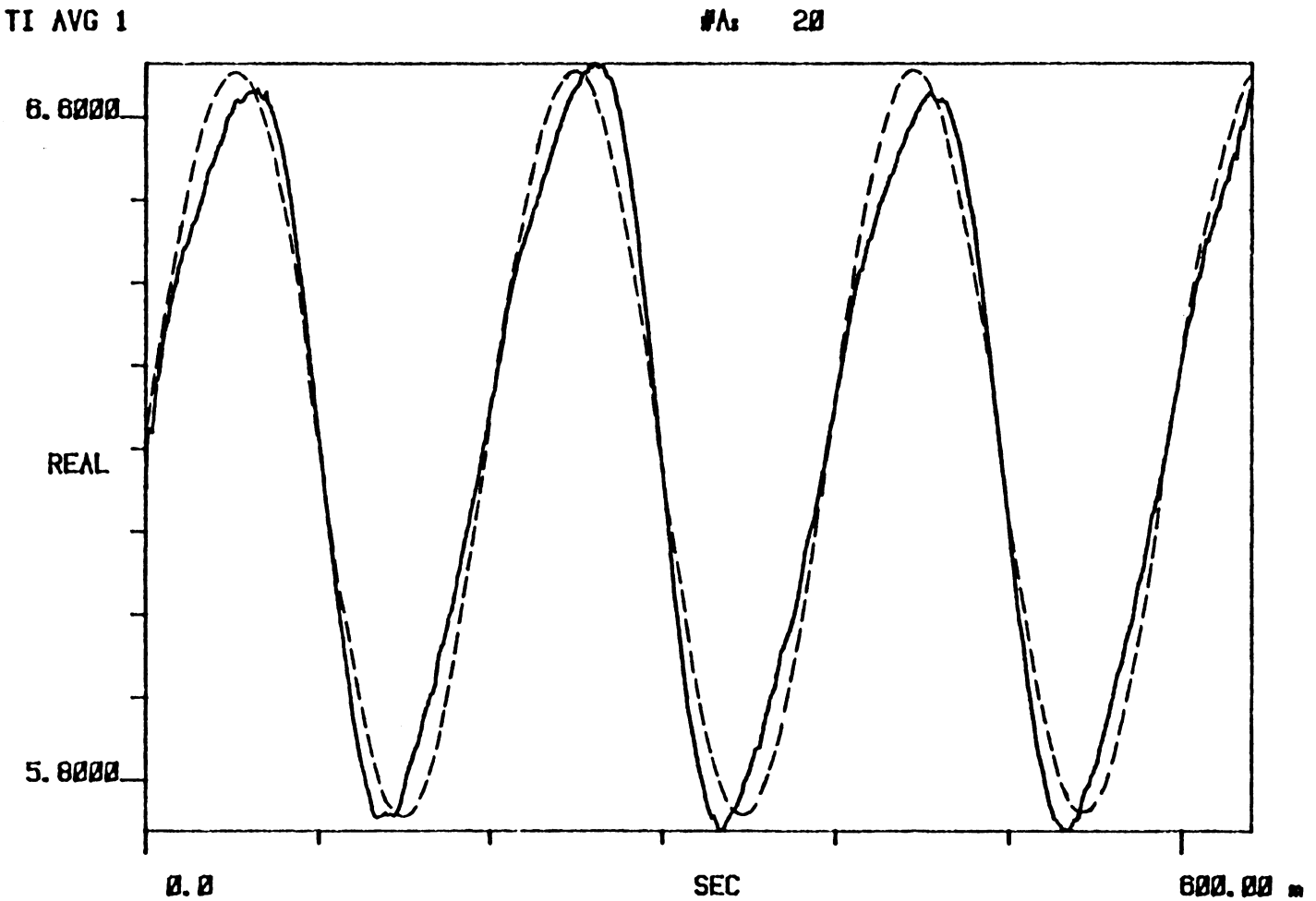

FIGURE 29: THE BEST VELOCITY WAVEFORM FOR SHUTTERS SETTING B AT 5.0 Hz. BOTH PLATES ARE REMOVED (U = 17 m/sec).

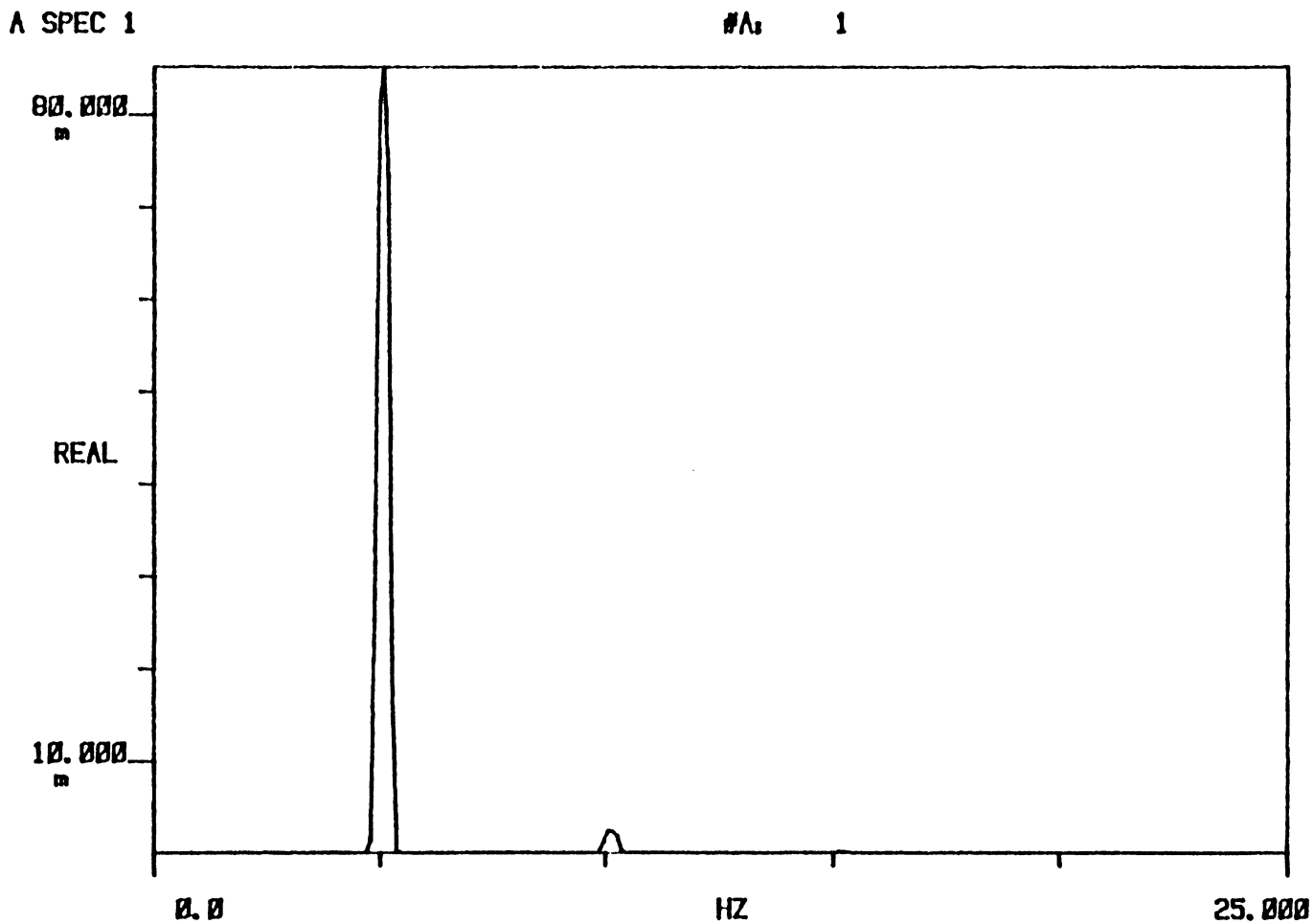

FIGURE 30: THE FREQUENCY SPECTRUM AT 5.0 Hz FOR SHUTTERS SETTING B. BOTH PLATES ARE REMOVED (U = 17 m/sec).

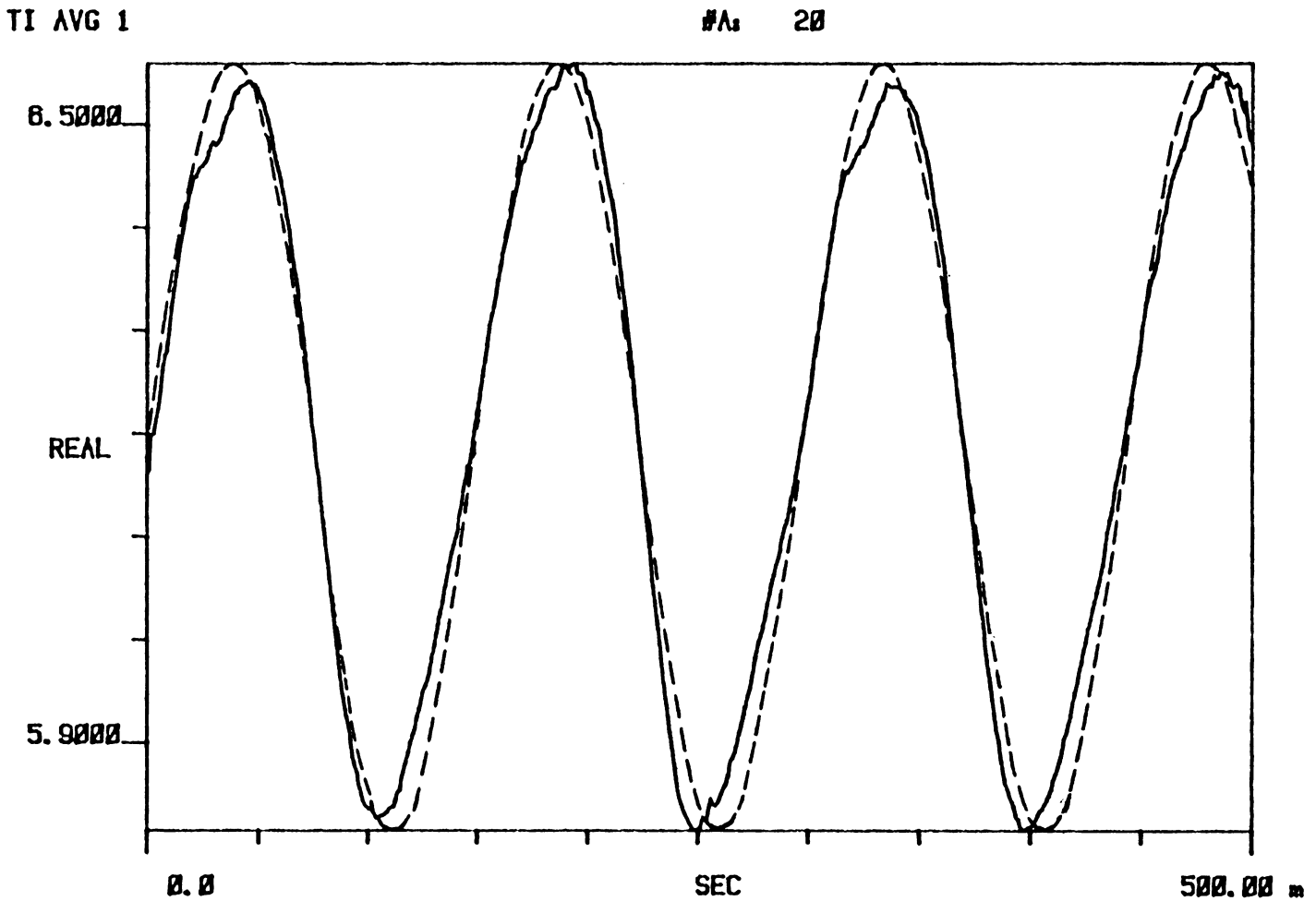

FIGURE 31: THE BEST VELOCITY WAVEFORM FOR SHUTTERS SETTING B AT 6.8 Hz. BOTH PLATES ARE REMOVED (U = 17 m/sec).

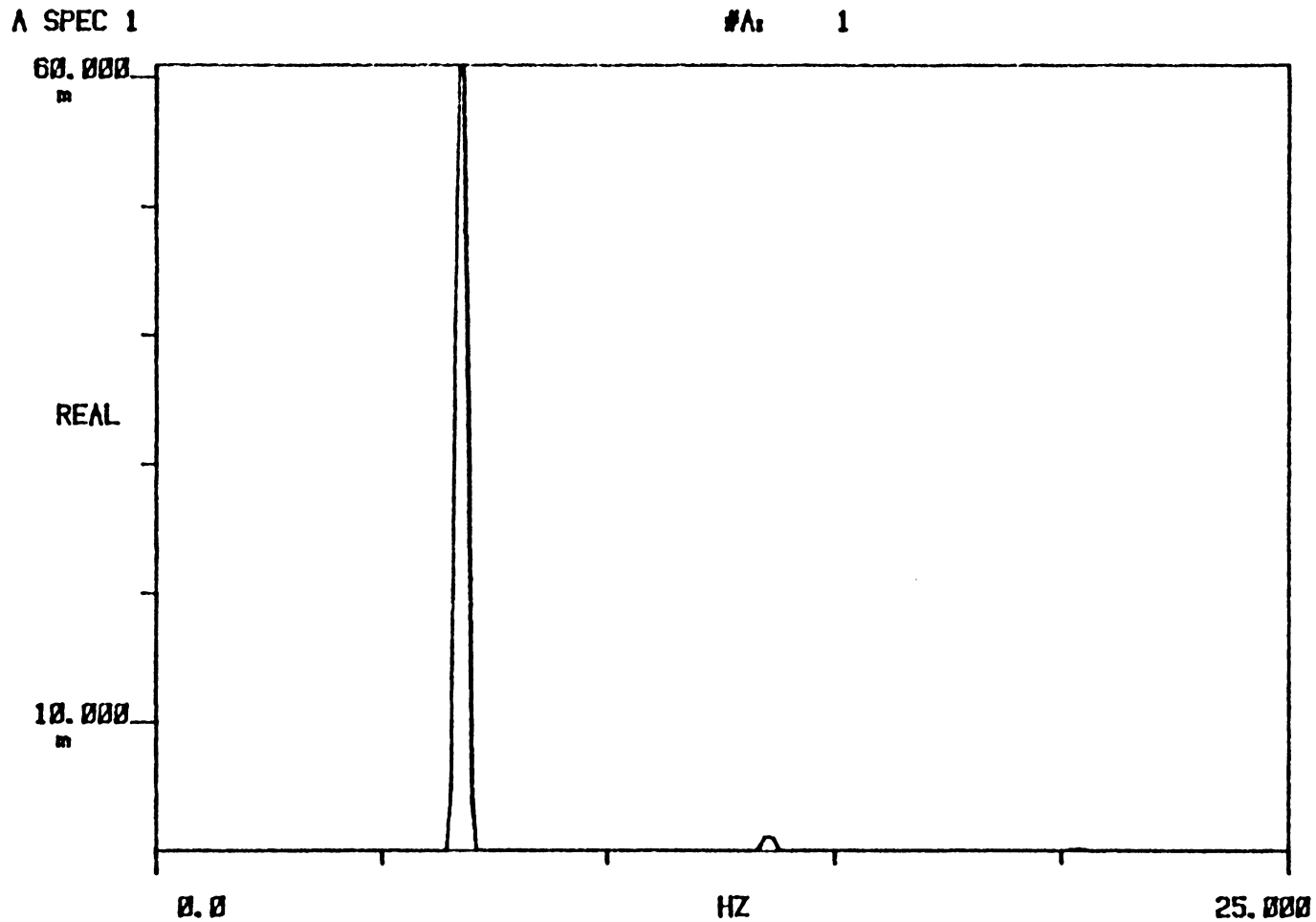

FIGURE 32: THE FREQUENCY SPECTRUM AT 6.8 Hz FOR SHUTTERS SETTING B. BOTH PLATES ARE REMOVED (U = 17 m/sec).

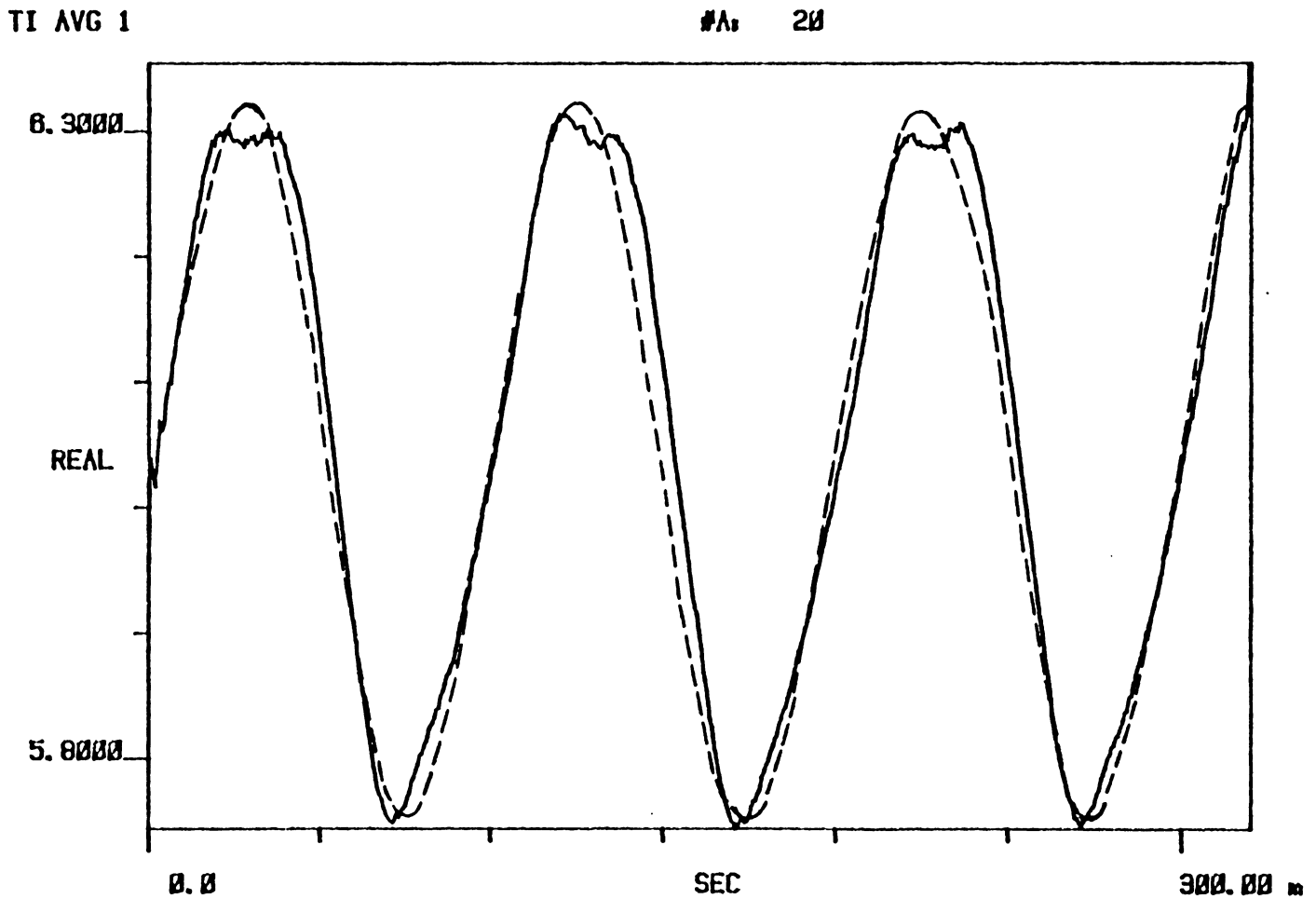

FIGURE 33: THE BEST VELOCITY WAVEFORM FOR SHUTTERS SETTING B at 10.0 Hz BOTH PLATES ARE REMOVED (U = 17 m/sec).

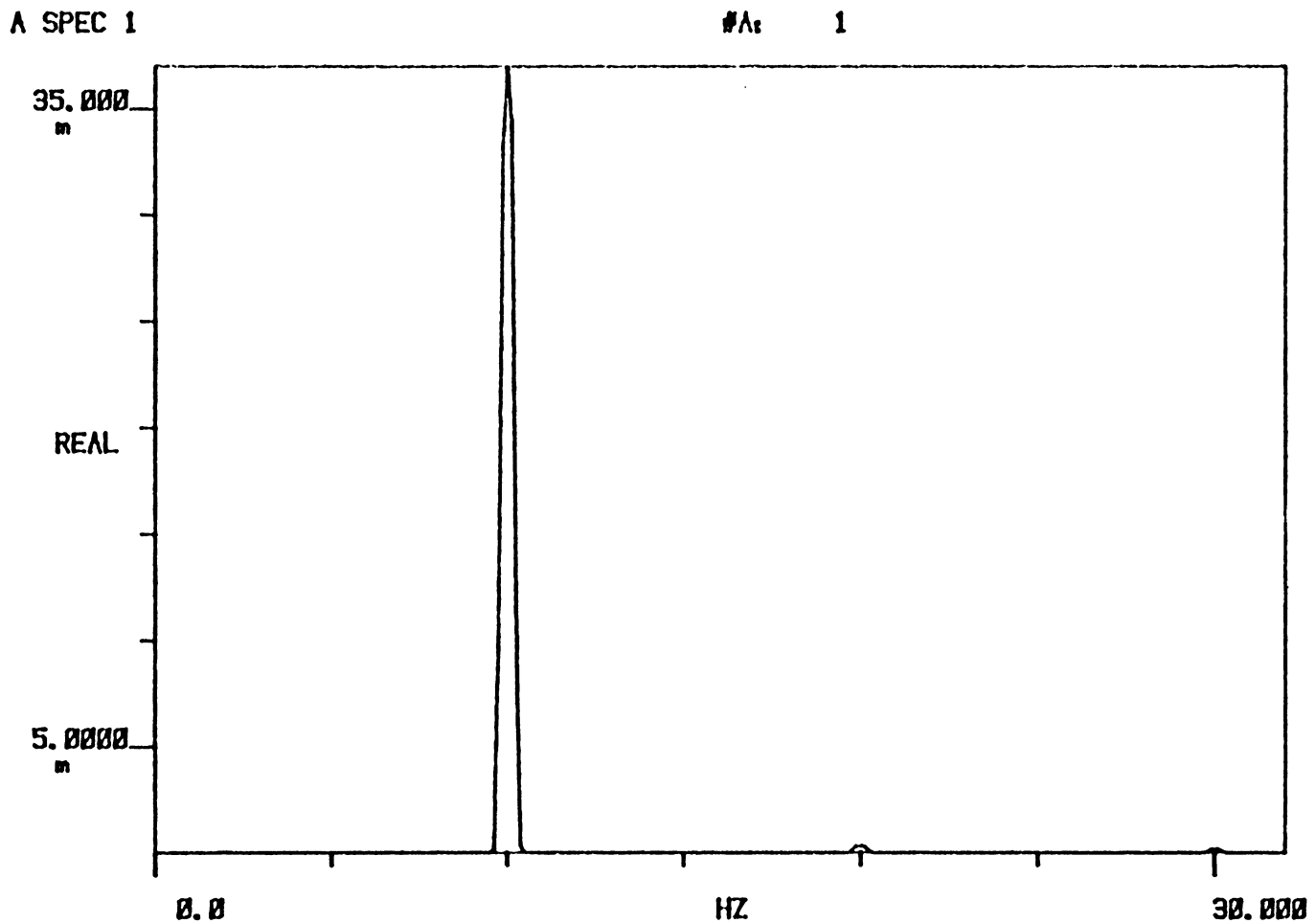

FIGURE 34: THE FREQUENCY SPECTRUM AT 10 Hz FOR SHUTTERS SETTING B. BOTH PLATES ARE REMOVED (U = 17 m/sec).

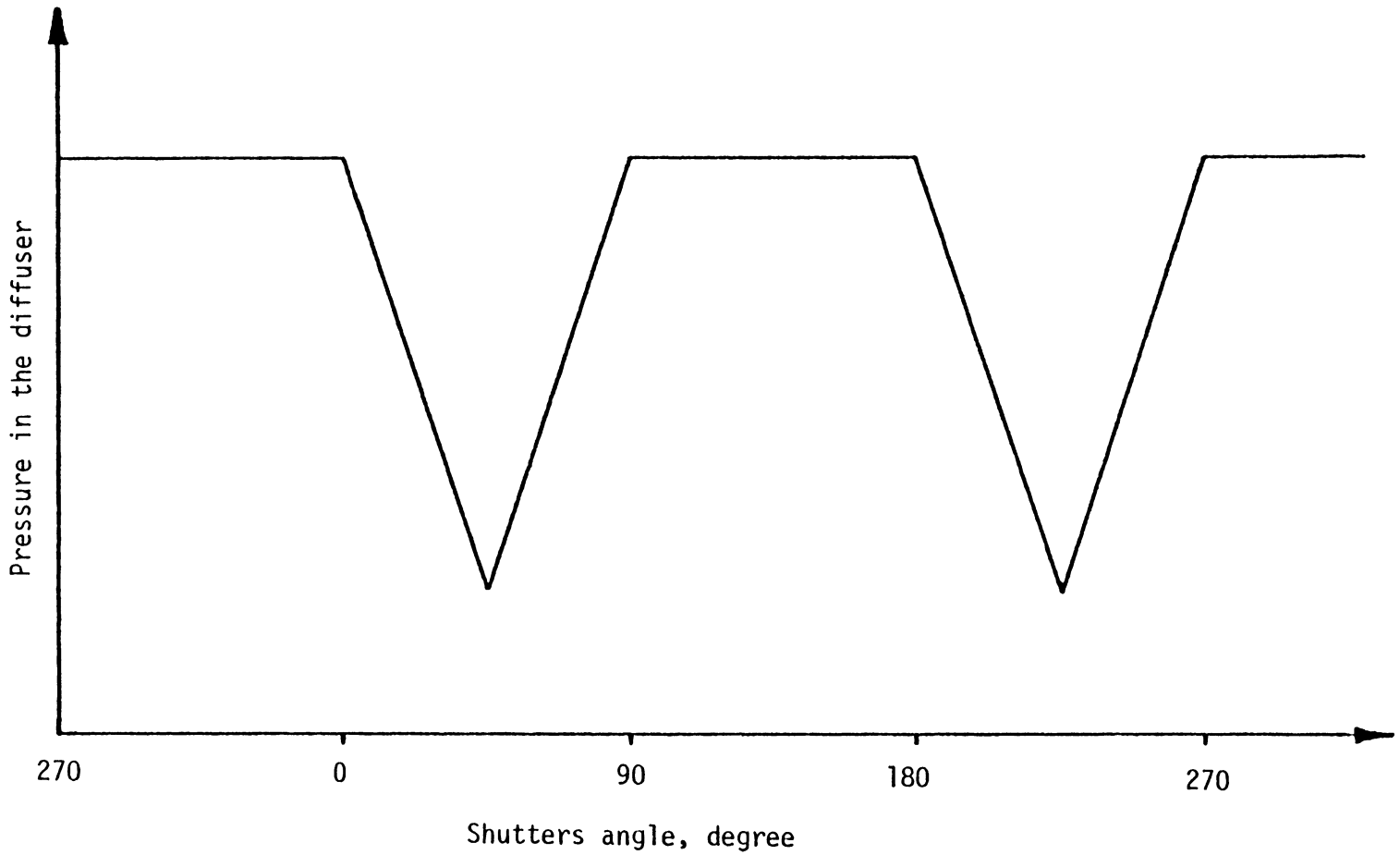

Figure 35: Waveform No. 4 of the pressure distributions for Table 20.

and conditions was much higher than other settings and conditions for these frequencies. The velocity waveforms and corresponding frequency spectra are shown in Figures 36 through 39.

The typical pressure waveform at this higher frequency range was different from the one at low frequency range and is shown in Figure 40.

The best velocity waveform at 31.3 Hz shown in Figure 41 was obtained when the flow was blocked at the blower inlet and the upper plate of the shutters box removed for shutters setting B. The amplitude obtained with this setting and conditions was not much lower than the case with both plates removed and flow not blocked. The typical pressure waveform at this frequency is the same as pressure wave over the frequency range of 16 to 19.2 Hz shown in Figure 40.

The fractions of power at the fundamental frequency are determined from the frequency power spectra and are listed in Table 16. Most of the energy occurs at the fundamental frequency as indicated by the area under the frequency power spectra. The second harmonic contains only a small amount of energy and the third harmonic has essentially none. The quantitative estimate of power at the fundamental frequency is 95% of the total. The power fraction is slightly lower at 3.4 Hz and slightly higher at 19.2 Hz. The power fraction for the original velocity waveforms (setting A, U = 30 $\frac{m}{sec}$, i.e., Figure 17) is as low as 50%. Therefore, the estimated power for the best velocity waveforms shows a big improvement over the original velocity waveforms at setting A. It must be observed that the frequency spectra indicate only the real parts of the energy. There may be some changes regarding the total power of

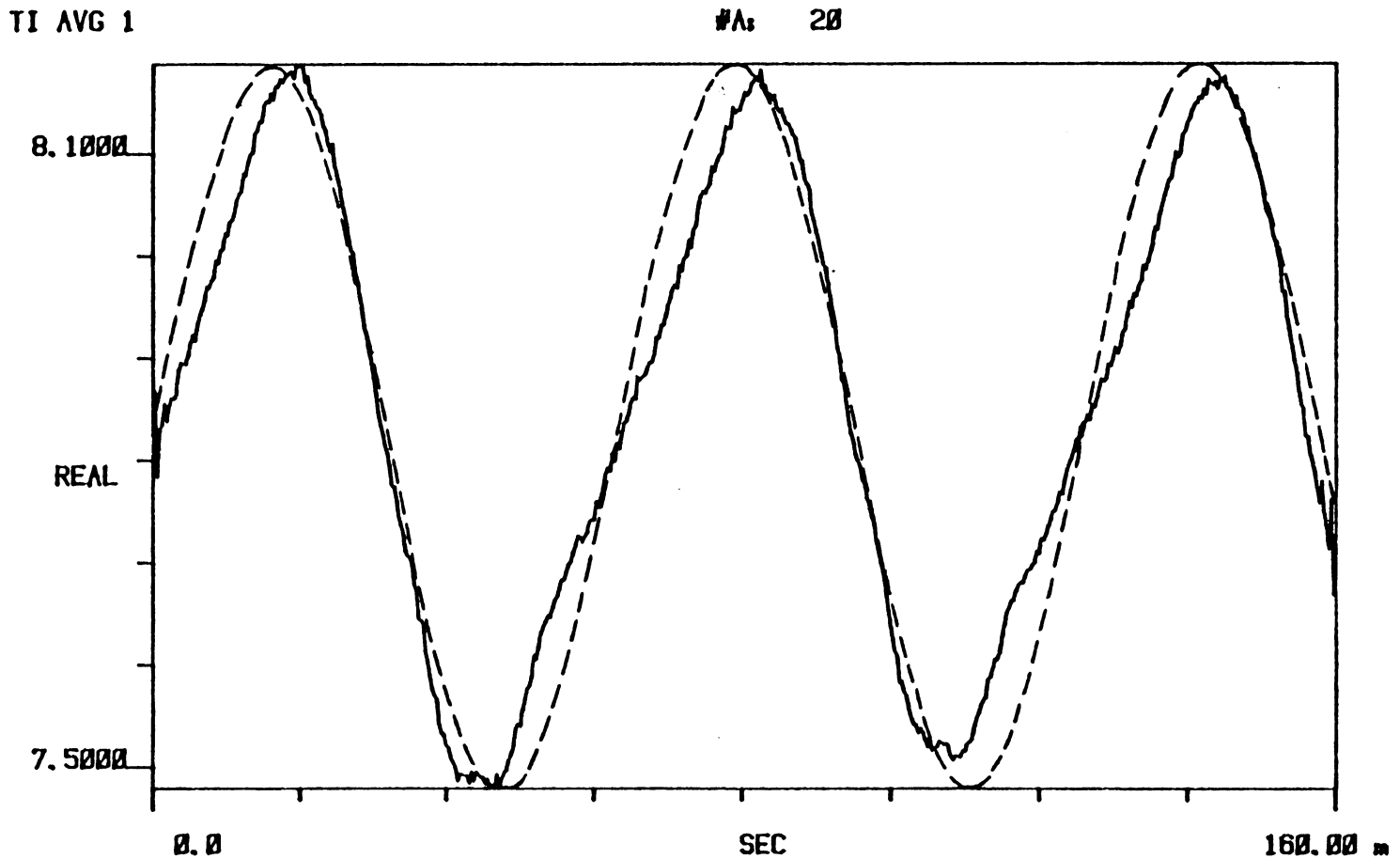

FIGURE 36: THE BEST VELOCITY WAVEFORM FOR SHUTTERS SETTING B AT 16 Hz. UPPER PLATE IS REMOVED (U = 22 m/sec).

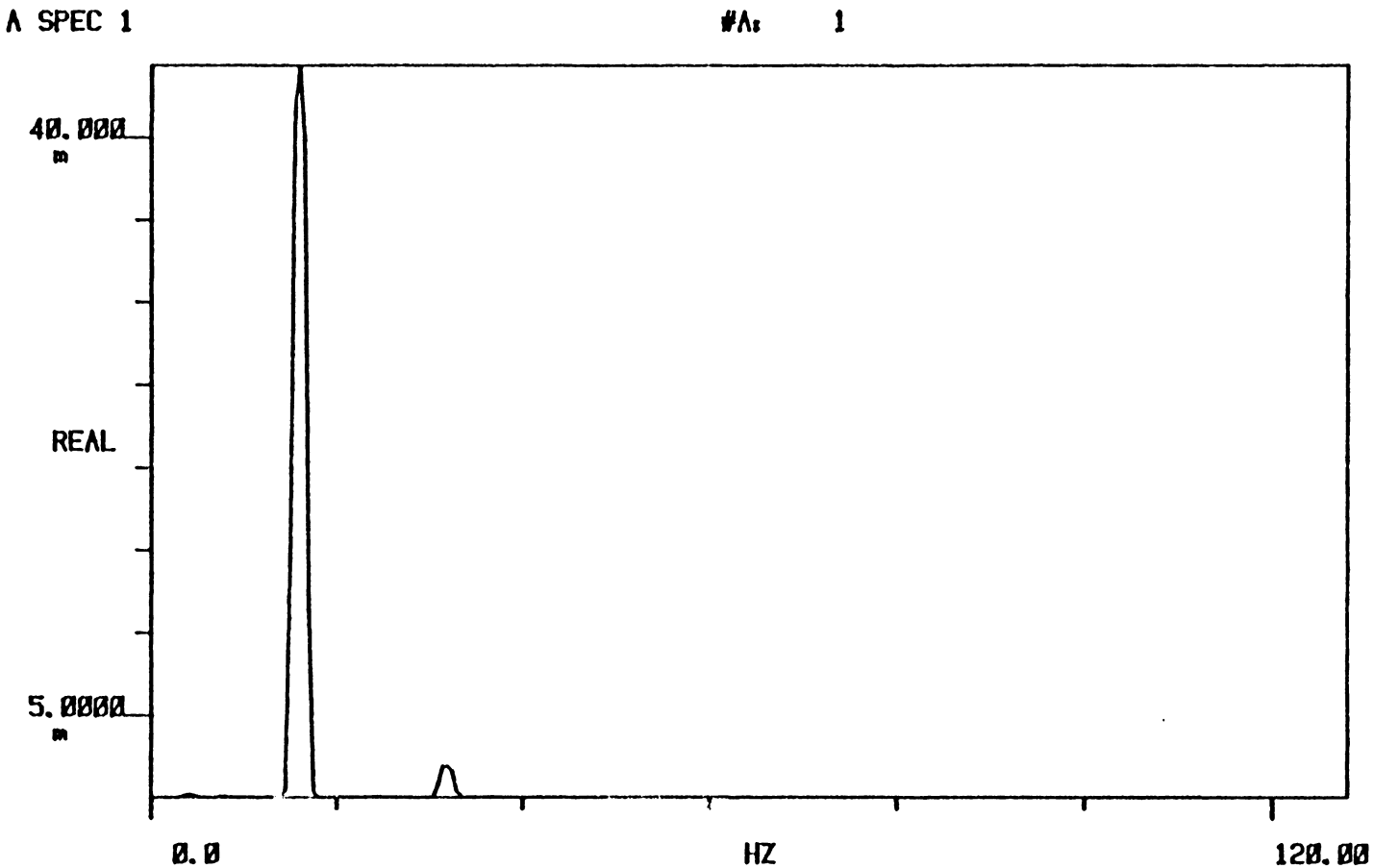

FIGURE 37: THE FREQUENCY SPECTRUM AT 16 Hz FOR SHUTTERS SETTING B. UPPER PLATE IS REMOVED (U = 22 m/sec).

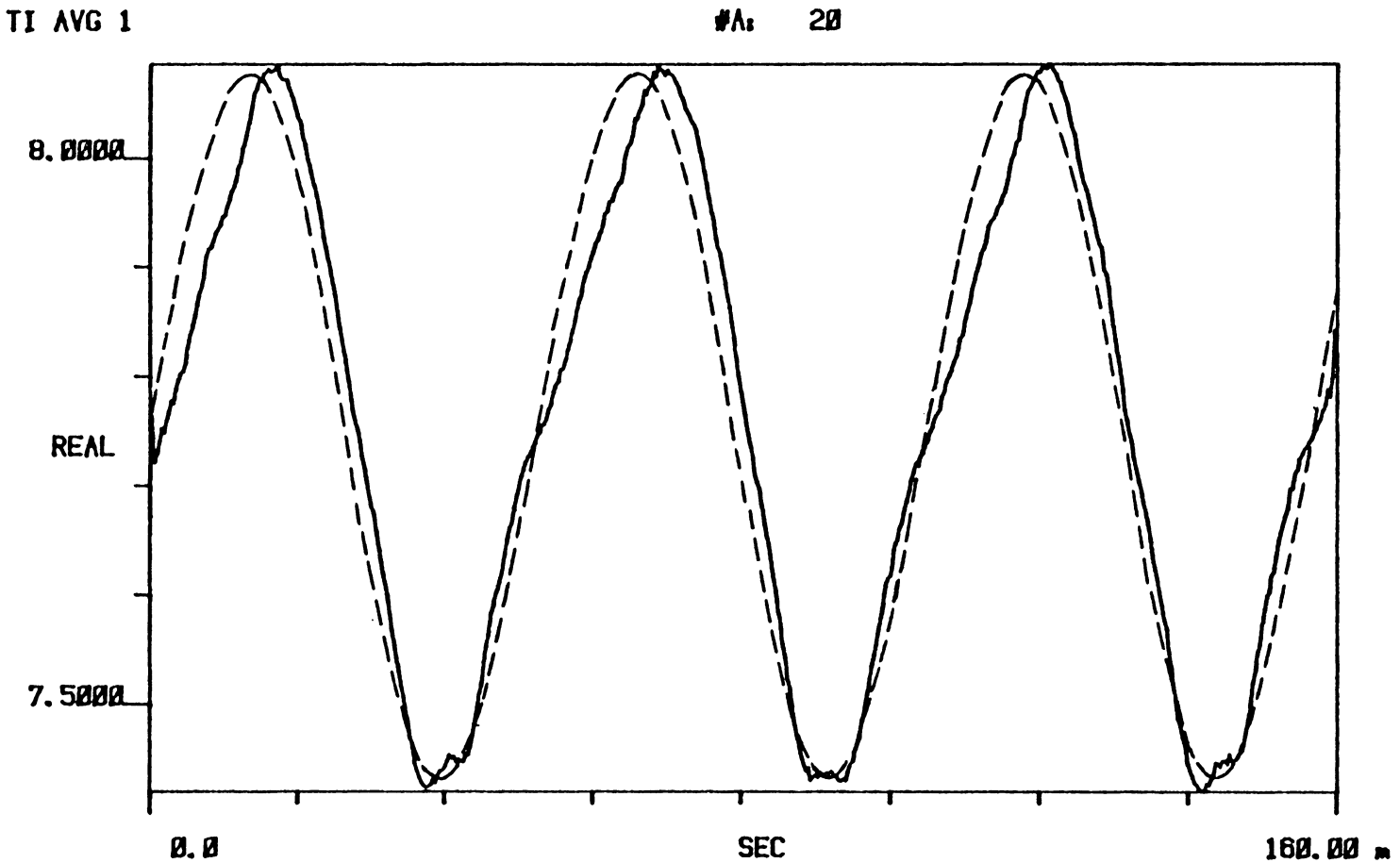

FIGURE 38: THE BEST VELOCITY WAVEFORM FOR SHUTTERS SETTING B AT 19.2 Hz. UPPER PLATE IS REMOVED (U = 22 m/sec).

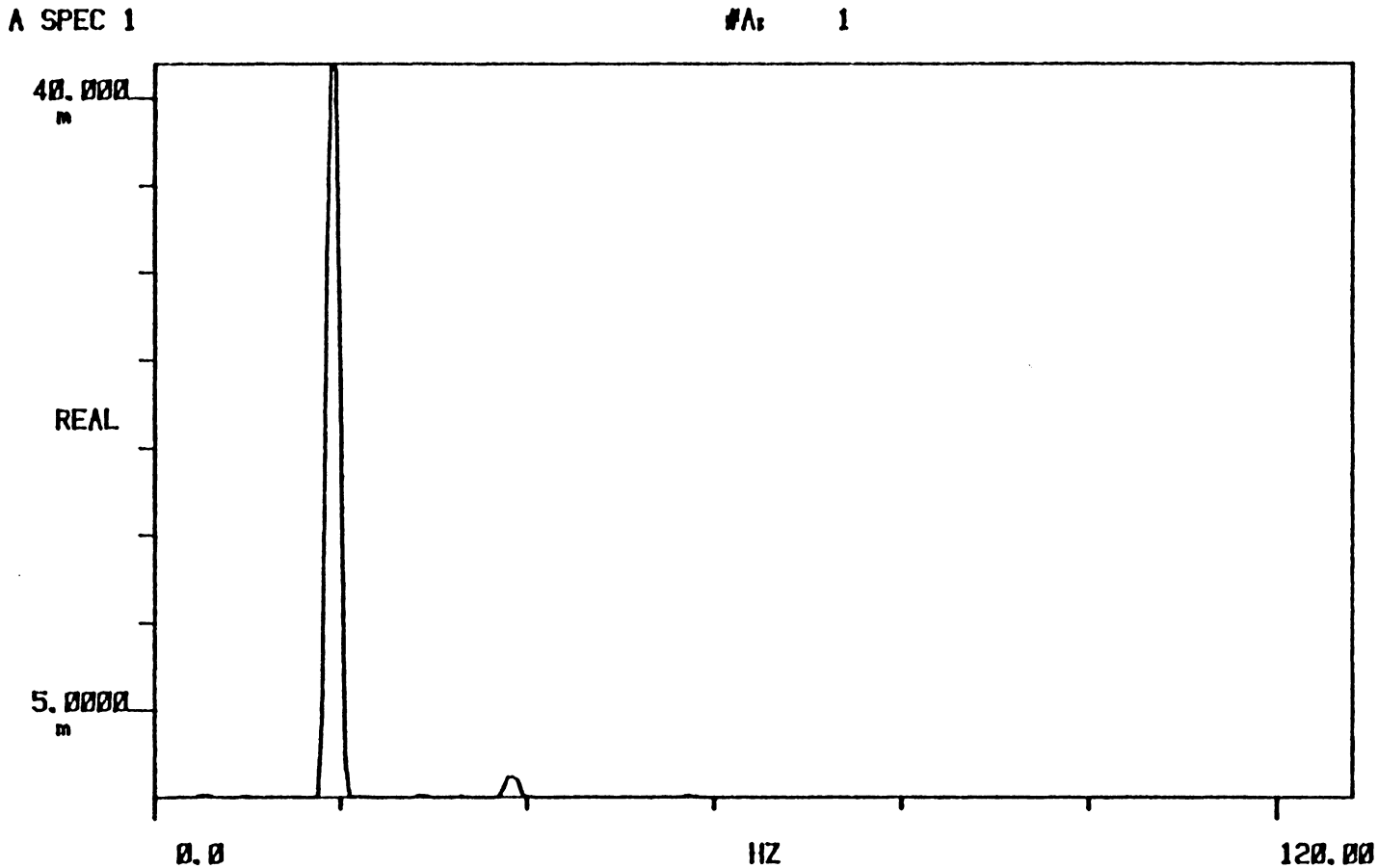

FIGURE 39: THE FREQUENCY SPECTRUM AT 19.2 Hz FOR SHUTTERS SETTING B. UPPER PLATE IS REMOVED (U = 22 m/sec).

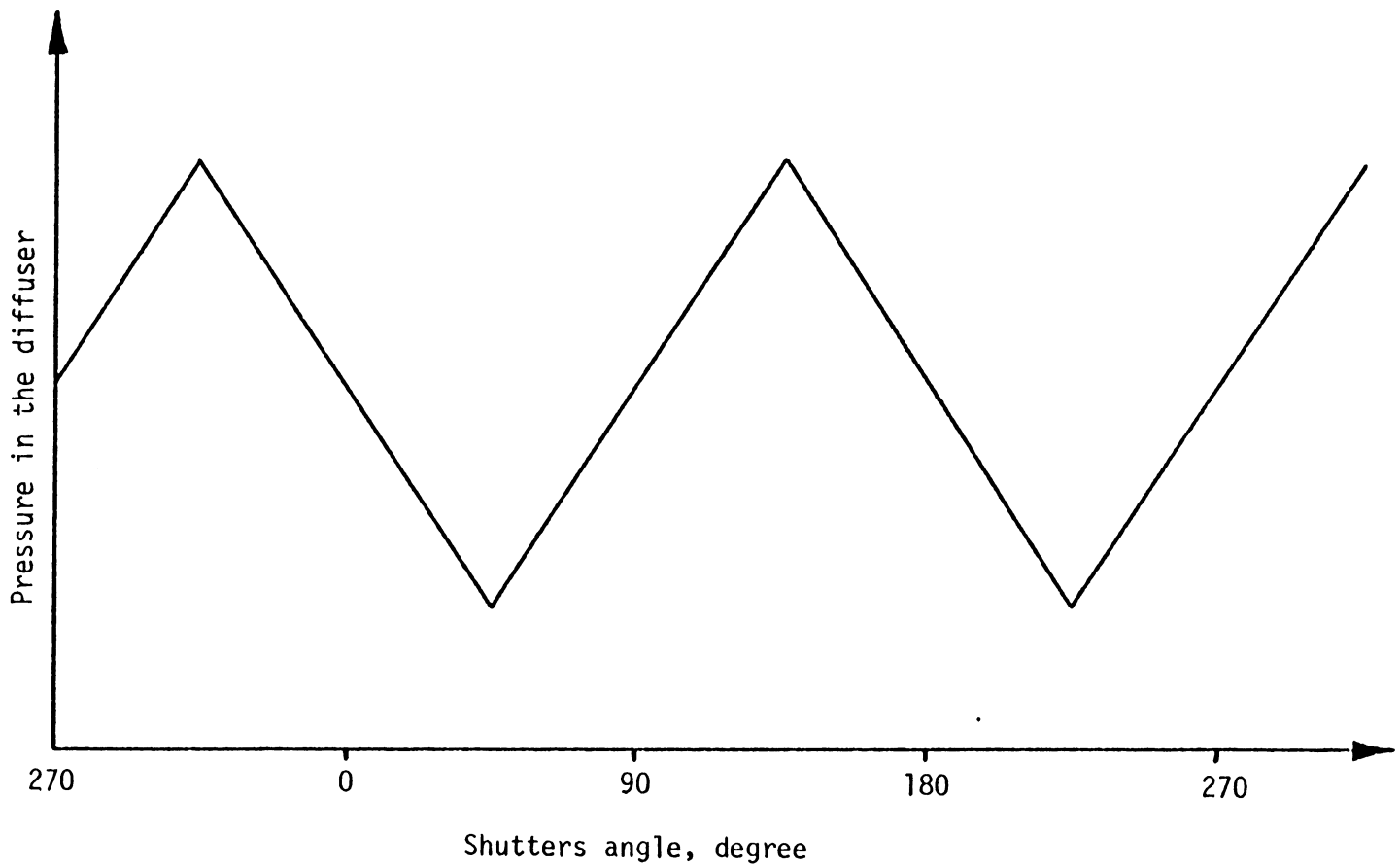

FIGURE 40: WAVEFORM NO. 5 OF THE PRESSURE DISTRIBTIONS FOR TABLE 21.

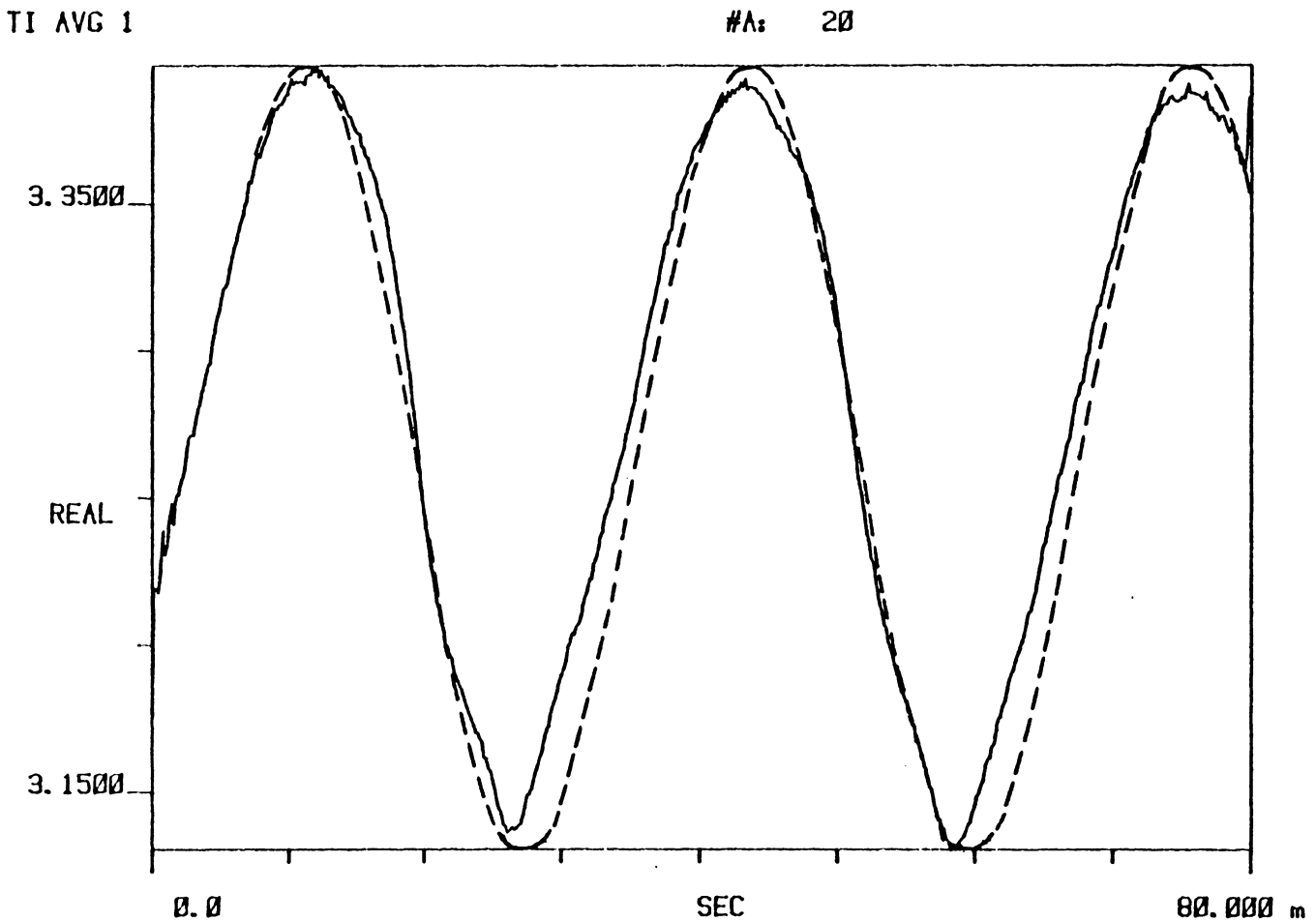

FIGURE 41: THE BEST VELOCITY WAVEFORM FOR SHUTTERS SETTING B AT 31.3 Hz. UPPER PLATE IS REMOVED (U = 10 m/sec).

TABLE 16: THE ENERGY UNDER FREQUENCY SPECTRA

Flow frequency, Hz	Fraction of power at the fundamental frequency (%)
3.38	93.0
5.08	95.0
6.8	96.4
10.0	97.6
16.0	93.5
19.2	95.4

the frequency spectra which must be taken into account.

8. DISCUSSION OF THE RESULTS

From the preliminary results, it was found that the transient pressure changes in the diffuser affect velocity waveforms. The goals of this analysis were to understand how specific pressure waveforms and amplitudes were produced and how these affected the velocity waveforms. Therefore, the pressure variations in the diffuser were grouped into different categories for various shutters settings and conditions at different frequencies. Consequently, five different types of pressure waveforms were identified and all of the pressure measurements for all conditions and frequencies could be grouped into these five types except for five curves.

The velocity waveforms (solid curves) shown in Figures 27, 29, 31, 33, 36, 38, and 41 indicate that they are in a close agreement with the true sinusoidal waveforms (dashed curves). As the velocity increases (decreases) the slope of the measured velocity waveform is less (more) than the true sinusoidal waveform. The slope changes occur at low frequency range.

The air flow was also examined for uniformity in the test section and it was shown to be uniform at different points for steady and unsteady state conditions. One of the velocity waveforms obtained at point ($\frac{y}{h_o} = 0.5$, $\frac{z}{w_o} = 0.5$) is shown in Figure 42 for shutters setting A at 3.4 Hz when both upper and lower plates of the shutters box removed. The uniformity results have been presented in Tables 4 through 7.

Table 17 indicates the peak-to-peak and base pressures for the

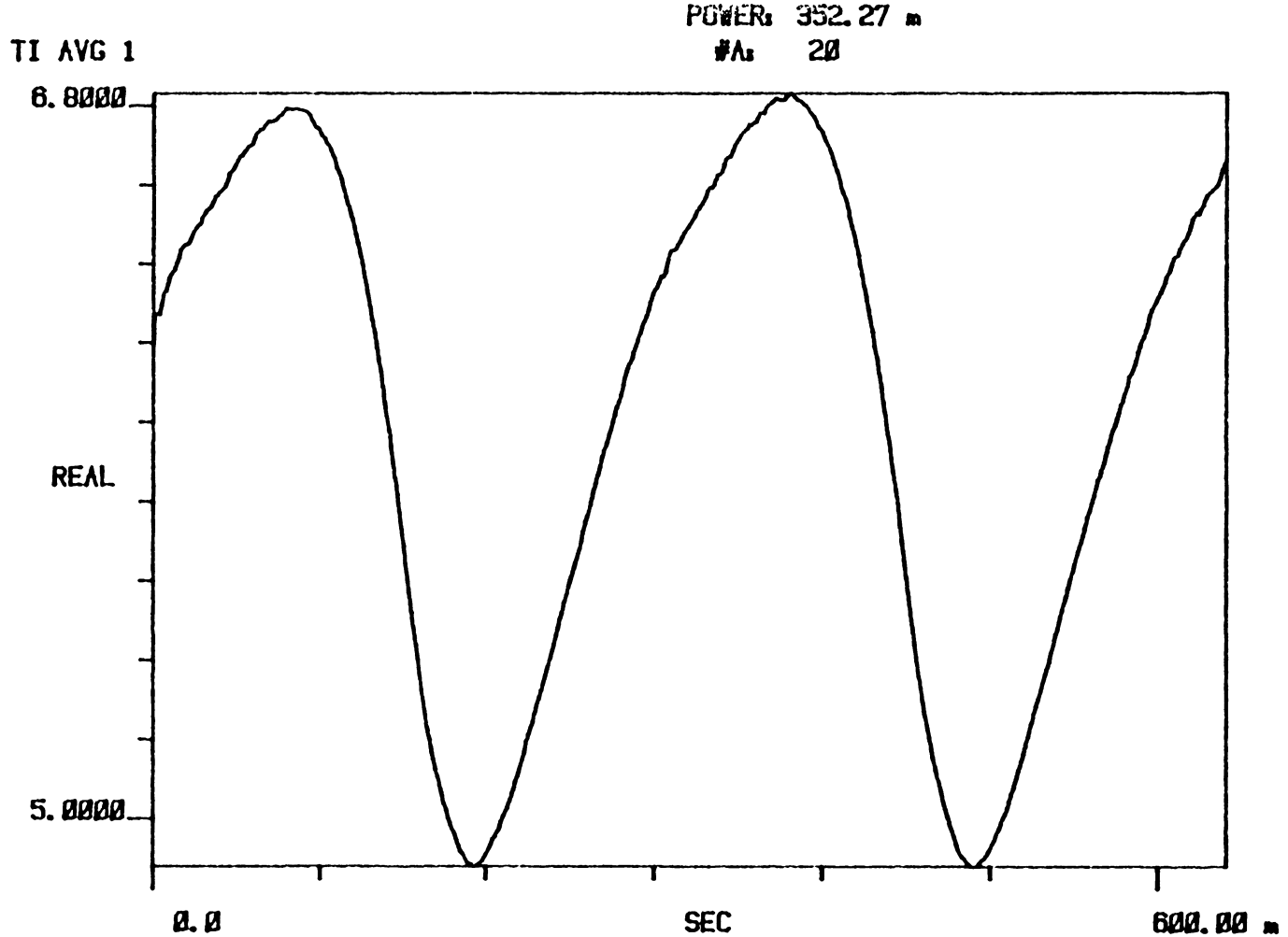

FIGURE 42: SAMPLE VELOCITY WAVEFORM FOR SHUTTERS SETTING A AT POINT ($\frac{y}{h_o}$ = 0.5, $\frac{z}{w_o}$ = 0.5) FOR FLOW UNIFORMITY AT 3.4 Hz. BOTH PLATES ARE REMOVED (U = 16 m/sec).

TABLE 17: VARIATION OF PRESSURE CORRESPONDING TO WAVEFORM NO. 1 FOR THE FOLLOWING SHUTTERS SETTINGS AND CONDITIONS.

Flow Frequency, Hz	Peak-to-Peak Pressure, in H_2O	Base Pressure, in H_2O	Flow Frequency, Hz	Peak-to-Peak Pressure, in H_2O	Base Pressure, in H_2O
	Shutters Setting A, Degree			Shutters Setting A, Degree	
	0 0 0 0 0 0			0 0 0 0 0 0	
	U = 30 m/sec			U = 15 m/sec	
3.38	1.11	2.44	3.38	0.42	1.1
5.08	1.72	1.58	5.08	0.20	1.1
6.8	1.72	1.82	6.8	0.26	1.07
10.0	2.48	1.82	31.34	0.8	1.1

TABLE 17: cont'd.

Flow Frequency, Hz	Peak-to-Peak Pressure, in H_2O			Base Pressure, in H_2O		
	Shutters Setting B, Degree					
	0	30	0	0	30	0
	U = 30 m/sec					
3.38	0.36			1.1		
5.08	0.55			1.1		
6.8	0.46			1.12		
10.0	1.17			1.1		
31.34	1.27			1.58		

Flow Frequency, Hz	Peak-to-Peak Pressure, in H_2O			Base Pressure, in H_2O		
	Shutters Setting B, Degree					
	0	30	0	0	30	0
	U = 15 m/sec					
3.38	0.045			0.015		
5.08	0.040			0.015		
6.8	0.015			0.015		
10.0	0.05			0.015		
16.0	0.114			0.015		
19.2	0.284			0.016		
31.34	0.704			0.016		

TABLE 17: cont'd.

Flow Frequency, Hz	Peak-to-Peak Pressure, in H_2O			Base Pressure, in H_2O		
	Shutters Setting B, Degree					
	0	30	0	0	30	0
	Upper plate is removed (U = 22 m/sec)					
10.0	1.26			1.1		
31.34	2.3			1.95		

TABLE 17: cont'd.

Flow Frequency, Hz	Peak-to-Peak Pressure, in H_2O			Base Pressure, in H_2O			Peak-to-Peak Pressure, in H_2O			Base Pressure, in H_2O		
	Shutters Setting A, Degree						Shutters Setting B, Degree					
	0	0	0	0	0	0	0	30	0	0	30	0
	Both plates are removed ($U \approx 16$ m/sec)						Both plates are removed ($U \approx 17$ m/sec)					
31.34	1.35			0.47			1.10			0.35		

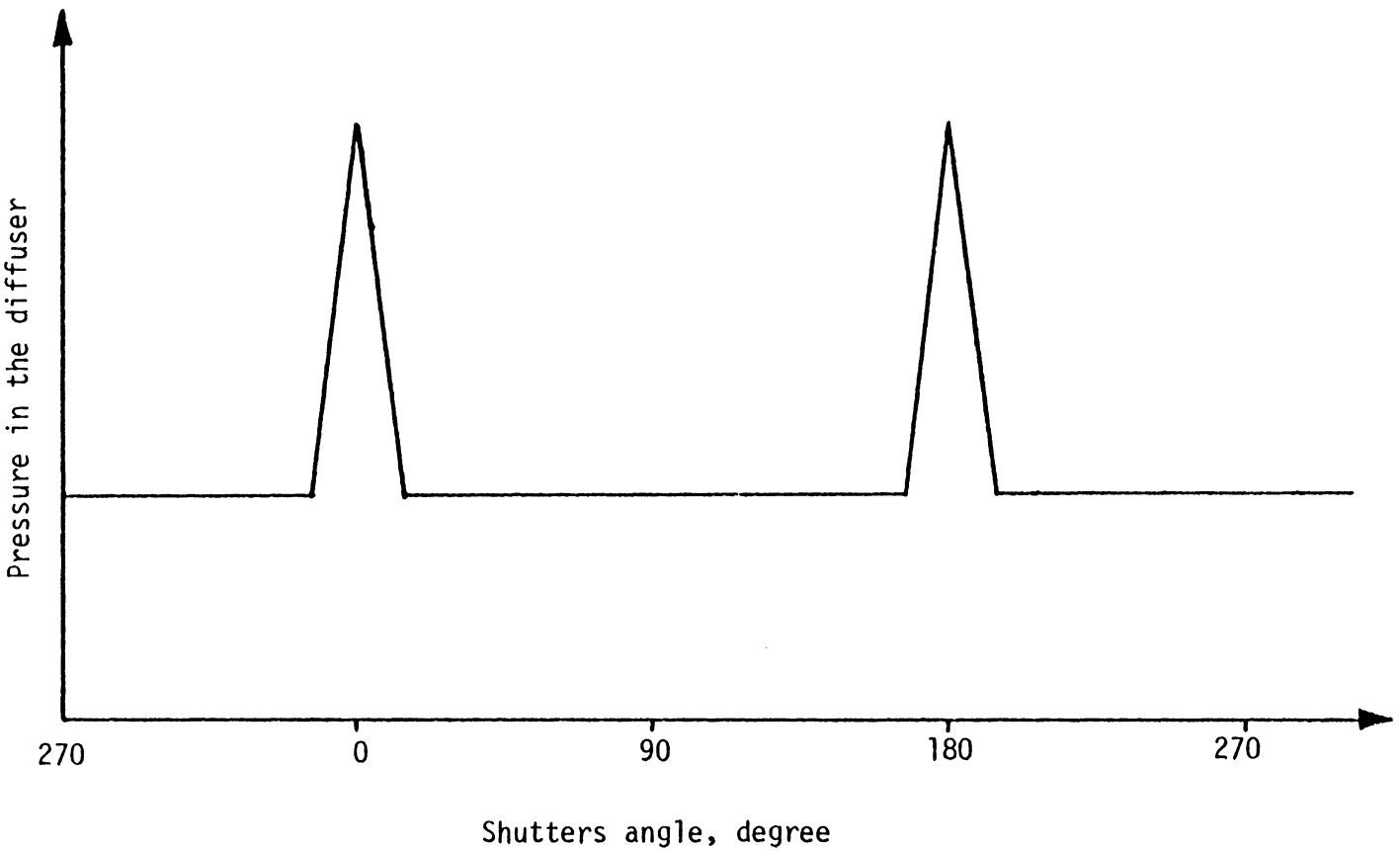

FIGURE 43: WAVEFORM No. 1 OF THE PRESSURE DISTRIBUTIONS FOR TABLE 17.

shutters settings and conditions listed. The corresponding pressure waveform is shown in Figure 43. For the conditions in Table 17 the pressure fluctuation in the diffuser caused by shutters rotation remains constant when the shutters are open until they are closed. At the closed position of the shutters the pressure increased sharply because the shutters vertical placing caused a large area of flow blockage and hence larger pressure fluctuation in the diffuser. As the shutters opened the pressure returned to the base pressure value because the area of flow blockage was small compared to the closed position of the shutters. One significant exception was shutters setting B when the flow was blocked at the blower inlet. In this case, part of the pressure build-up in the diffuser was lowered by blocking the incoming flow. The entire frequency range gave this type of pressure waveform, although the amplitude was very small. The amplitude of this type of pressure waveform was relatively small but still resulted in blips on velocity waveform. This type of pressure waveform occurred mostly at the low frequency range of 3.4 to 10.0 Hz and at the higher frequency of 31.3 Hz.

The second type of pressure waveform in the diffuser is shown in Figure 44 for the shutters settings and conditions listed in Table 18. This waveform showed a sharp decrease in pressure when the shutters were closed over the frequency range of 3.4 to 19.2 Hz. This occurred primarily when the plates of the shutters box were removed. Therefore, the pressure in the diffuser was released through the openings of the shutters box. The pressure then increased when the shutters reached a

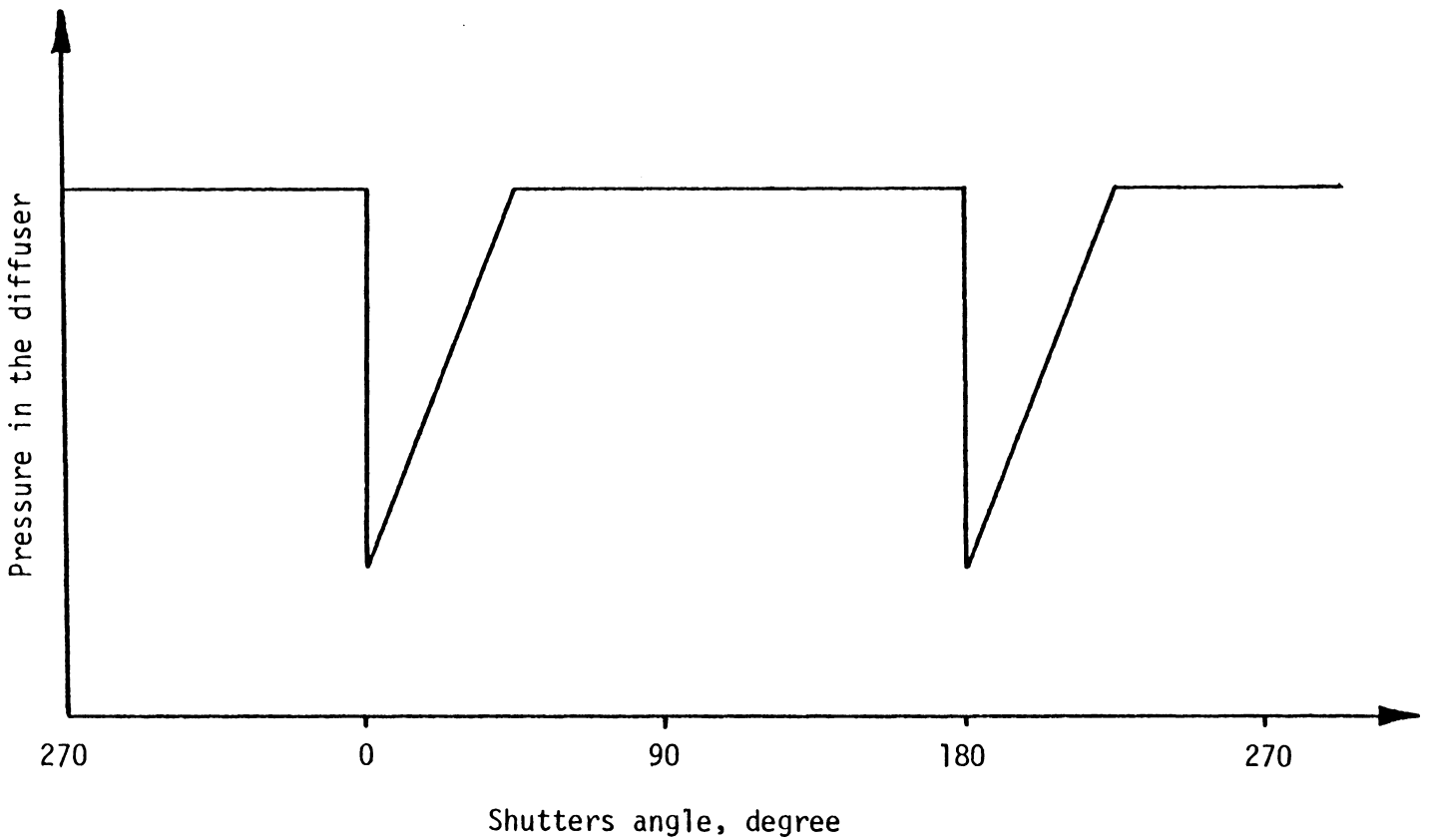

FIGURE 44: WAVEFORM NO. 2 OF THE PRESSURE DISTRIBUTIONS FOR TABLE 18.

TABLE 18: VARIATION OF PRESSURE CORRESPONDING TO WAVEFORM NO. 2 FOR THE FOLLOWING SHUTTERS SETTING AND CONDITIONS.

Flow Frequency, Hz	Peak-to-Peak Pressure, in H_2O			Base Pressure, in H_2O		
	Shutters Setting A, Degree					
	0	0	0	0	0	0
	U = 30 m/sec					
16.0	1.80			2.68		

Flow Frequency, Hz	Peak-to-Peak Pressure, in H_2O			Base Pressure, in H_2O		
	Shutters Setting A, Degree					
	0	0	0	0	0	0
	U = 15 m/sec					
16.0	0.94			0.74		
19.2	1.11			0.96		

TABLE 18: cont'd

Flow Frequency, Hz	Peak-to-Peak Pressure, in H_2O	Base Pressure, in H_2O
	Shutters Setting A, Degree	
	0 0 0	0 0 0
	Upper plate is removed (U = 20 m/sec)	
3.38	0.28	1.1
5.08	0.85	1.1
6.8	1.12	1.1
10.0	1.24	1.1
16.0	1.24	1.1
19.2	1.24	1.1

Flow Frequency, Hz	Peak-to-Peak Pressure, in H_2O	Base Pressure, in H_2O
	Shutters Setting A, Degree	
	0 0 0	0 0 0
	Both plates are removed (U = 16 m/sec)	
3.38	1.15	1.1
6.8	1.27	1.1
10.0	1.31	1.1
16.0	1.25	1.04
19.2	1.27	1.04

45 degrees angle and it remained constant until the next closing of the shutters where it decreased sharply again. The assymetry of the waveform can be explained by the guidance of flow out through the openings when the shutters were between 0° and 45°. This is illustrated in Figure 45. The amplitude of the pressure waveform was comparatively high and directed the pressure to decrease. This gave reasonable sinusoidal velocity waveforms. It is interesting to note that only shutters setting A with four different conditions has this type of pressure waveform.

The pressure waveform in Figure 46 described the pressure fluctuation in the diffuser for higher frequencies of 19.2 Hz and 31.3 Hz. The pressure increased sharply at the time of triggering (at 270 degrees) until the shutters closed where it sharply decreased. The pressure then increased sharply to its base pressure until the next shutters closing occurred where it sharply decreased again. The decrease in pressure occurred when the shutters were open, and it increased when the shutters were closed due to a larger area of flow blockage. This did not provide good sinusoidal velocity waveforms at these frequencies, although the pressure amplitude was relatively high. The results are indicated in Table 19 for various shutters settings.

The pressure waveform shown in Figure 47 was obtained at low frequency range of 3.4 to 10.0 Hz. This waveform correspond to the conditions when both the upper and lower plates of the shutters box were removed and flow was not blocked. It gave the best velocity waveforms. The shutters were in open position (270 degrees) when the

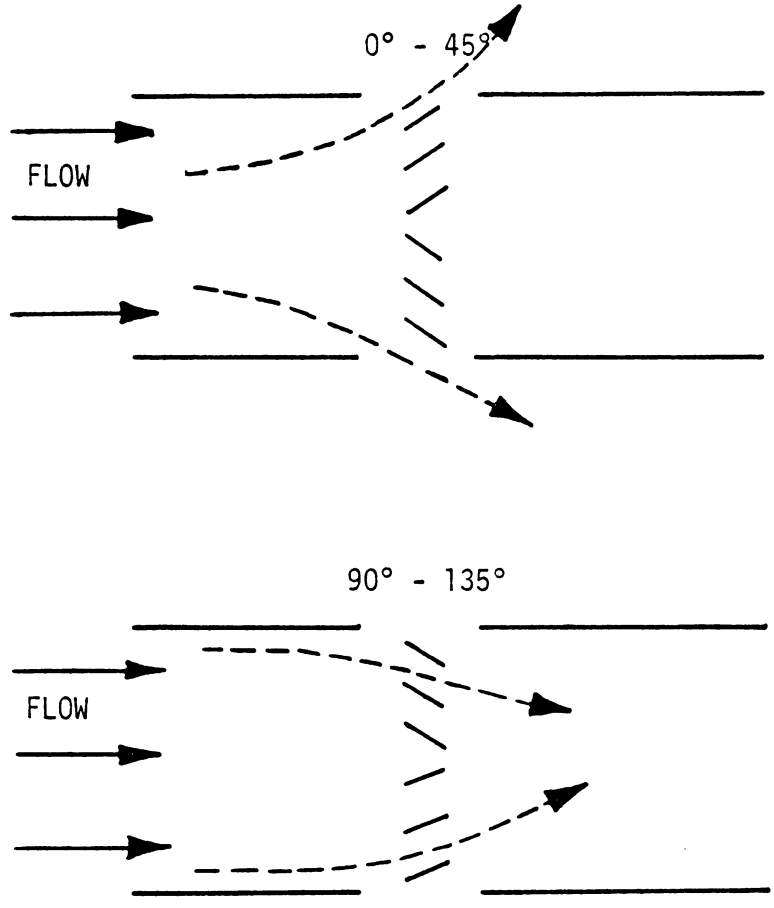

FIGURE 45: INDICATION OF SMALL AREA OF FLOW BLOCKAGE (0° - 45°) AND LARGE AREA OF FLOW BLOCKAGE (90° - 135°).

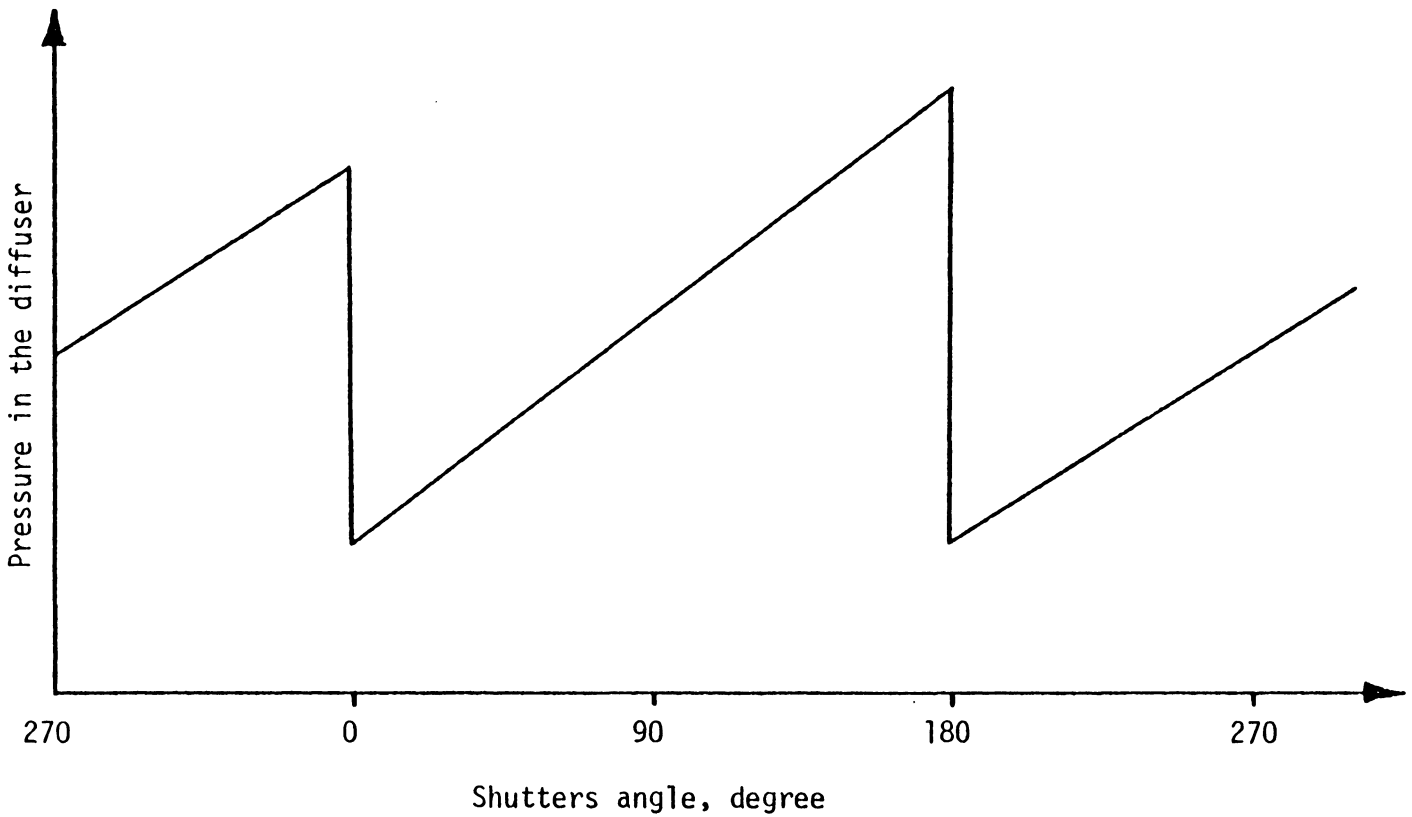

FIGURE 46: WAVEFORM NO. 3 OF THE PRESSURE DISTRIBUTIONS FOR TABLE 19.

TABLE 19: VARIATION OF PRESSURE CORRESPONDING TO WAVEFORM NO. 3 FOR THE FOLLOWING SHUTTERS SETTINGS AND CONDITIONS

Flow Frequency, Hz	Peak-to-Peak Pressure, in H_2O			Base Pressure, in H_2O		
	Shutters Setting A, Degree					
	0	0	0	0	0	0
	U = 30 m/sec					
19.2	2.11			3.54		
31.34	2.7			0.84		

Flow Frequency, Hz	Peak-to-Peak Pressure, in H_2O			Base Pressure, in H_2O		
	Shutters Setting B, Degree					
	0	30	0	0	30	0
	U = 30 m/sec					
19.2	1.96			2.54		

TABLE 19: cont'd.

Flow Frequency, Hz	Peak-to-Peak Pressure, in H_2O			Base Pressure, in H_2O		
	Shutters Setting A, Degree					
	0	0	0	0	0	0
	Upper plate is removed (U = 20 m/sec)					
31.34	1.75			1.05		

Flow Frequency, Hz	Peak-to-Peak Pressure, in H_2O			Base Pressure, in H_2O		
	Shutters Setting A, Degree					
	0	0	0	0	0	0
	Both plates are removed (U = 16 m/sec)					
5.08	1.16			0.84		

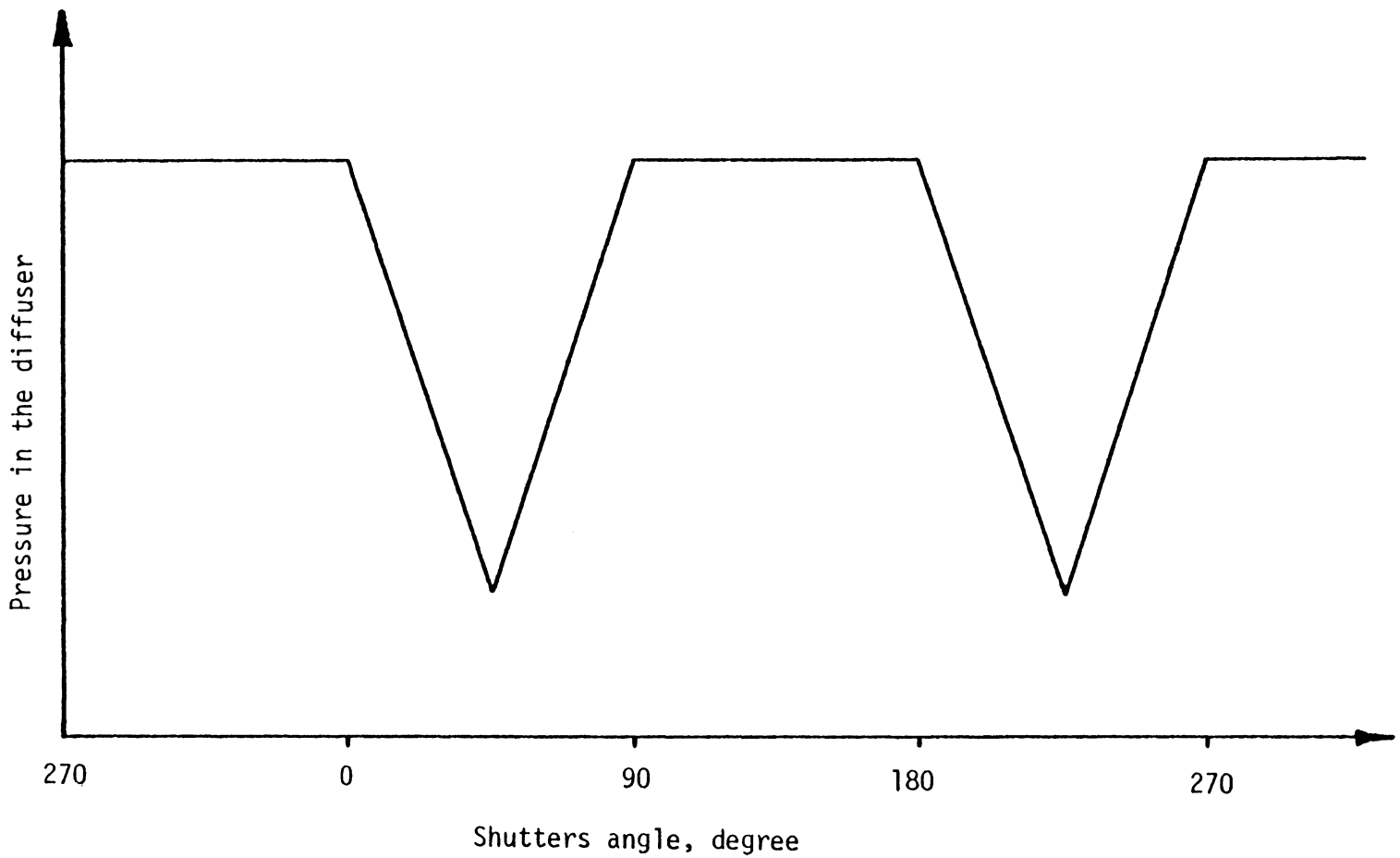

FIGURE 47: WAVEFORM NO. 4 OF THE PRESSURE DISTRIBUTIONS FOR TABLE 20.

triggering occurred and the pressure remained constant until they were in closed position (zero degree) where the pressure dropoed sharply to its base value. The pressure decrease was because some of the air flow escaped the tunnel through the openings of the shutters box. The mechanism was the same as for the waveform No. 2, illustrated in Figure 45. The two shutters at 30° offset for setting B, however, gave a longer transient in the pressure behind the shutters. The minimum pressure occurred at shutters angle of 45 degrees where the shutters area of flow blockage was less compared to shutters angle at zero degree. The 45-degree angle gave more openings to the flow to escape the tunnel and release the pressure build-up in the diffuser. The pressure then increased to its base value at 90 degrees because the relative positioning of the shutters did not allow the release of pressure build-up and guided the flow in the streamwise direction. At 90 degrees the pressure remained constant again until the shutters were closed at 180 degrees where the pressure decreased sharply to its peak at 225 degrees and then increased sharply until the shutters were open at 270 degrees. Table 20 shows the peak-to-peak and base pressures for different conditions and shutters setting B.

It is interesting to note that Table 20 indicates that all cases of pressure waveform shown in Figure 47 are for shutters setting B, which is similar to pressure waveform shown in Figure 44, both at relatively low frequency range.

A different pressure waveform was obtained at higher frequency range of 16 to 31.3 Hz shown in Figure 48. The pressure increased to

TABLE 20: VARIATION OF PRESSURE CORRESPONDING TO WAVEFORM NO. 4 FOR THE FOLLOWING SHUTTERS SETTING AND CONDITIONS.

Flow Frequency, Hz	Peak-to-Peak Pressure, in H_2O			Base Pressure, in H_2O		
	Shutters Setting B, Degree					
	0	30	0	0	30	0
	U = 30 m/sec					
16.0	1.47			1.58		

Flow Frequency, Hz	Peak-to-Peak Pressure, in H_2O			Base Pressure, in H_2O		
	Shutters Setting B, Degree					
	0	30	0	0	30	0
	Both plates are removed (U = 17 m/sec)					
3.38	0.18			1.1		
5.08	0.13			1.1		
6.8	1.25			1.05		
10.0	1.35			1.05		

TABLE 20: cont'd

Flow Frequency, Hz	Peak-to-Peak Pressure, in H_2O			Base Pressure, in H_2O		
	Shutters Setting B, Degree					
	0	30	0	0	30	0
	Upper plate is removed (U = 22 m/sec)					
3.38	0.54			2.46		

Flow Frequency, Hz	Peak-to-Peak Pressure, in H_2O			Base Pressure, in H_2O		
	Shutters Setting B, Degree					
	0	30	0	0	30	0
	Both plates are removed (U = 17 m/sec)					
3.38	0.13			0.01		

its maximum value at 315 degrees when the triggering occurred at 270 degrees. It then decreased sharply to its minimum value at 45 degrees where it increased to its base value at 135 degrees. Starting at this angle the pressure decreased until the shutters reached a 225 degrees angle where the shutters positioning allowed some of the flow to escape through the plates openings. The pressure then increased to its base at 270 degrees for the next triggering. This type of pressure waveform with reasonably high amplitude gave nearly sinusoidal velocity waveforms at higher frequency range specified above.

It is interesting to note that Table 21 indicates that all cases of pressure waveform shown in Figure 48 are for shutters setting B, which is similar to pressure waveform shown in Figure 46 (both at higher frequencies).

A few of the pressure curves could not be fit to any general listed waveform. There are a number of possible reasons. The resolution on some of the curves was not adequate to confidently determine a pressure waveform. Some of the peak-to-peak pressure values were small and the noise in the measurement masked the waveform details. These results are indicated in Table 22.

Among the five different pressure waveforms obtained from the pressure variations in the diffuser only two of them led to best velocity waveforms (closest to sinusoidal) measured in the test section. The pressure waveform in Figure 47 resulted in the best velocity waveforms at low frequency range of 3.4 to 10 Hz when both the upper and lower plates of the shutters box were removed and flow was not blocked at the

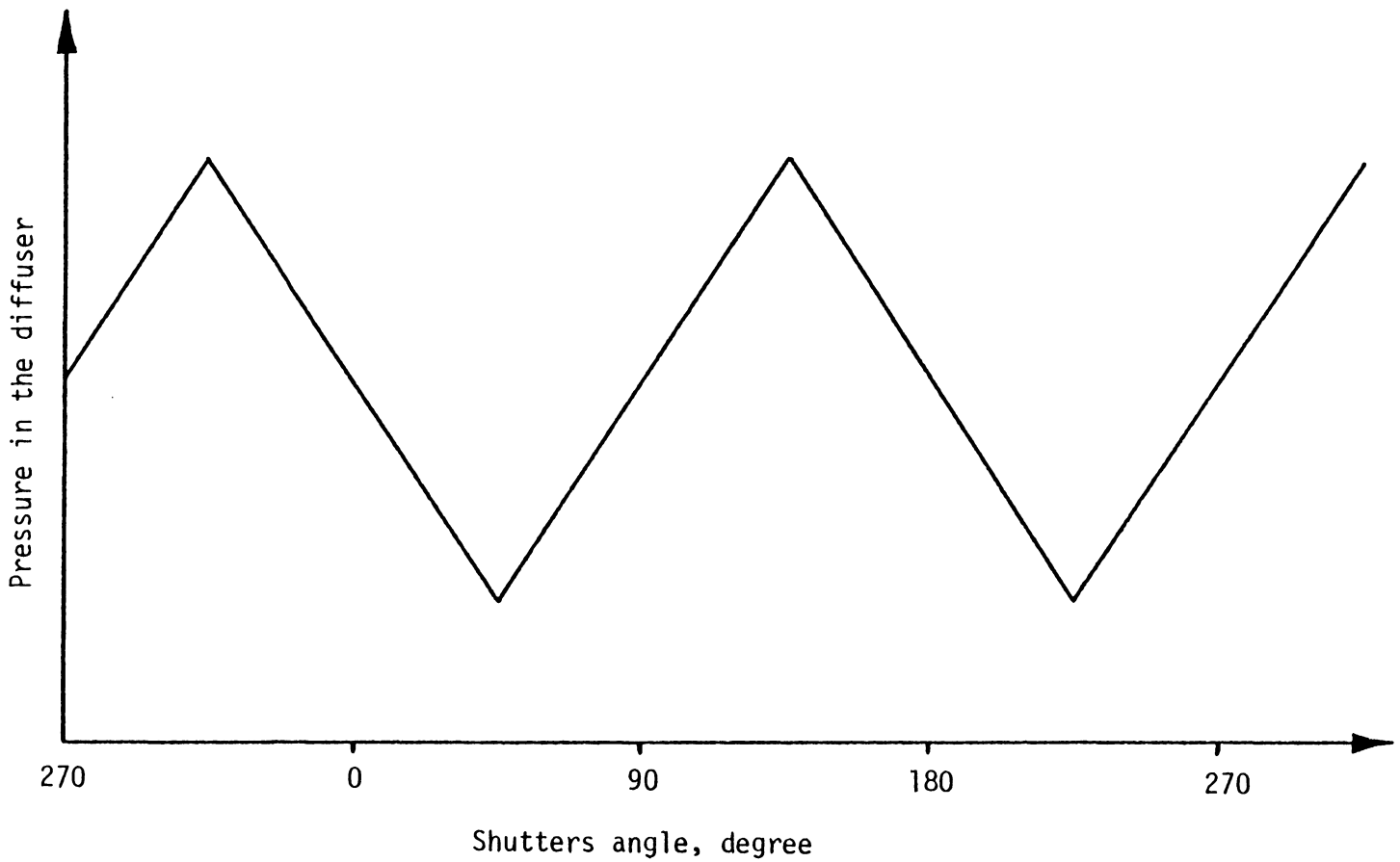

FIGURE 48: WAVEFORM NO. 5 OF THE PRESSURE DISTRIBUTIONS FOR TABLE 21.

TABLE 21: VARIATION OF PRESSURE CORRESPONDING TO WAVEFORM NO. 5 FOR THE FOLLOWING SHUTTERS SETTING AND CONDITIONS.

Flow Frequency, Hz	Peak-to-Peak Pressure, in H_2O			Base Pressure, in H_2O			Flow Frequency, Hz	Peak-to-Peak Pressure, in H_2O			Base Pressure, in H_2O		
	Shutters Setting B, Degree							Shutters Setting B, Degree					
	0	30	0	0	30	0		0	30	0	0	30	0
	Upper plate is removed (U = 22 m/sec)							Upper plate is removed (U = 10 m/sec)					
5.08	1.33			2.32			6.8	0.85			1.25		
6.8	1.20			1.1			10.0	0.62			1.15		
10.0	1.09			1.1			31.34	1.47			0.84		

TABLE 21: cont'd

Flow Frequency, Hz	Peak-to-Peak Pressure, in H_2O			Base Pressure, in H_2O		
	Shutters Setting B, Degree					
	0	30	0	0	30	0
	Both plates are removed (U = 17 m/sec)					
16.0	1.0			0.84		
19.2	1.0			0.84		

TABLE 22: VARIATION OF PRESSURE FOR UNKNOWN WAVEFORM FOR THE FOLLOWING SHUTTERS SETTINGS AND CONDITIONS.

Flow Frequency, Hz	Peak-to-Peak Pressure, in H_2O			Base Pressure, in H_2O		
	Shutters Setting A, Degree					
	0	0	0	0	0	0
	U = 15 m/sec					
10.0	0.66			1.1		

TABLE 22: cont'd.

Flow Frequency, Hz	Peak-to-Peak Pressure, in H_2O			Base Pressure, in H_2O		
	Shutters Setting B, Degree					
	0	30	0	0	30	0
	Upper plate is removed (U = 22 m/sec)					
6.8	1.2			1.1		

Flow Frequency, Hz	Peak-to-Peak Pressure, in H_2O			Base Pressure, in H_2O		
	Shutters Setting B, Degree					
	0	30	0	0	30	0
	Upper plate is removed (U = 10 m/sec)					
5.08	0.15			1.1		
16.0	0.48			1.15		
19.2	0.38			1.05		

blower inlet. The shutters setting B allowed release of pressure transients in the diffuser. The same reasoning was true at higher frequency range of 16 to 31.3 Hz when only the upper plate of the shutters box was removed. At higher frequency range the pressure waveform shown in Figure 48 gave the best nearly sinusoidal waveforms for the same shutters setting mentioned above. Again this setting resulted in releasing the pressure transients in the diffuser.

The shutters setting B that gave the best velocity waveforms does not have geometrical similarity in terms of shutters angles, but is symmetric with time. For instance, at time zero all the shutters are set at zero degree except shutters No. 2 and 5 at 30 degrees. At a later time when the shutters are rotated by 30 degrees in the clockwise sense (see Figure 12) relative to shutter No. 1, shutter No. 5 returns to zero degree and partly blocks the flow. The same condition is applicable to shutter No. 2 at some other time when the shutters are rotated by 330 degrees in the clockwise sense relative to shutter No. 1 and shutter No. 2 partly blocks the flow this time. Therefore, the setting indicates to be symmetric with time at two different angles. This is illustrated in Figure 49.

The shutters tip velocities (ωr) and mean velocities (u) in the settling chamber were calculated for the different shutters settings and frequencies. These are listed in Appendix A. The ratio of shutters tip velocity to mean velocity, $\frac{\omega r}{u}$, was then compared with the velocity phase lag obtained from the velocity waveforms. The velocity phase lags for different shutters settings and frequencies are listed

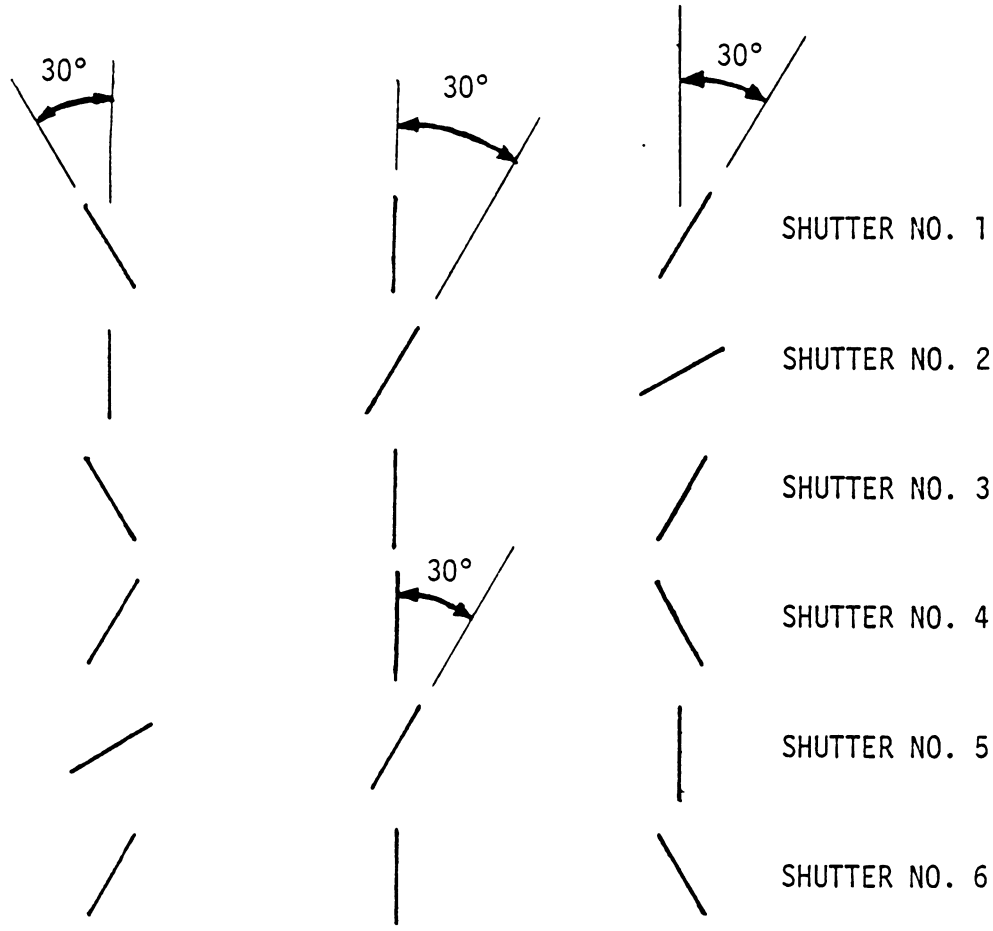

FIGURE 49: SYMMETRY OF THE SHUTTERS IN TERMS OF RELATIVE POSITIONING.

in Appendix B. Tables 23 through 27 list the average of velocity phase lags and ratio of $\frac{\omega r}{u}$ for five different conditions and two shutters settings. The corresponding plots of the phase lag versus ratio of shutters tip velocity to mean velocity (in the settling chamber) follow in Figures 50 through 52. The plots indicate that as the mean velocity in the settling chamber was reduced (because of pressure release), their slopes decreased. It also became apparent that the velocity phase lag increased with $\frac{\omega r}{u}$.

It was thought that the ratio $\frac{\omega r}{u}$ should have some effect on the shape of velocity waveforms. As it is indicated in the tables of Appendix A, the ratio of $\frac{\omega r}{u}$ remains almost constant for two different shutters settings with the same conditions at the same frequency. The ratio almost doubles when the flow is blocked at the blower inlet compared to the case for flow not blocked. Blocking the flow makes the mean velocity drop by a factor of about 2.0. These results did not indicate any significant correlation between the shape of velocity waveforms and ratio of $\frac{\omega r}{u}$. This ratio was also compared at a frequency for a mean velocity of 30 $\frac{m}{sec}$ (in the test section) with twice of the frequency for a mean velocity of 15 $\frac{m}{sec}$ (in the test section), at the same shutters setting, which did not show any effect on the shape of velocity waveforms. The ratio of $\frac{\omega r}{u}$ was then compared at a frequency for a mean velocity of 15 $\frac{m}{sec}$ (in the test section) with twice of the frequency for a mean velocity of 30 $\frac{m}{sec}$ (in the test section), at the same setting, and it remained fairly constant but no significant effect was observed on the shape of velocity waveforms. The shape of velocity waveforms and

TABLE 23: THE AVERAGE OF VELOCITY PHASE LAGS AND RATIO OF $\frac{\omega r}{u}$ FOR A MEAN VELOCITY OF 30 m/sec FOR TWO SHUTTERS SETTINGS

Flow Frequency, Hz	Shutters Setting A, Degree					
	0	0	0	0	0	0
	Shutters Setting B, Degree					
	0	30	0	0	30	0
	Phase lags average, degree			Average of $\frac{\omega r}{u}$		
3.38	14			0.15		
5.08	30			0.21		
6.8	33			0.29		
10.0	46			0.43		
16.0	52			0.69		
19.2	71			0.82		
31.34	73			1.44		

TABLE 24: THE AVERAGE OF VELOCITY PHASE LAGS AND RATIO OF $\frac{\omega r}{u}$ FOR A MEAN VELOCITY OF 15 m/sec FOR TWO SHUTTERS SETTINGS

Flow Frequency, Hz	Shutters Setting A, Degree					
	0	0	0	0	0	0
	Shutters Setting B, Degree					
	0	30	0	0	30	0
	Phase lags average, degree			Average of $\frac{\omega r}{u}$		
3.38	10			0.24		
5.08	25			0.37		
6.8	26			0.52		
10.0	28			0.78		
16.0	44			1.25		
19.2	47			1.52		
31.34	58			2.43		

TABLE 25: THE AVERAGE OF VELOCITY PHASE LAGS AND RATIO OF $\frac{\omega r}{u}$ FOR TWO SHUTTERS SETTINGS. THE FLOW IS NOT BLOCKED AND UPPER PLATE OF THE SHUTTERS BOX IS REMOVED.

Flow Frequency, Hz	Shutters Setting A, Degree					
	0	0	0	0	0	0
	Shutters Setting B, Degree					
	0	30	0	0	30	0
	Phase Lags average, degree			Average of $\frac{\omega r}{u}$		
3.38	19			0.19		
5.08	29			0.28		
6.8	29			0.38		
10.0	30			0.55		
16.0	35			0.88		
19.2	43			1.06		
31.34	57			1.85		

TABLE 26: THE AVERAGE OF VELOCITY PHASE LAGS AND RATIO OF $\frac{\omega r}{u}$ FOR ONE SHUTTERS SETTING AT DIFFERENT FREQUENCIES. THE FLOW IS BLOCKED AND UPPER PLATE OF SHUTTERS BOX IS REMOVED.

Flow Frequency, Hz	Shutters Setting B, Degree					
	0	30	0	0	30	0
	Phase lags average, degree			Average of $\frac{\omega r}{u}$		
3.38	21			0.4		
5.08	26			0.59		
6.8	34			0.78		
10.0	31			1.19		
16.0	40			1.89		
19.2	48			2.27		
31.34	55			3.81		

TABLE 27: THE AVERAGE OF VELOCITY PHASE LAGS AND RATIO OF $\frac{\omega r}{u}$ FOR TWO SHUTTERS SETTINGS. FLOW IS NOT BLOCKED AND BOTH THE UPPER AND LOWER PLATES OF THE SHUTTERS BOX ARE REMOVED.

Flow Frequency, Hz	Shutters Settings A, Degree					
	0	0	0	0	0	0
	Shutters Settings B, Degree					
	0	30	0	0	30	0
	Phase lags average, degree			Average of $\frac{\omega r}{u}$		
3.38	23			0.24		
5.08	35			0.35		
6.8	37			0.48		
10.0	31			0.70		
16.0	39			1.12		
19.2	38			1.35		
31.34	49			2.36		

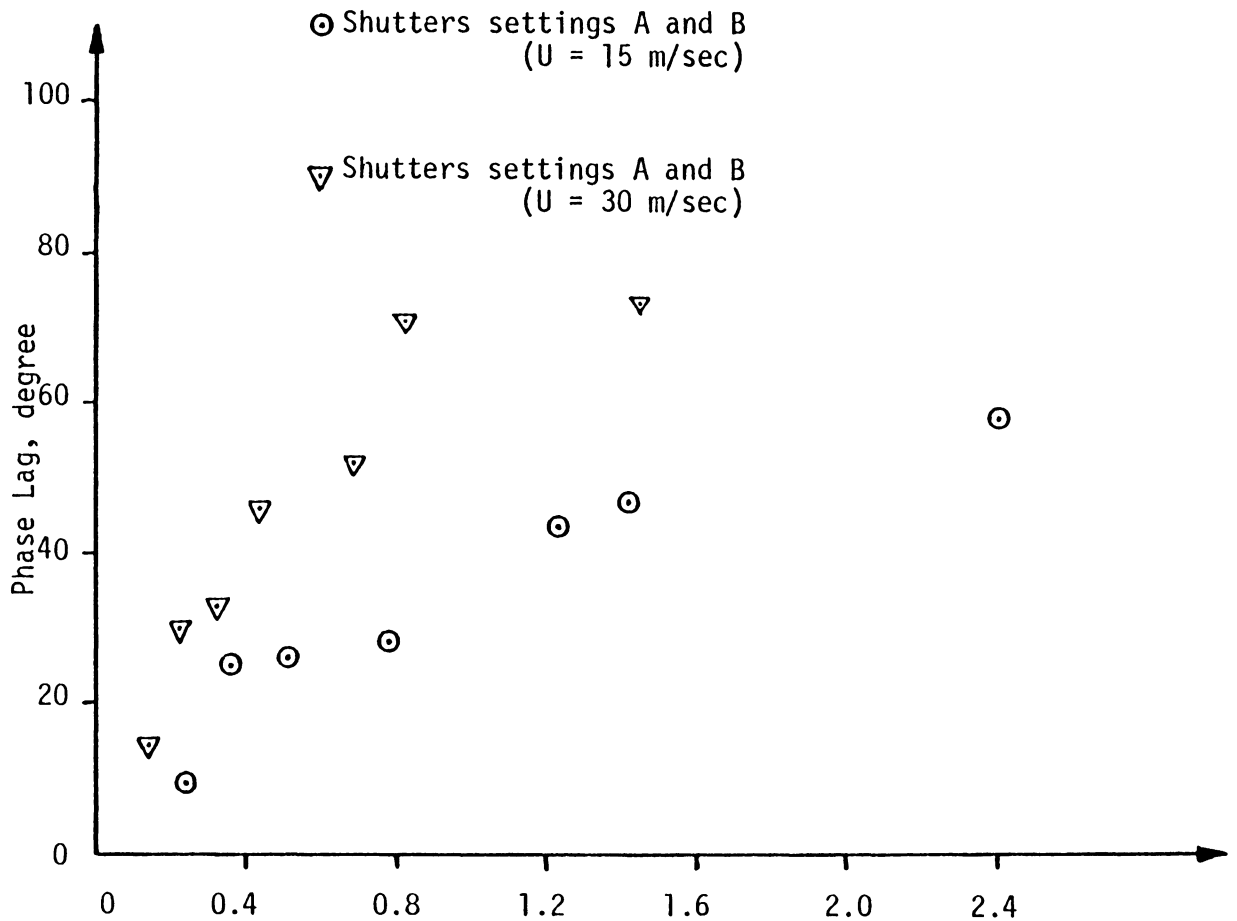

FIGURE 50: PLOT OF VELOCITY PHASE LAG VERSUS RATIO OF $\frac{\omega r}{u}$

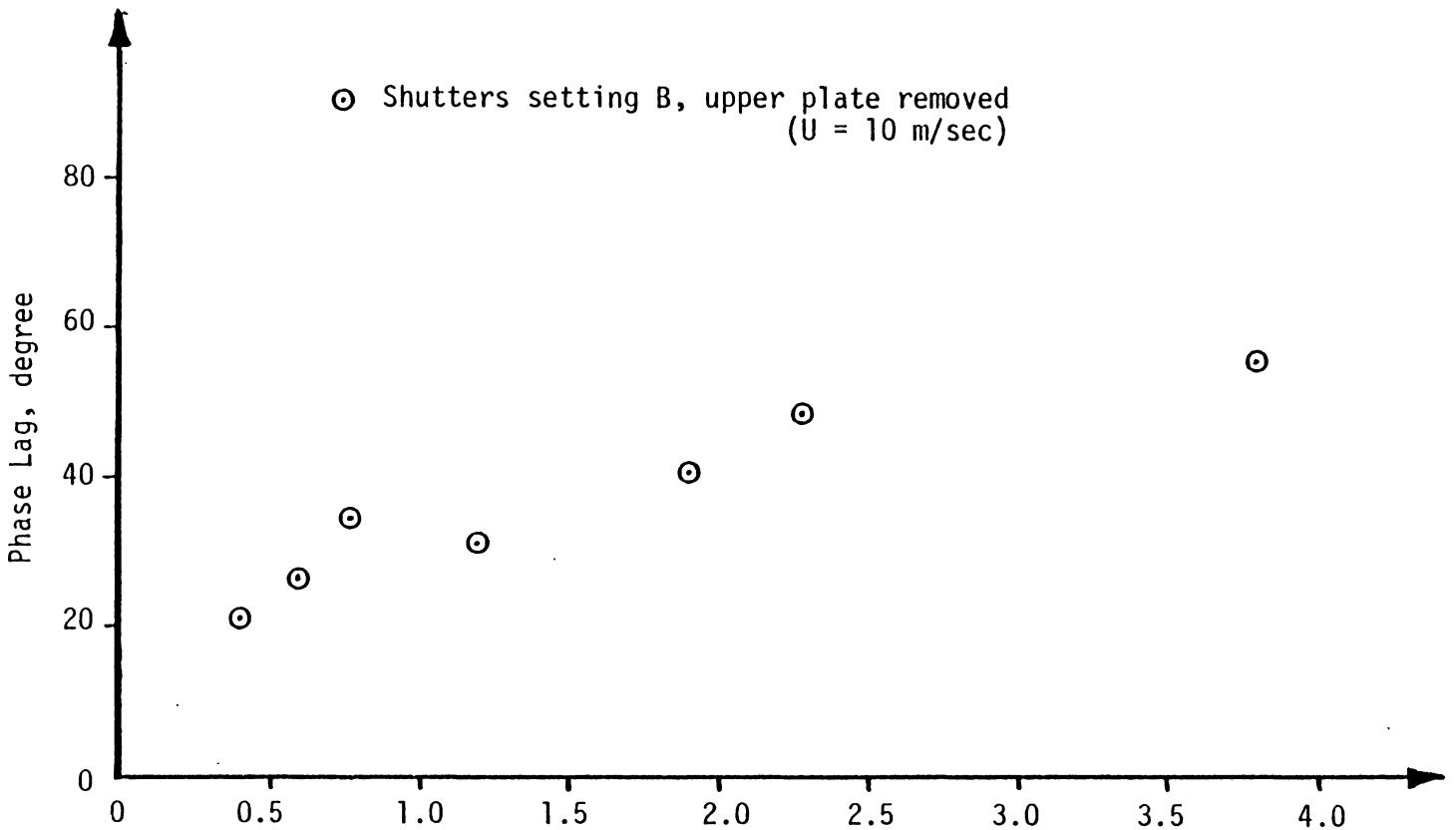

FIGURE 51: PLOT OF VELOCITY PHASE LAG VERSUS RATIO OF $\frac{\omega r}{u}$

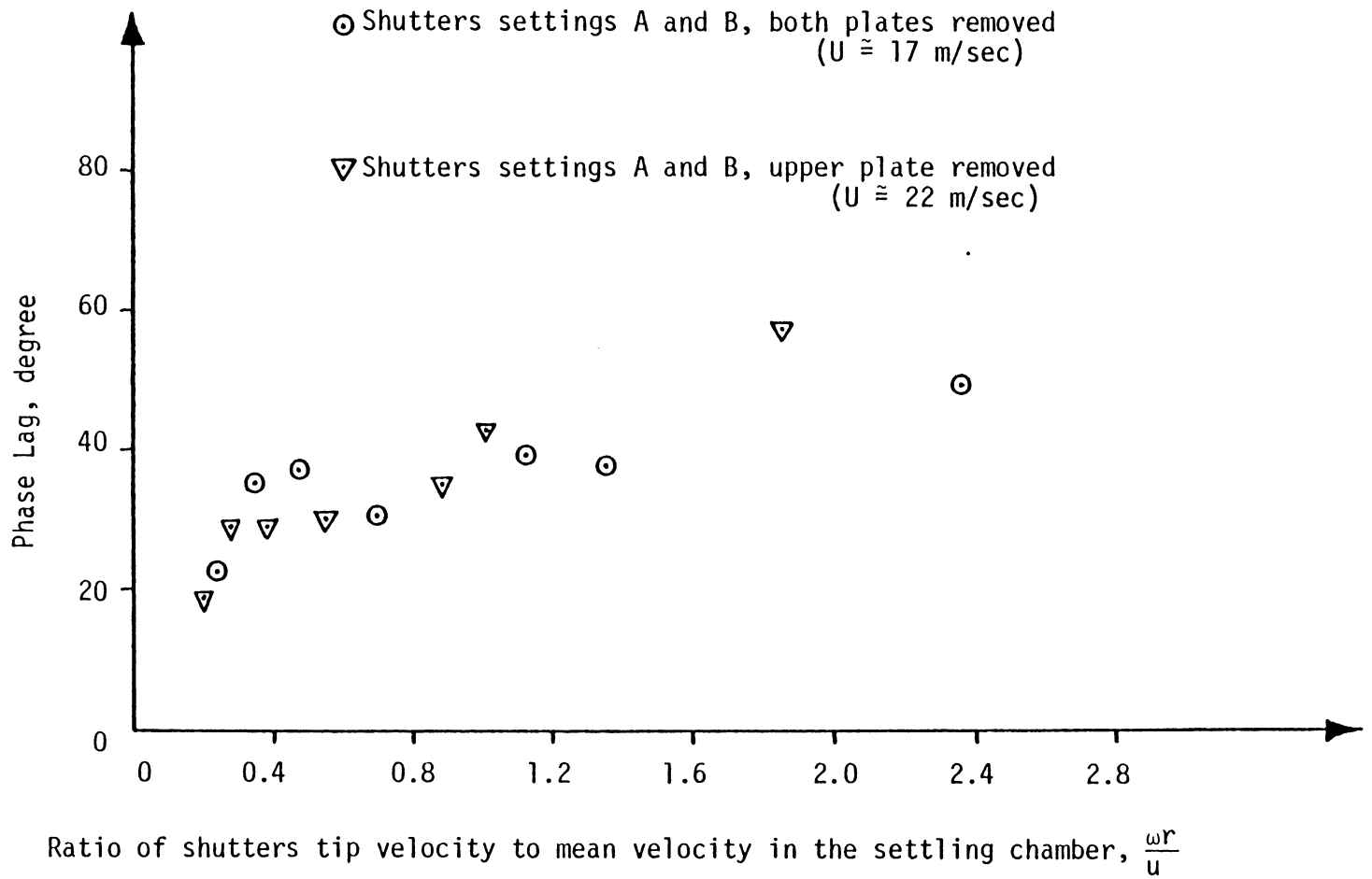

FIGURE 52: PLOT OF VELOCITY PHASE LAG VERSUS RATIO OF $\frac{\omega r}{u}$

corresponding pressure fluctuations in the diffuser were compared at different frequencies and shutters settings. This comparison indicated that as the pressure was released through the openings of the shutters box, better shape of velocity waveforms were obtained. The velocity waveforms had different types of pressure waveform at different shutters settings and frequencies.

9. LARGER SCALE WIND TUNNEL

This section presents the actual size and dimensions of the large wind tunnel. The alteration and recommendation on the numbers of shutters to be used are also included.

It was decided to double the size of the small tunnel for the larger one. The dimensions and requirements for the large wind tunnel components are given below.

The 124 cm (49-in) long test section has a 51 cm height x 71 cm width (20-in x 28-in) cross sectional area.

The contraction area ratio, c, is to remain the same at 6 and its length is 163 cm (64-in).

The settling chamber has a cross sectional area of 152 cm height x 142 cm width (60-in x 56-in) within a 178 cm (70-in) length.

The size of the diffuser is variable but it must be such that the angles of the diffuser remain between 6 to 8 degrees, or a diffuser with an area ratio of 1.6 within an approximately 132 cm (52-in) length which connects to the blower. The dimensions of the diffuser inlet depend on the dimensions of the blower discharge. A 15-hP centrifugal blower is sufficient to supply the tunnel.

There are two alternatives to build the shutters box. The first alternative is to have six shutters which will have larger dimensions and spacing compared to the shutters dimensions for the small tunnel. The following calculations are given for the dimensions and spacing in this case. It must be noted that the pressure losses through the

tunnel and the pressure at each section of the tunnel with or without the shutters will remain about the same as before except the required blower power, the spacing between the shutters, and the height of the shutters. The required power of the blower is also given below.

$$\text{Power} = P_5 \; V_2 \; A_2$$

$$\text{Power} = (758.8 \; \frac{N}{m^2})(25 \; \frac{m}{sec})(51cm \times 71cm \times \frac{1m^2}{10000cm^2})$$

$$\text{Power} = 6869 \; \frac{N \cdot m}{sec} \; (\frac{J}{sec})$$

$$\text{Power} = 6869 \; w = 6.87 \; kw$$

$$HP = \frac{(6.87 \; kw)(1.341 \; \frac{HP}{kw})}{0.75}$$

$$HP = 12.3$$

Therefore, a 15-hP blower will have enough power to drive room air through the tunnel.

The spacing between the six shutters and their height in the large tunnel will be twice as large as the ones in the small tunnel, which are determined below.

$$V_2 \; A_2 = V_s \; A_s \; C_d$$

$$A_s = \frac{V_2 \; A_2}{V_s \; C_d}$$

$$A_s = \frac{(12 \; \frac{m}{sec})(51cm \times 71cm)}{(3.2 \; \frac{m}{sec})(0.8)}$$

$$A_s = 1697 \; cm^2 \; (263\text{-}in^2)$$

But $A_s = 5(S)(W)$, and hence

$$S = \frac{A_s}{5W}$$

$$S = \frac{1697 \text{ cm}^2}{5(142 \text{ cm})}$$

$$S = 2.38 \text{ cm (0.93-in)}$$

The height of the shutters is calculated as follows:

$$h = 6\ h_s + 5S + 2S_t$$

$$152 \text{ cm} = 6\ h_s + 5(2.38 \text{ cm}) + 2\ (1.18 \text{ cm})$$

$$h_s = 23 \text{ cm (9.06-in)}$$

According to the previous results obtained from the small tunnel with six shutters, the large tunnel would probably indicate nearly sinusoidal velocity waveforms with six shutters of dimensions given above.

The best velocity waveforms in the small tunnel were obtained at shutters setting B when the pressure build-up in the diffuser was released through the shutters openings. These velocity waveforms were nearly sinusoidal. Therefore, using six shutters for the large tunnel will probably provide the same type of velocity waveforms. This must be examined for certainty.

There are two advantages of also having six shutters in the large tunnel. The first advantage is because the area ratio of shutters area to shutters opening area will be maintained the same as that of the small tunnel. The second advantage is because there already exists enough information about the pressure distribution in the diffuser and the shutters setting for the best velocity waveforms with the highest

obtainable amplitude at the desired frequency range. This information will be useful in obtaining good velocity waveforms. The disadvantage of having six shutters in the large tunnel is that the ratio of $\frac{\omega r}{u}$ will be different.

The second alternative is to maintain the same spacing between the shutters and their height as used for the small tunnel. In this case, twelve shutters will be used because of the following calculation:

$$h = nhs + (n-1)\ S + 2\ S_t$$

$$152\ cm = n(11.5\ cm) + (n-1)(1.18\ cm) + 2(.59\ cm)$$

$$n = 12$$

where n is denoted to be the number of shutters, and all the other parameters remain the same as before.

The advantage of using twelve shutters instead of six is in maintaining the same spacing and height of the shutters as before and the same area of flow blockage. The other advantage is that the ratio of $\frac{\omega r}{u}$ will be the same.

Using twelve shutters will create better mixing of the flow and hence uniformly distributed pressure behind the shutters since less force is acted on each shutter over the same area of flow blockage. The better mixing of the flow and uniformity will also probably result in smaller turbulence level of the flow in the tunnel.

The only disadvantage that will be encountered is how to set the shutters at appropriate angles to obtain sinusoidal velocity waveforms with the highest amplitude. For this case, it is worthwhile to first try to obtain velocity waveforms for shutters No. 3, 4, 9 and 10 set at

30 degrees and the rest at zero degree. The reason is because it seems that shutters No. 3 with 4 and 9 with 10 correspond to shutters No. 2 and 5, respectively for the case with six shutters which result in nearly sinusoidal velocity waveforms.

In the small tunnel, the pressure build-up was released through the openings of the upper and lower plates of shutters box. Releasing the pressure through these openings of 12.7cm x 71cm (5-in x 28-in) may not be desirable for the large tunnel since this produces a substantial decrease in the core velocity. Although, the velocity waveforms obtained are nearly sinusoidal at the desired shutters setting and frequencies in the small tunnel.

Two methods are recommended to release the pressure build-up in the diffuser of the large tunnel. The first method is achieved by hinging the upper and lower plates of the shutters on one side. The plates are connected by two bars, where their openings can be controlled to adequately release enough pressure build-up. The thickness of this opening depends on how much of pressure release is needed and is recommended to have a thickness of about 25cm x 142cm(10-in x 56-in) where it can be varied to desirable opening.

The second alternative is to have perforated shutters. Using perforated (or porous) shutters will accomplish the same decrease in average stagnation pressure on the shutters as removing the plates of the shutters box in the small tunnel. This way the flow bled through the porous shutters will reduce the velocity impinging on the shutters, thus, reducing the stagnation pressure.

10. CONCLUSIONS

On the basis of the experimental measurements investigated, the following conclusions are presented for the pulsating flow with six shutters in the small tunnel. The frequency range tested is between 3.4 to 31.3 Hz.

1. The shape of velocity waveforms can be controlled by adjusting the relative shutter orientations and providing release of the transient pressures in the diffuser. Acceptable velocity waveforms are obtained over the frequency range of 3.4 to 31.3 Hz.
2. Controlling the pressure waveform in the diffuser is the key to controlling the velocity waveform.
3. The non-dimensional parameter $\frac{\omega r}{u}$ is correlated with the phase lag of velocity waveform, but not the waveform shape.
4. Vibration of the tunnel components can be a problem. The structure must be stiffened and isolated to prevent excessive noise and vibration.

Precaution must be observed in providing a constant pressure, upstream of the shutters box (in the diffuser), in order to obtain the best velocity waveforms with the highest obtainable amplitude at the desired frequency range in the large tunnel.

REFERENCES

1. Pope, Alan, and Harper, John J., "Low-Speed Wind Tunnel Testing," pp. 36-82, 1966.

2. Mehta, R. D. and Bradshaw, P., "Design Rules for Small Low Speed Wind Tunnels", Aeronautical Journal, November 1979, Paper No. 718, pp. 443-449.

3. Liiva, J., et al., "Two-Dimensional Tests of Airfoils Oscillating Near Stall," U.S. Army Aviation Material Lab., Fort Eustis, Va. Tech Report 68-13. April 1968; also, Journal of Aircraft, Vol. 6, No. 1, January 1969, pp. 46-51.

4. Long, J. D., "Experimental Results for an Airfoil with Oscillating Spoiler and Flap," Symposium on Unsteady Aerodynamics, Kinney, R. B., ed., University of Arizona, Tucson, 1975, pp. 55-80; also, Journal of Aircraft, Vol. 13, No. 9, Sept. 1976, pp. 687-694.

5. Maresca, C., Rebont, J., and Valensi, J., "Separation and Reattachment of the Boundary Layer on a Symmetrical Airfoil Oscillating at Fixed Incidence in a Steady Flow," Symposium on Unsteady Aerodynamics, Kinney, R. B., ed., University of Arizona, Tucson, 1975, pp. 35-53.

6. Maresca, C., Rebont, J., and Valensi, J., "Caracteristiques Aerodynamiques d'un Profil d'Aile en Mouvement Instationnaire," Proc. IUTAM 14th International Congress of Theoretical and Applied Mechanics, Delft, Sept. 1976, to be published by Springer-Verlag, Berlin.

7. Saxena, L. S., Fejer, A. A., and Morkovin, M. V., "Effects of Periodic Changes in Free Stream Velocity on Flows over Airfoils near Static Stall," Nonsteady Fluid Dynamics, eds., Crow, D. E., and Miller, J. A., December 1978, pp. 111-116.

8. Saxena, L. S., Fejer, A. A., and Morkovin, M. V., "Features of Unsteady Flow over Airfoils," Paper No. 22, Proc. AGARD Conference on Unsteady Aerodynamics, AGARD, Cp-277, 1977.

9. Maresca, C., Favier, D., Rebont, J., Jones, G., and Telionis, D., "Measurement and Visualization of a Stalling Airfoil in Translational Oscillation," AIAA 12th Fluid and Plasma Dynamics Conference, July 23-25, 1979/Williamsburg, Virginia.

10. Schachenmann, A. A., and Rockwell, D. O., "Oscillating Turbulent Flow in a Conical Diffuser," Journal of Fluids Engineering, Transactions of the ASME, December 1976, pp. 695-701.

11. Charnay, G., and Mathieu, J., "Periodic Flow in a Wind Tunnel Produced by Rotating Shutters," Journal of Fluids Engineering, Transactions of the ASME, Vol. 98, 1976.

12. Miller, J. A., and Fejer, A. A., "Transition Phenomena in Oscillating Boundary Layer Flows," Journal of Fluid Mechanics, Vol. 18, 1964, pp. 438-448.

13. Obremski, H. J., and Fejer, A. A., "Transition in Oscillating Boundary Layer Flows," Journal of Fluid Mechanics, Vol. 29, 1967, pp. 93-111.

14. Duhamed, P., "Contribution a' l'Etudes des Taches Turbulentes de Transition Pour un Ecovlement Pulse' sur une Plaque Plane," Thesis at University of Nancy, 1971.

15. Karlesson, S. K. F., "An Unsteady Turbulent Boundary Layer," Journal of Fluid Mechanics, Vol. 5, 1959, pp. 622-636.

16. Simpson, R. L., Sallas, J. J., and Nasburg, R. E., "Tailoring the Waveform of a Periodic Flow with a Programmable Damper," Journal of Fluids Engineering, Transactions of the ASME, Vol. 100, September 1978, pp. 287-290.

17. Mehta, R. D., "The Aerodynamics Design of Blower Tunnels with Wide-Angle Diffusers," Prog. Aerospace Sci., Vol. 18, pg. 59, 1977.

18. Mehta, R. D., "Aspects of the Design and Performance of Blower Tunnel Components," Ph.D. Thesis, Imperial College, University of London, 1978.

APPENDIX A

THE RATIO OF SHUTTERS TIP SPEED TO MEAN VELOCITY (IN THE SETTLING CHAMBER), $\frac{\omega r}{u}$, FOR DIFFERENT SHUTTERS SETTINGS AND FREQUENCIES.

TABLE 28: THE RATIO OF SHUTTERS TIP SPEED TO MEAN VELOCITY ($\frac{\omega r}{u}$) FOR DIFFERENT SHUTTERS SETTINGS AND FREQUENCIES. THE FLOW IS NOT BLOCKED.

Flow Frequency, Hz	Shutters Tip Speed(ωr), $\frac{m}{sec}$	SHUTTERS SETTING A, DEGREE						SHUTTERS SETTING B, DEGREE						Average of Ratio $\frac{\omega r}{u}$
		0	0	0	0	0	0	0	30	0	0	30	0	
		Mean Velocity(u), $\frac{m}{sec}$			$\frac{\omega r}{u}$			Mean Velocity(u), $\frac{m}{sec}$			$\frac{\omega r}{u}$			
3.38	0.61	3.7			0.17			4.9			0.12			0.15
5.08	0.91	3.7			0.25			4.9			0.18			0.21
6.8	1.23	3.7			0.33			4.9			0.25			0.29
10.0	1.81	3.73			0.49			4.9			0.37			0.43
16.0	2.90	3.75			0.77			4.8			0.61			0.69
19.2	3.47	3.8			0.91			4.7			0.73			0.82
31.34	5.67	3.9			1.44			3.9			1.44			1.44

TABLE 29: THE RATIO OF SHUTTERS TIP SPEED TO MEAN VELOCITY ($\frac{\omega r}{u}$) FOR DIFFERENT SHUTTERS SETTINGS AND FREQUENCIES. THE FLOW IS BLOCKED.

Flow Frequency, Hz	Shutters Tip Speed(ωr), $\frac{m}{sec}$	SHUTTERS SETTING A, DEGREE						SHUTTERS SETTING B, DEGREE						Average of Ratio $\frac{\omega r}{u}$
		0	0	0	0	0	0	0	30	0	0	30	0	
		Mean Velocity(u), $\frac{m}{sec}$			$\frac{\omega r}{u}$			Mean Velocity(u), $\frac{m}{sec}$			$\frac{\omega r}{u}$			
3.38	0.61	2.7			0.23			2.40			0.26			0.24
5.08	0.91	2.6			0.35			2.40			0.38			0.37
6.8	1.23	2.3			0.53			2.40			0.51			0.52
10.0	1.81	2.3			0.80			2.40			0.76			0.78
16.0	2.90	2.3			1.29			2.40			1.22			1.25
19.2	3.47	2.2			1.57			2.4			1.46			1.52
31.34	5.67	2.3			2.49			2.4			2.38			2.43

TABLE 30: THE RATIO OF SHUTTERS TIP SPEED TO MEAN VELOCITY ($\frac{\omega r}{u}$) FOR DIFFERENT SHUTTERS SETTINGS AND FREQUENCIES. THE FLOW IS NOT BLOCKED AND UPPER PLATE OF THE SHUTTERS BOX IS REMOVED

Flow Frequency, Hz	Shutters Tip Speed(ωr), $\frac{m}{sec}$	SHUTTERS SETTING A, DEGREE						SHUTTERS SETTING B, DEGREE						Average of Ratio $\frac{\omega r}{u}$
		0	0	0	0	0	0	0	30	0	0	30	0	
		Mean Velocity(u), $\frac{m}{sec}$			$\frac{\omega r}{u}$			Mean Velocity(u), $\frac{m}{sec}$			$\frac{\omega r}{u}$			
3.38	0.61	3.3			0.19			3.3			0.19			0.19
5.08	0.91	3.2			0.28			3.3			0.28			0.28
6.8	1.23	3.2			0.38			3.3			0.37			0.375
10.0	1.81	3.2			0.56			3.3			0.54			0.55
16.0	2.90	3.2			0.90			3.4			0.85			0.875
19.2	3.47	3.2			1.1			3.4			1.02			1.06
31.34	5.67	3.1			1.86			3.1			1.83			1.845

TABLE 31: THE RATIO OF SHUTTERS TIP SPEED TO MEAN VELOCITY ($\frac{\omega r}{u}$) FOR ONE SHUTTERS SETTING AT DIFFERENT FREQUENCIES. THE FLOW IS BLOCKED AND UPPER PLATE OF THE SHUTTERS BOX IS REMOVED.

Flow Frequency, Hz	Shutters tip Speed(ωr), $\frac{m}{sec}$	SHUTTERS SETTING B, DEGREE					
		0	30	0	0	30	0
		Mean Velocity(u), $\frac{m}{sec}$			$\frac{\omega r}{u}$		
3.38	0.61	1.5			0.4		
5.08	0.91	1.5			0.59		
6.8	1.23	1.6			0.78		
10.0	1.81	1.5			1.19		
16.0	2.90	1.5			1.89		
19.2	3.47	1.5			2.27		
31.34	5.67	1.5			3.91		

TABLE 32: THE RATIO OF SHUTTERS TIP SPEED TO MEAN VELOCITY ($\frac{\omega r}{u}$) FOR DIFFERENT SHUTTERS SETTINGS AND FREQUENCIES. THE FLOW IS NOT BLOCKED AND BOTH THE LOWER AND UPPER PLATES OF THE SHUTTERS BOX ARE REMOVED

Flow Frequency, Hz	Shutters Tip Speed(ωr), $\frac{m}{sec}$	SHUTTERS SETTING A, DEGREE						SHUTTERS SETTING B, DEGREE						Average of Ratio $\frac{\omega r}{u}$
		0	0	0	0	0	0	0	30	0	0	30	0	
		Mean Velocity(u), $\frac{m}{sec}$			$\frac{\omega r}{u}$			Mean Velocity(u), $\frac{m}{sec}$			$\frac{\omega r}{u}$			
3.38	0.61	2.5			0.24			2.6			0.23			0.24
5.08	0.91	2.5			0.36			2.6			0.34			0.35
6.8	1.23	2.5			0.49			2.7			0.46			0.48
10.0	1.81	2.5			0.72			2.7			0.68			0.70
16.0	2.9	2.6			1.14			2.6			1.11			1.12
19.2	3.47	2.6			1.36			2.6			1.34			1.35
31.34	5.67	2.4			2.36			2.4			2.36			2.36

APPENDIX B

THE VELOCITY PHASE LAG FOR DIFFERENT SHUTTERS SETTINGS AND FREQUENCIES

TABLE 33: THE VELOCITY PHASE LAG WHEN THE FLOW IS NOT BLOCKED FOR DIFFERENT SHUTTERS SETTINGS AND FREQUENCIES.

Flow Frequency, Hz	VELOCITY PHASE LAG, DEGREE												Phase Lags Average, Degree
	SHUTTERS SETTING A, DEGREE						SHUTTERS SETTING B, DEGREE						
	0	0	0	0	0	0	0	30	0	0	30	0	
3.38	12						15						13.5
5.08	28						32						30
6.8	32						33						32.5
10.0	47						41						46
16.0	50						53						51.5
19.2	70						71						70.5
31.34	73						73						73

TABLE 34: THE VELOCITY PHASE LAG WHEN THE FLOW IS BLOCKED FOR DIFFERENT SHUTTERS SETTINGS AND FREQUENCIES.

Flow Frequency, Hz	VELOCITY PHASE LAG, DEGREE												Phase Lags Average, Degree
	SHUTTERS SETTING A, DEGREE						SHUTTERS SETTING B, DEGREE						
	0	0	0	0	0	0	0	30	0	0	30	0	
3.38	8						11						9.5
5.08	24						26						25
6.8	27						25						26
10.0	27						29						28
16.0	40						47						43.5
19.2	47						46						46.5
31.34	49						67						58

TABLE 35: THE VELOCITY PHASE LAG WHEN THE FLOW IS NOT BLOCKED FOR DIFFERENT SHUTTERS SETTINGS AND FREQUENCIES. THE UPPER PLATE OF THE SHUTTERS BOX IS REMOVED.

Flow Frequency, Hz	VELOCITY PHASE LAG, DEGREE												Phase Lags Average, Degree
	SHUTTERS SETTING A, DEGREE						SHUTTERS SETTING B, DEGREE						
	0	0	0	0	0	0	0	30	0	0	30	0	
3.38	13						24						18.5
5.08	25						32						28.5
6.8	24						34						29
10.0	23						37						30
16.0	33						37						35
19.2	43						42						42.5
31.34	55						58						56.5

TABLE 36: THE VELOCITY PHASE LAG WHEN THE FLOW IS BLOCKED FOR ONE SHUTTERS SETTING AT DIFFERENT FREQUENCIES. THE UPPER PLATE OF THE SHUTTERS BOX IS REMOVED.

Flow Frequency, Hz	VELOCITY PHASE LAG, DEGREE					
	SHUTTERS SETTING B, DEGREE					
	0	30	0	0	30	0
3.38	21					
5.08	26					
6.8	34					
10.0	31					
16.0	40					
19.2	48					
31.34	55					

TABLE 37: THE VELOCITY PHASE LAG WHEN THE FLOW IS NOT BLOCKED FOR DIFFERENT SHUTTERS SETTINGS AND FREQUENCIES. BOTH THE UPPER AND LOWER PLATES OF THE SHUTTERS BOX ARE REMOVED.

Flow Frequency, Hz	VELOCITY PHASE LAG, DEGREE												Phase Lags Average, Degree
	SHUTTERS SETTING A, DEGREE						SHUTTERS SETTING B, DEGREE						
	0	0	0	0	0	0	0	30	0	0	30	0	
3.38	18						27						22.5
5.08	32						38						35
6.8	33						41						37
10.0	23						38						30.5
16.0	30						48						39
19.2	40						35						37.5
31.34	43						55						49

The vita has been removed from the scanned document

DESIGN OF EVALUATION OF

A PULSATING FLOW WIND TUNNEL

by

Amir Tavakoli

(ABSTRACT)

A wind tunnel was designed and built to produce a pulsating flow. The pulsation was achieved by a series of shutters (rotating with constant angular velocity) placed upstream of the settling chamber inlet. The system was optimized to obtain nearly sinusoidal velocity waveforms with the highest obtainable amplitudes over the frequency range of 3.4 to 31.3 Hz. The velocity and pressure waveforms are given for different shutters settings and conditions.

It was found that the velocity waveform shape and amplitude, obtained in the test section, are a strong function of pressure build-up in the diffuser upstream of the shutters box. An explanation is given, for various shutters settings and conditions, of how pressure release is achieved and how the pressure waveforms are generated.